Archives of Computational Methods in Engineering (2021) 28:3721–3780
https://doi.org/10.1007/s11831-020-09523-0

ORIGINAL PAPER

# Thirty Years of the Finite Volume Method for Solid Mechanics

P. Cardiff[1] · I. Demirdžić[2]

Received: 21 May 2020 / Accepted: 14 December 2020 / Published online: 2 February 2021


**Abstract**
Since early publications in the late 1980s and early 1990s, the finite volume method has been shown suitable for solid mechanics analyses. At present, there are several flavours of the method, which can be classified in a variety of ways, such as grid arrangement (cell-centred vs. staggered vs. vertex-centred), solution algorithm (implicit vs. explicit), and stabilisation strategy (Rhie–Chow vs. Jameson–Schmidt–Turkel vs. Godunov upwinding). This article gives an overview, historical perspective, comparison and critical analysis of the different approaches where a close comparison with the de facto standard for computational solid mechanics, the finite element method, is given. The article finishes with a look towards future research directions and steps required for finite volume solid mechanics to achieve more widespread acceptance.

## 1 Introduction

"*Now however I recognise the FVM/FEM dichotomy as being comparable with those between Protestant and Catholic, or Sunni and Shia. That is to say that it promotes needless conflict; and expense; and loss of opportunity.*" [1] With these words, Brian Spalding highlighted the, at times, unproductive nature of the debate around the relative merits of the finite volume (FVM) and finite element (FEM) methods. Although accepted in the computational fluid dynamics (CFD) field, there remains a reluctance and general confusion around the application of the finite volume method to solid mechanics. The aim of this article is to clarify this confusion, by: providing an overview of the significant developments within the field; linking variants of the finite volume method for solid mechanics analyses; comparing finite volume methods with standard finite element methods; and, finally, identifying future directions for the field.

Building on the foundations of the finite difference method, the finite volume method is a generalisation in terms of geometry and topology: simple finite volume schemes reduce to finite difference schemes. Whereas the finite difference method is based on nodal relations for *differential* equations, the finite volume method balances forces acting on control volumes, directly discretising the *integral* form of the conservation laws. A number of prior developments within CFD provided the foundation for the earliest paper on the cell-centred finite volume method for solid mechanics by Demirdžić et al. [2]. In the subsequent three decades the finite volume method for solid mechanics has developed in a number of directions, differing in terms of discretisation, solution methodology and overall philosophy. The varied approaches may be classified in a number of ways, including, for example:

- *Grid arrangement*: cell-centred [2, 3] vs. vertex-centred [4–12] vs. staggered-grid [13–19], as well as more recently face-centred [20, 21] and meshless [22, 23];
- *Solution algorithm*: implicit [3, 24, 25] vs. explicit (matrix-free) [26–28];
- *Stabilisation approach*: Rhie–Chow [29, 30] vs. Jameson–Schmidt–Turkel [31] vs. Godunov *two-sided* upwinding [27, 32].

There are countless other ways to classify the approaches, for example, based on force discretisation at the control volume face, however, the current article will base its discussion primarily around the three classification types above.

The essential characteristic of a finite volume method is the integration of the governing conservation equation over finite control volumes. In this sense, the *cell-centred* vs.

✉ P. Cardiff
philip.cardiff@ucd.ie

[1] Bekaert University Technology Centre, School of Mechanical and Materials Engineering, University College Dublin, Belfield, Ireland

[2] Mašinski fakultet Sarajevo, Vilsonovo šetalište 9, 71000 Sarajevo, Bosnia-Herzegovina

*vertex-centred* vs. *staggered-grid* approaches primarily differ in *how* these control volumes are constructed. Cell-centred approaches use the primary mesh control volumes, whereas vertex-centred approaches construct a *dual mesh* with control volumes surrounding the vertices of the primary mesh. On the other hand, staggered-grid approaches create multiple secondary meshes, one for each scalar component of the primary solution vector, constructed about the primary mesh faces. Despite their close relationship, as explored further in Sect. 3, approaches based on differing grid arrangements often differ greatly in terms of philosophy: as noted by Baliga and Atabaki [33], the cell-centred method is often thought of as a control-volume finite difference method, combining ideas borrowed from finite volume and finite difference methods; whereas, the vertex-centred approach is viewed as a control-volume finite element method, formulated by amalgamating concepts native to finite volume and finite element methods.

Regardless of the chosen grid arrangement, spatio-temporal integration of the governing equations may adopt an *implicit* or *explicit* solution algorithm. Implicit algorithms are characterised by the solution of a linear system of equations and are unconditionally stable with respect to the time increment size. In contrast, explicit or matrix-free algorithms avoid the need to construct such a system of linear equations but the time increment size is restricted by the classic Courant–Friedrichs–Lewy constraint [34]. The choice of solution algorithm often depends on the problems of interest, with implicit methods favoured for elliptic and parabolic cases (steady-state and quasi-steady-state) and explicit methods for hyperbolic (high rates, wave propagation). Once the grid arrangement and solution algorithm are selected, care must be taken in the construction of a stable discretisation that does not suffer from unphysical instabilities in the solution field. To this end, a variety of stabilisation approaches have been proposed. Generally, each approach can be viewed upon as adding some form of diffusion to the surface force discretisation with the purpose of quelling high-frequency oscillations. Rhie–Chow-style stabilisation is common in the implicit approaches originating from the work of Demirdžić and Muzaferija [29], while Godunov upwinding and Jameson–Schmidt–Turkel approaches are more commonly seen in the explicit approaches, rooted in the solution of compressible gas flow Euler equations.

From afar, each of these main variants of finite volume method can seem quite distinct; however, upon closer inspective, they share many similarities in terms of discretisation and solution algorithm. Nevertheless, the fragmented nature of the finite volume solid mechanics community is evident from many recent publications in the area, where authors, reviewers and editors tend to be unaware of developments within the field, for example, see [35]. In addition, and more generally, there is a lack of awareness in the computational mechanics community around the capabilities of the finite volume method for solid mechanics. Accordingly, a comparative and critical review of the finite volume method for solid mechanics is timely, relevant and essential for the future progress of the field. Within this domain, there are a number of open questions: What are the strengths and weaknesses of the various approaches? Which approaches show the greatest potential and widest applicability? Are there possibilities for the various methods to be combined to produce superior methods? How do the finite volume approaches relate to finite element methods? Are there directions of development which are missing? This article will attempt to provide answers to these questions, as well as providing a unifying framework for the discussion of finite volume methods for solid mechanics, and their relationship with finite element methods. Given the scale of the field, it is outside the scope of the article to provide an exhaustive review of all formulations; instead, the article aims to provide detailed analysis on the main variants of approach common in the literature. The primary novel contributions of the current article are twofold: (i) The first detailed review of the finite volume solid mechanics field is presented; and (ii) The first analysis of similarities and differences between all main variants of the finite volume method for solid mechanics is detailed.

The remainder of the article is constructed as follows: Sect. 2 provides a chronological overview of the prominent finite volume developments for solid mechanics. Section 3 compares and contrasts the three main flavours of the finite volume method for solid mechanics. In Sect. 4, the finite volume method for solid mechanics is compared to the "standard" continuous Bubnov–Galerkin finite element method, highlighting similarities and differences in terms of discretisation, solution methodology and overall philosophy. Section 5 reviews the variety of structural applications to which the finite volume method has been applied in its thirty year history. The penultimate section briefly reviews software that use, or have previously used, the finite volume method for solid mechanics simulations. Finally, Sect. 7 summaries the main conclusions of the article and considers the current challenges facing the field.

## 2 History of the Finite Volume Method for Computational Solid Mechanics

The development of the finite volume method for solid mechanics has occurred independently in a number of forms, with finite difference methods, computational fluid mechanics algorithms, and finite element methods providing much of the inspiration. This section gives an overview of the historical development of these finite volume methods. The treatise is primarily partitioned based on the grid

arrangement, where comments regarding the solution algorithm and stabilisation scheme are given where appropriate. In-depth dissections of the technical details are left to Sect. 3. While the field is small and fragmented, there are a number of notable reviews worth mentioning, including those of Maneeratana [36], Vaz Jr. et al. [37] and Cavalcante et al. [38].

Before delving into details of influential publications, it is insightful to first consider the literature landscape as a whole. To this end, Fig. 1 presents a histogram of the publications in the area to-date, separated into journal articles, conferences, Ph.D. theses, Masters theses and books. Of course, exact records of each publication type are difficult to track and consequently the data should be taken as indicative. To complement this, Fig. 2 lists the most popular international journals for publishing finite volume solid mechanics articles; only journals with greater than five articles have been included. Furthermore, a table of the most cited articles related to the finite volume method for solid mechanics can be found in "Appendix 1".

A perspective on the literature landscape is gained from the *co-authorship network* presented in Fig. 3, which has been generated using the VOSviewer software [39]. A co-authorship network is a visual method to assess research collaborations within a field, as well as observe detached regions of research. Referring to Fig. 3, the three larger sub-networks broadly correspond to: implicit cell-centred approaches indicated by the red sub-network centred on *demirdžić* and *ivanković*; implicit vertex-centred approaches indicated by the green sub-network centred on *cross*, *bailey* and *fallah*; and a specialised form of finite volume method for microstructural analysis indicated by the blue sub-network centred on *aboudi*, *pindera* and *cavalcante*. Although the co-authorship graph is not a direct measure

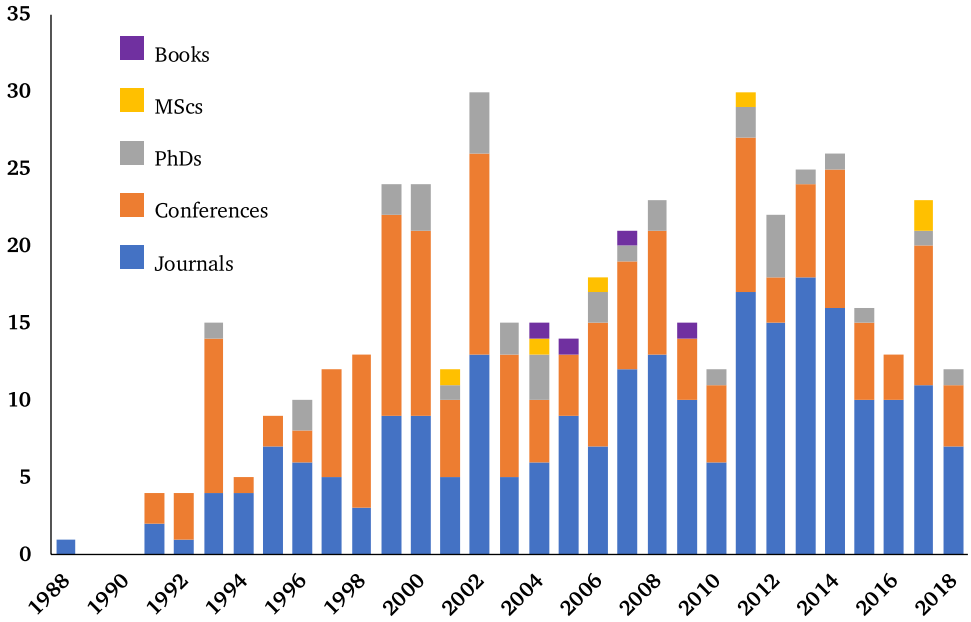


**Fig. 1** Histogram of the finite volume method for solid mechanics publications to-date. (Color figure online)

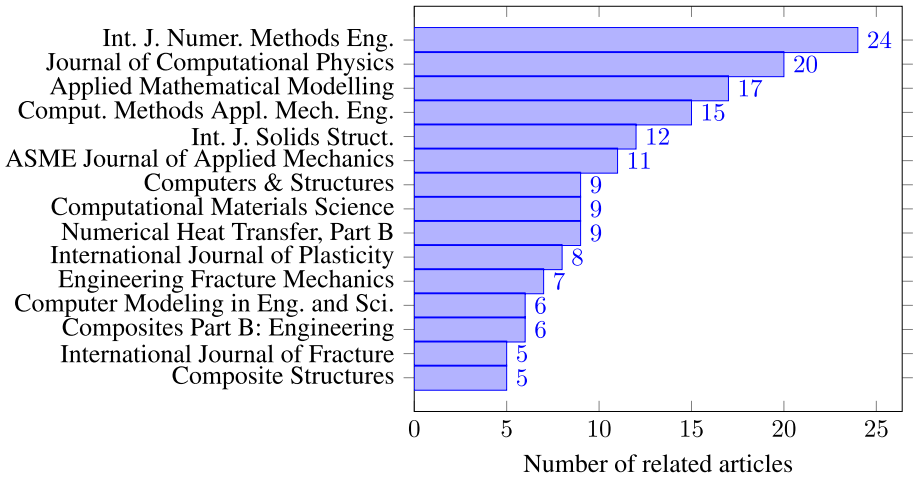


**Fig. 2** Number of publications per journal related to computational solid mechanics using the finite volume method, based on the cited references, where only journals with greater than five articles have been counted. (Color figure online)

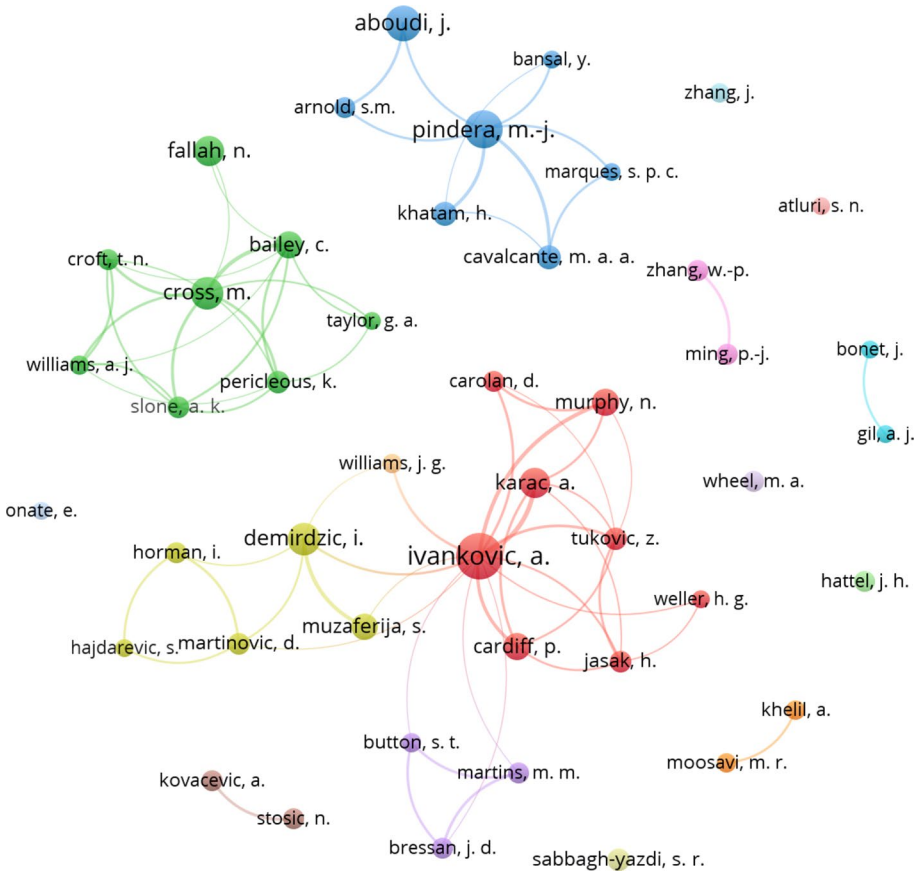


**Fig. 3** Co-authorship network of the finite volume method for solid mechanics, generated using the VOSviewer software [39]. To maintain interpretability, only authors with five or more related peer-reviewed publications have been included in the network. The network provides insight into collaborations within the field but is not a direct measure of contribution. (Color figure online)

of contribution to the field, it does provide insight into the collaboration between authors and subdivisions within the domain. In the graph, individual authors are represented by filled circles, and a co-authored publication between two individual authors is symbolised by a line connecting the two filled circles; the line thickness increases with increasing number of co-authored publications; the size of an author's filled circle is directly proportional to the number of their related publications. To maintain interpretability, only authors with five or more related publications have been included in the network, and only peer-reviewed publications have been incorporated.

Finally, before considering individual contributions, we will clarify the meaning of a number of terms in the current context to avoid any confusion. For the domain spatial discretisation, this will be referred to interchangeably as the "mesh" or "grid"; each sub-domain in a finite volume mesh will be equivalently referred to as a "control volume", a "cell", or even an "element"; similarly, each sub-domain in the finite element mesh will be referred to as an "element" or "cell'. The term "node" indicates the mesh location where the solution variable is stored, which could be a vertex, face-centre or cell-centre depending on the method.

## 2.1 Cell-Centred Approaches

Thirty years ago, Demirdžić et al. [2] proposed the first application of the cell-centred finite volume method in its modern form to solid mechanics. Subsequently, cell-centred developments have primarily focussed on two relatively disconnected approaches:

- *Implicit* cell-centred approaches based on the original approach of Demirdžić et al. [2], and
- *Explicit* Godunov-type cell-centred approaches stemming from the work of Trangenstein and Colella [40].

The cell-centred approach takes its name from the dependent variable(s) residing at the cell centres (control volume centroids); equivalently, the approach has been termed the *colocated*, *co-located* or *collocated* finite volume method, as the dependent variables share their location at the cell centres/centroids.

### 2.1.1 Implicit Cell-Centred Methods

Considering first the implicit methods: in the original approach of Demirdžić et al. [2], a structured rectangular 2-D method was applied to the simulation of thermal

deformations in welded workpieces (Fig. 4a). The displacement was assumed to vary linearly between computational nodes, and the small strain material behaviour was described by the *Duhamel–Neumann* form of Hooke's law. A distinguishing feature of the proposed solution algorithm was the partitioning of the surface force term into a compact-stencil *implicit* term and a larger stencil *explicit* term. As a result, the linear momentum *vector* equation was temporarily decoupled into three *scalar* component equations that were independently solved, where outer fixed-point/Gauss–Seidel/Picard iterations provided the required coupling. This form of solution methodology is termed a *segregated* approach, as the governing conservation of linear momentum equation is segregated into three scalar equations during solution. This style of implicit segregated solution algorithm was inspired by the methods adopted in similar CFD procedures, where the restrictive computer memory sizes available at the time necessitated memory efficient procedures.

The original 2-D method was later generalised to 3-D convex polyhedral cells by Demirdžić and Muzaferija [41] (Fig. 4b). This form of the cell-centred approach has since been extended to deal with a wide variety of solid and multi-physics phenomena, including:

- Elastoplasticity [3, 25, 36, 42–54] and viscoelasticity [55–60];
- Thermo-elasticity [2, 41, 61–65] and hygro-thermo-elasticity [66–77];
- Poro-elasticity [78–85];
- Anisotropy [66, 67, 69, 72–75, 86–89] and heterogeneous material properties [79, 84, 90–92].
- Incompressibility and quasi-incompressibility [93–100];
- Contact mechanics [25, 101–105];
- Finite strains and rotations [25, 36, 88, 95, 106–117];
- Fracture mechanics [60, 79, 80, 82, 84, 91, 118–132];
- Casting, melting, solidification and residual stresses [44, 45, 133–137];
- Fluid–solid interaction [29, 93, 94, 96, 98, 99, 113, 138–166];
- Beams, plates and shells [59, 89, 145, 146, 150, 167–187];
- Solid–electrostatic interaction [188, 189] and wave propagation [42, 190–192];

Of particular note are the developments of Weller et al. [193] and Jasak and Weller [194], where the same implicit cell-centred form has been demonstrated to be well-suited to running on distributed-memory supercomputers. The *domain decomposition method* was used where the solution domain is decomposed into a number of sub-domains, each solved on a separate central processing unit (CPU) core; necessary coupling between the sub-domains is performed using a message-passing protocol, initially *parallel virtual machine*, but *message passing interface* in later publications. The Weller et al. [193] and Jasak and Weller [194] implementations form a component of the popular open-source C++ library OpenFOAM, formerly commercial software FOAM. Many of the subsequent developments in the implicit cell-centred field have been based on the OpenFOAM platform, for example, [25, 30, 77, 78, 83, 88, 90, 104, 112, 113, 131, 195]. It should, however, be noted that the explicit Godunov-type approaches have also been implemented in OpenFOAM [28, 196].

The essence of the implicit cell-centre finite volume method has been the use of a displacement approach combined with a segregated algorithm; however, alternative solution methodologies have also been developed, including geometric multi-grid procedures [86, 120, 142, 143, 197], block-coupled algorithms [30, 188, 189, 198, 199], hybrid/mixed pressure–displacement formulations [46, 95, 97, 100, 138, 139, 200, 201], Aitken acceleration [78, 160,

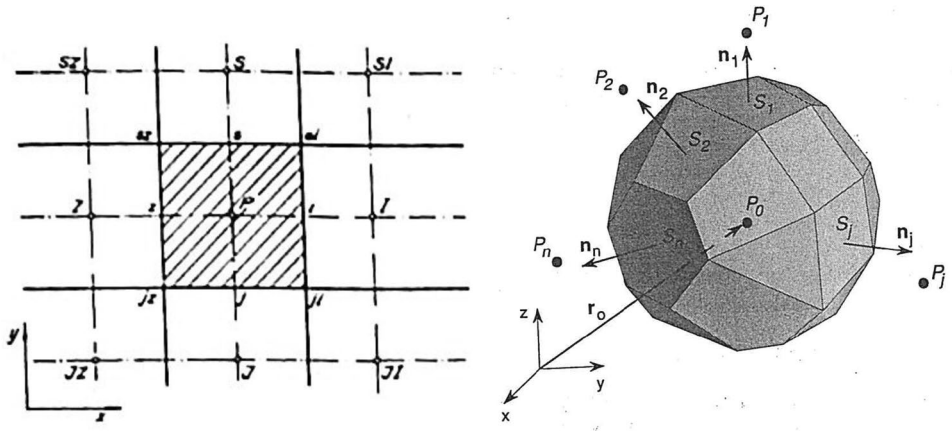


**(a)** 2-D structured quadrilateral mesh from Demirdžić et al. [2]

**(b)** 3-D general convex polyhedral control volume from Demirdžić and Muzaferija [41]

**Fig. 4** Original 2-D structured quadrilateral mesh of Demirdžić et al. [2] (left) and the subsequent generalisation to 3-D unstructured convex polyhedra [41] (right). (Color figure online)

199], and curvilinear formulations [43, 202]. In addition, fourth-order accuracy variants have been proposed [203] as well as novel gradient and tractions calculation methods [25, 157, 160, 199, 204–208]. Apart from the standard *continuum* approaches, a number of authors have proposed implicit cell-centred finite volume methods for beams, plates and shells [59, 89, 145, 146, 150, 167, 173, 174, 181, 185, 186, 209, 210].

#### 2.1.2 Explicit Cell-Centred Methods

Explicit Godunov-type finite volume methods were first proposed for the solution of hyperbolic problems characterised by waves and shocks [32, 211, 212], and have been popularised for the solution of Euler compressible gas flow equations. The typical approach, which casts the conservation laws as a system of first-order hyperbolic equations, is characterised by the solution of a Riemann problem (propagation of a solution discontinuity) at the control volume faces to determine forces. The resulting discretisation evaluates the force at a control volume face as a weighted average of the force evaluated at each side of the face. Godunov-type methods were first applied to structural problems by Trangenstein and Colella, when they modelled the 1-D propagation of waves in elasto-plastic solids [40, 213, 214]; in their approach, the primitive conservation variables were the linear momentum vector and the deformation gradient (or displacement gradient) tensor. Subsequently, the method has been extended to unstructured 3-D grids in a variety of forms, differing in terms of discretisations and primitive variables [20, 21, 26–28, 32, 196, 215–236], for example, see Fig. 5. Although cell-centred formulations are the most common form of Godunov-type method, vertex-centred [31, 237] and, recently, face-centred approaches [20, 21] have also been explored.

To-date, Godunov-type approaches have been used to model a wide range of physical mechanisms:

- Linear elasticity [21, 40, 213, 232];
- Material nonlinearity [26, 28, 196, 216, 218, 222–224, 226–236];
- Fracture and cavitation [216, 226];
- Finite strains [28, 196, 222–224, 226–229, 231, 233–236];
- Material heterogeneity [217, 219];
- Wave propagation and impacts [32, 40, 213–219, 222–229, 231–236].

A distinctive characteristic of Godunov-type methods is the adoption of fully explicit solution algorithms, where the time increment size is restricted by the standard Courant–Friedrichs–Lewy constraint [34].

From an implementation and philosophy perspective, the implicit approaches stemming from Demirdžić et al. [2] differ greatly from the explicit approaches deriving from Trangenstein and Colella [40]. The most obvious difference is the need of the implicit approach to form and solve a linear system of equations, and the time increment size restriction for explicit methods. In addition to this, the implicit methods have typically assumed a smooth variation of the primitive variable within each cell (or across cell faces); in contrast, the explicit approaches have aimed to directly approximate the propagation of solution discontinuities. Many of these technical distinctions are discussed further in Sect. 3. It should be noted that *explicit* cell-centred approaches that do *not* adopt a Godunov approach are also possible, for example, as developed by Selim et al. [238, 239].

### 2.2 Vertex-Centred Approaches

#### 2.2.1 Implicit Vertex-Centred Methods

Fryer et al. [5] was the first to propose a vertex-centred finite volume method for solid mechanics. The approach, initially termed a *control volume-unstructured mesh*

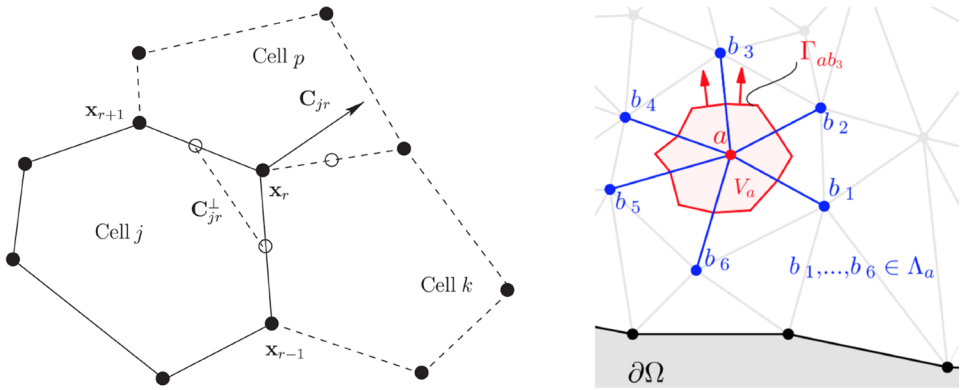


**(a)** 2-D unstructured cell-centred polygonal mesh from Kluth and Després [26]

**(b)** 2-D/3-D unstructured vertex-centred polygonal/polyhedral mesh from Aguirre et al. [237]

**Fig. 5** Forms of mesh employed by Kluth and Després [26] and Aguirre et al. [237]. (Color figure online)

procedure, could analyse complex 2-D geometry using both quadrilateral and triangular cells (Fig. 6a). The method of Fryer et al. [5] followed closely the approach of Baliga and Patankar [240] from a decade earlier, who developed a so-called *control-volume-based finite element method* for convection–diffusion equations on unstructured triangular grids.

In addition to the designation *vertex-based finite volume method*, the formulation is referred to by a number of other names, including *vertex-centred finite volume method*, *cell-vertex finite volume method*, *control volume procedure*, *control-volume finite element method*, *control-volume-based finite-element method*, and *element-based finite volume method*.

In contrast to cell-centred and staggered-grid approaches, vertex-centred approaches store the primary unknowns at the *primary* mesh vertices and integrate the governing equation over secondary/*dual* mesh control volumes surrounding each *primary* mesh vertex.

The original 2-D approach of Fryer et al. [5] was subsequently extended to three dimensions by Bailey and Cross [24] (Fig. 6b) and has since been applied to a wide range of physical phenomena:

- Compressible and incompressible elasticity [24, 242–250];
- Elasto-plasticity, elasto-visco-plasticity, creep and material nonlinearity [179, 183, 241, 251–253];
- Finite strains and geometric nonlinearity [254–260];
- Beams, plates and shells [168, 261, 262];
- Multi-physics and fluid–solid interaction [249, 263–280];
- Casting [4, 7, 9, 10, 264–267, 281–284], extrusion and forging [285–287];
- Welding [288, 289];
- Contact mechanics [290];
- Functionally graded solids [291, 292] and wood drying [293, 294];
- Micropolar/Cosserat elasticity (shear stress may not be symmetric) [295, 296];
- Vibrations, acoustics and wave propagation [178, 297–299].

Alternative solution methodologies have been examined, including mixed displacement-rotation approaches [300–302], and addressing parallelisation on distributed memory supercomputers [303, 304]. Also of note are the developments of Maitre et al. [305] and Souhail [306], who proposed a higher order extension of the vertex-based approach.

It is important to note the distinction between *overlapping* and *non-overlapping* vertex-centred methods: the more common approach involves non-overlapping control volumes, where the control volumes about each primary mesh vertex do not overlap with the control volumes of neighbouring primary mesh vertices. In the less popular overlapping control volumes approaches, for example, as discussed by Oñate et al. [12], primary mesh vertices partly share control volumes with primary mesh neighbouring vertices, resulting in the governing equations being integrated more than once over regions of the domain; this overlapping local integration domain approach is more similar to the finite element method. Additionally, Tsui et al. [249] proposed a variation on the common approach to construct the control volumes: the primary mesh cell centres are joined together to make the control volumes, rather than joining the cell-centres to the face-centres as per the classic vertex-based method.

### 2.2.2 Explicit Vertex-Centred Methods

Similar to cell-centred methods, both implicit and explicit solution algorithms have been developed, although explicit vertex-centred methods have seen less development. Within the category of explicit vertex-centred methods, there exists a variety of sub-classes, including: so-called

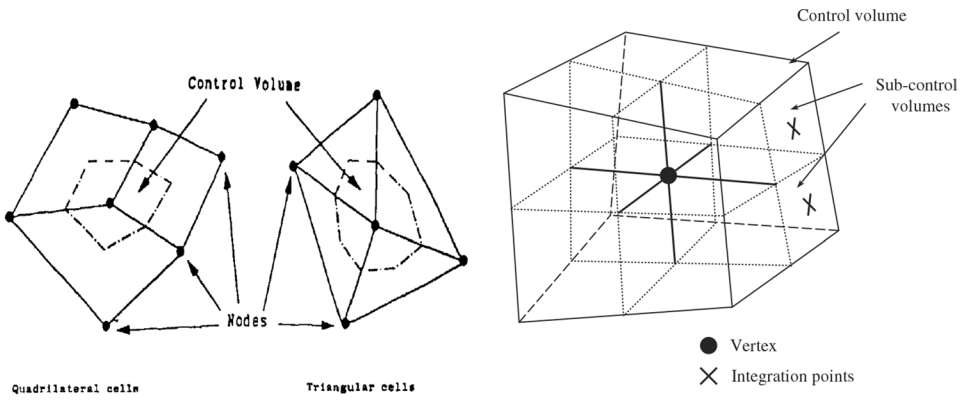


**(a)** 2-D unstructured quadrilateral and trianglular mesh from Fryer et al. [5]

**(b)** 3-D unstructured mesh from Taylor et al. [241]

**Fig. 6** Vertex-based finite volume formulation of Fryer et al. [5] (left) showing the construction of control volumes around a mesh vertex for quadrilateral and triangular 2-D cells, and of Taylor et al. [241] showing the extension to 3-D cells. (Color figure online)

dual-time-stepping explicit methods, where the solution is calculated in an explicit manner and a linear system is not directly formed [248, 249, 277, 279, 297]; Godunov-type approaches [31, 237] similar to those seen in cell-centred approaches, as noted in Sect. 2.1; and the so-called *grid method* [307–312]. Regarding the grid-method, the originators of the method, Zhang and Liu [307], argue for the distinction between the grid method and the vertex-based finite volume method, however, the authors of the current article believe this distinction is unwarranted: like other finite volume methods, the grid method starts from the governing momentum equation in strong integral form and approximates the forces over the boundaries of the control volumes; although there are minor differences in the techniques used to approximate the surface forces, for example, comparing Dormy and Tarantola [313] and Zhang and Liu [308], the *grid method* still remains a form of vertex-centred finite volume method.

### 2.3 Staggered-Grid Approaches

In staggered-grid approaches, as originally proposed for CFD by Harlow and Welch [314], the components of the primary solution variable, for example, the $x$ and $y$ components of displacement, are stored at different locations. In addition, different sets of control volumes are used when integrating the discretised governing equation in each Cartesian direction. For example, the $x$-momentum component equation employs a different grid to the $y$-momentum component equation. The primary motivation for such staggered-grid approaches is the avoidance of solution instabilities, namely the "checker-boarding" phenomenon, where high frequency variations appear in the solution variables that are unobservable to the discretisation. Consequently, staggered-grid approaches do not need to explicitly included a stabilisation term, as is common in cell-centred methods. The extension of staggered-grid approaches to general unstructured 3-D meshes is, however, not trivial; and consequently, this major limitation has resulted in declining popularity for such approaches in solid mechanics.

The first application of a staggered-grid formulation to solid mechanics was by Beale and Elias [13, 14], who showed how the finite volume CFD code PHOENICS could be applied to stress analysis problems. In their method, Beale and Elias used the analogy between the stream functions in creeping-fluid-flow and the Airy stress functions in solid mechanics, where the stress components were the primary unknowns. This method was later generalised by Spalding et al. [15, 17, 315–321], where a displacement, rather than a force analogy, was adopted, having the major advantage of being more general in three dimensions. Spalding noted that a CFD solution procedure designed for computing velocities is suitable for computing displacements if the convection terms are set to zero and the volume/dilatation stress term is introduced by inclusion of a pressure- and temperature-dependent source term. As a consequence, the resulting solution method used an *implicit* SIMPLE algorithm [322, 323], still popular in modern CFD codes. The employed primitive variables were displacement and pressure, as opposed to velocity and pressure in standard fluid flow analyses.

The use of mixed displacement-pressure approaches, however, is not a requirement of staggered-grid approaches. Hattel, Hansen and collaborators [16, 18, 19, 324–336] demonstrated a staggered-grid approach where the sole primary variable was displacement. Hattel and Hansen [16] initially proposed their staggered-grid approach for the analysis of thermally induced stresses in casting problems, and subsequently extended it for a variety of thermo-elasto-plasticity problems. They termed their approach "a control volume based finite difference method", further indicating the close-relationship with finite difference methods. The authors noted that their method resulted in an elegant formulation for non-constant material properties, a benefit of the staggered grid approach.

In addition to the displacement and displacement-pressure approaches, a number of alternative staggered grid formulations have also been proposed: Spalding [319] proposed a staggered formulation where *rotation* and displacement were the primitive variables; Spalding surmised that the rotation-based method may provide a more efficient solution algorithm in certain situations. The approach is described in documentation from an early version of the PHOENICS software; however, issues with boundary conditions are noted and no further articles appear on the formulation. A similar idea was subsequently proposed by Wenke et al. [300–302] in the framework of vertex-based finite volume methods, where both displacements and rotations are considered the primitive variables. More recently, Wang and Melnik [337] put forward a staggered finite volume approach for analysis of shape memory alloys, defined on 2-D structured rectangular grids. In contrast to the majority of staggered grid approaches, which employ implicit solution algorithms, Rajagopal et al. [338] proposed a one-step explicit staggered grid finite volume approach to investigate the response of a layered viscoelastic plate.

### 2.4 Other Approaches

Across the spectrum of finite volume methods for solid mechanics, not all procedures align with the previously discussed divisions.

#### 2.4.1 Approaches for Periodic Heterogenous Microstructures

Although arguably not a fundamental class of finite volume method, there has been significant development related to specialised versions of the finite volume method for periodic microstructures. Depending on the formulation, the related methods can be referred to by a number of names, including: the *higher-order theory for functionally graded material* (HOTFGM) [339], the *high-fidelity generalised method of cells* (HFGMC) [340–343], the *finite volume direct averaging micromechanics* (FVDAM) theory [344, 345], or some variant thereof. Although there is some disagreement over the naming convention [342, 343, 345], these methods have a common origin in the *method of cells* and the *generalised method of cells* developed by Aboudi and Paley [346–348]. Recent discussions around the development of these methods can be found in Haj-Ali and Aboudi [343], Cavalcante et al. [38], Gong et al. [291], and Cavalcante and Pindera [349], along with reviews of the high fidelity generalised method of cells approaches by Aboudi [350] and of microstructural analysis approaches by Pindera et al. [351] and Charalambakis and Murat [352]. Reviews of the application of such methods can be found in Aboudi et al. [353] and Aboudi [354]. A brief overview of the discretisation used in HOTFGM/HFGMC/FVDAM approaches is given in "Appendix 2".

#### 2.4.2 Meshless Finite Volume Approaches

Meshless methods have been proposed to overcome the drawbacks of mesh-based finite element and finite volume methods, particularly related to large deformations and cracking. Atluri and Shen [355] were the first to propose a meshless finite volume formulation, based on the earlier generalised *Meshless Local Petrov–Galerkin (MLPG) method* by Atluri and Zhu [356]. The approach has subsequently been extended and applied to a variety of problems in elasto-statics, elasto-dynamics and fracture mechanics [357–374]. Based on the initial development of Atluri and Shen [355], Moosavi and Khelil [366] proposed a novel meshless form of the finite volume method for elasto-static analysis, that combined the finite volume concept with the meshless local Petrov–Galerkin approach with moving least squares interpolation. Moosavi and co-workers have since extended the method to elasto-dynamics, beams, plates, shells and crack problems [367–369, 373, 374], where the method has been named the *orthogonal meshless finite volume method*. Whereas the Atluri and Shen [355] approach uses overlapping control volumes, the meshless finite volume method developed by Ebrahimnejad et al. [22, 375, 376] employs non-overlapping control volumes. The method has been applied to 2-D elasticity with adaptive mesh refinement, and was later extended to problems with material discontinuities [23, 377], to free vibration analysis of laminated composite plates [378, 379], and to fractures in orthotropic media [380].

#### 2.4.3 Eulerian Approaches

There are many solid mechanics problems which can be equivalently considered from the fluid mechanics perspective, for example, in the analysis of extrusion and drawing. Eulerian "fluid" approaches are often used to solve such problems, for example, [46, 48, 50–52, 54, 286, 287, 381–393]. These methods are more closely related to CFD procedures and are not discussed further here.

#### 2.4.4 Miscellaneous

Teng et al. [394] and Chen et al. [395] developed a finite volume method to simulate the draping of woven fabrics, where the governing nonlinear equations were solved using a single-step full Newton–Raphson method. Martin and Pascal [396, 397] proposed a novel *discrete duality finite volume* method for solving linear elasticity problems on unstructured meshes; the main characteristic of the discretisation is the integration of the governing equations over two meshes: the given primal mesh and also over a dual mesh built from the primal one. Pietro et al. [398] proposed a novel discretisation scheme for linear elasticity with only one degree of freedom per control-volume face, corresponding to the normal component of the displacement.

## 3 Comparing Variants of the Finite Volume Method for Computational Solid Mechanics

The finite volume method, like other related numerical approaches, consists of the following main components:

(a) Discretisation of space and time;
(b) Discretisation of the mathematical model equations;
(c) Solution algorithm.

To facilitate comparison between the major variants, three popular formulations will be considered here:

- Implicit cell-centred approach originating from the work of Demirdžić et al. [2];
- Implicit vertex-centred approach of Fryer et al. [5] and Bailey and Cross [24];

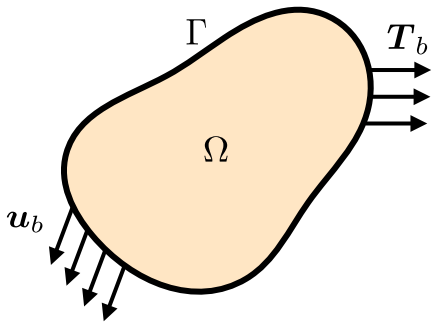


**Fig. 7** Generic solid body, with volume Ω and surface Γ, subjected to boundary displacements, $\boldsymbol{u}_b$, and boundary tractions, $\boldsymbol{T}_b$. (Color figure online)

- Explicit cell-centred approach emanating from Trangenstein and Colella [40].

Analysis and insight into the similarities and differences between these variants is provided.

## 3.1 Mathematical Model for Dynamic Linear Elasticity

To allow a clear comparison of the methods, the dynamic behaviour of a body with volume Ω and surface Γ is analysed (Fig. 7), where part of its boundary is subjected to a specified displacement, $\boldsymbol{u}_b$, and the remainder is subjected to a specified traction, $\boldsymbol{T}_b$.

Assuming the relationship between stress and strain to be described by Hooke's law, the governing conservation of linear momentum equation, a generalisation of Newton's second law, can be given in strong integral form as:

$$\underbrace{\int_\Omega \rho \frac{\partial^2 \boldsymbol{u}}{\partial t^2}\,\mathrm{d}\Omega}_{\text{Inertia forces}} = \underbrace{\oint_\Gamma \boldsymbol{n}\cdot\left[\mu\boldsymbol{\nabla u} + \mu(\boldsymbol{\nabla u})^T + \lambda\,\mathrm{tr}(\boldsymbol{\nabla u})\mathbf{I}\right]\mathrm{d}\Gamma}_{\text{Surface forces}} + \underbrace{\int_\Omega \rho \boldsymbol{f}_b\,\mathrm{d}\Omega}_{\text{Body forces}} \tag{1}$$

Small deformations are assumed i.e. no distinction is made between the initial and deformed configurations; $\rho$ is the initial density, $\boldsymbol{u}$ is the unknown total displacement vector, $\boldsymbol{n}$ is the outward-pointing surface unit normal vector, $\boldsymbol{\nabla}$ is the del operator, $\lambda$ is the first Lamé parameter, $\mu$ is the second Lamé parameter, synonymous with the shear modulus, $\mathbf{I}$ is the second-order identity tensor, and $\boldsymbol{f}_b$ is a body force acceleration. To avoid unnecessary complexity, the material properties ($\rho$, $\mu$ and $\lambda$) are assumed to be uniform and isotropic; however, this assumption is not required. It should be noted that the finite volume method directly discretises this strong integral form of the governing equation, without requiring weighting functions, the weak form of the equation or the use of the Gauss divergence theorem.

## 3.2 Implicit Cell-Centred Approach

In this sub-section, the implicit cell-centred approach stemming from Demirdžić et al. [2] is described.

### 3.2.1 Discretisation of Time

For all described variants of the finite volume method, discretisation of the solution domain comprises time discretisation and space discretisation. The total specified simulation time is divided into a finite number of time increments, $\Delta t$, and the discretised governing equations are solved in a time-marching manner.

### 3.2.2 Discretisation of Space

For the implicit cell-centred approach, the spatial domain is divided into a finite number of contiguous convex polyhedral cells bounded by polygonal faces that do not overlap and fill the space completely. A typical control volume is shown in Fig. 8, with the computational node $P$ located at the cell centre/centroid, and the cell volume is $\Omega_P$; $N_f$ is the centroid of a neighbouring control volume, which shares face $f$ with the current control volume; $\boldsymbol{\Gamma}_f$ is the area vector of face $f$, vector $\boldsymbol{d}_f$ joins $P$ to $N_f$, and $\boldsymbol{x}$ is a positional vector. No distinction is made between different cell volume shapes, as all general convex polyhedra are discretised in the same fashion.

### 3.2.3 Discretisation of the Mathematical Model Equations

The governing conservation law (Eq. 1) is applied to each polyhedral cell in the mesh. The discretisation of each of the

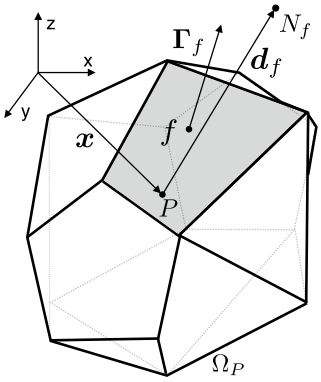


**Fig. 8** General convex polyhedral control volume. Adapted from [25, 29, 155]. (Color figure online)

three terms (inertia, surface forces, body forces) within the equation is now discussed in turn.

Considering first the spatial discretisation of the inertia term in Eq. (1). The term can be approximated by making an assumption about the variation of the displacement vector $\boldsymbol{u}$ over the cell; typically in the implicit cell-centred approach a linear variation is assumed. This linear variation can be expressed in terms of a truncated Taylor series expansion about the cell centre:

$$\boldsymbol{u}(\boldsymbol{x}) = \boldsymbol{u}_P + (\boldsymbol{x} - \boldsymbol{x}_P) \cdot (\boldsymbol{\nabla u})_P \tag{2}$$

This expression says that the displacement $\boldsymbol{u}(\boldsymbol{x})$ at any point in the cell can be calculated using the cell-centre displacement $\boldsymbol{u}_P$ and the constant gradient of displacement within the cell $(\boldsymbol{\nabla u})_P$. This approximation is second-order order in space i.e. as the mesh spacing is reduced, the error in this approximation reduces at second-order rate. In principle, any other distribution could be used; for example, Demirdžić [203] extended the approach to use a fourth-order cubic distribution.

Using the approximation in Eq. (2), the inertia term can be calculated using the midpoint rule as a function of the cell-centred values:

$$\int_\Omega \rho \frac{\partial^2 \boldsymbol{u}}{\partial t^2} \, \mathrm{d}\Omega \approx \rho \left( \frac{\partial^2 \boldsymbol{u}}{\partial t^2} \right)_P \Omega_P \tag{3}$$

where the subscript $P$ on the density has been dropped as a uniform density field is assumed i.e. $\rho_P = \rho$.

The acceleration $\partial^2 \boldsymbol{u}/\partial t^2$ may be discretised in time using any appropriate finite difference scheme; in the original cell-centred approach of Demirdžić et al. [2], the bounded first-order backward Euler method was used:

$$\left( \frac{\partial^2 \boldsymbol{u}}{\partial t^2} \right)_P \approx \frac{\boldsymbol{u}_P - 2\boldsymbol{u}_P^{[m-1]} + \boldsymbol{u}_P^{[m-2]}}{\Delta t^2} \tag{4}$$

where $m$ is the time-step counter; the superscript on the unknown current time value of displacement has been dropped for brevity. Here it is assumed that the time-step size $\Delta t$ is constant; however, the method can be generalised to variable time-step sizes. There are numerous other temporal discretisations that may be used; for example, the unbounded second-order backward Euler scheme [194], the second-order trapezoidal rule [199], or the second-order Newmark schemes that are popular with the finite element method.

The final discretised inertia term is:

$$\int_\Omega \rho \frac{\partial^2 \boldsymbol{u}}{\partial t^2} \, \mathrm{d}\Omega \approx \rho \, \frac{\boldsymbol{u}_P - 2\boldsymbol{u}_P^{[m-1]} + \boldsymbol{u}_P^{[m-2]}}{\Delta t^2} \, \Omega_P \tag{5}$$

In a similar fashion, the body force term (second term on the right-hand side of Eq. (1)) is approximated by assuming $\boldsymbol{f}_b$ to vary over the cell according to Eq. (2). Consequently, the term can be approximated in terms of the cell-centre values using the midpoint rule as:

$$\int_\Omega \rho \boldsymbol{f}_b \, \mathrm{d}\Omega \approx \rho \boldsymbol{f}_{b_P} \Omega_P \tag{6}$$

Towards the discretisation of the surface force term, the closed surface integral in Eq. (1) is converted into a sum of surface integrals over each polygonal face:

$$\begin{aligned} &\oint_\Gamma \boldsymbol{n} \cdot \left[ \mu \boldsymbol{\nabla u} + \mu (\boldsymbol{\nabla u})^T + \lambda \, \mathrm{tr}(\boldsymbol{\nabla u}) \mathbf{I} \right] \mathrm{d}\Gamma \\ &= \sum_{f=1}^{nFaces} \int_{\Gamma_f} \boldsymbol{n} \cdot \left[ \mu \boldsymbol{\nabla u} + \mu (\boldsymbol{\nabla u})^T + \lambda \, \mathrm{tr}(\boldsymbol{\nabla u}) \mathbf{I} \right] \mathrm{d}\Gamma \end{aligned} \tag{7}$$

where *nFaces* is the number of faces in the cell. This form represents a force balance for the cell. To approximate the stress term $[\mu \boldsymbol{\nabla u} + \mu (\boldsymbol{\nabla u})^T + \lambda \, \mathrm{tr}(\boldsymbol{\nabla u}) \mathbf{I}]$ at each cell face, the assumed variation of displacement in Eq. (2) is once again used; accordingly, the stress can be calculated in terms of the displacement gradient values at the face centre (centroid):

$$\begin{aligned} &\sum_{f=1}^{nFaces} \int_{\Gamma_f} \boldsymbol{n} \cdot \left[ \mu \boldsymbol{\nabla u} + \mu (\boldsymbol{\nabla u})^T + \lambda \, \mathrm{tr}(\boldsymbol{\nabla u}) \mathbf{I} \right] \mathrm{d}\Gamma \\ &\approx \sum_{f=1}^{nFaces} \boldsymbol{n}_f \cdot \left[ \mu (\boldsymbol{\nabla u})_f + \mu (\boldsymbol{\nabla u})_f^T + \lambda \, \mathrm{tr}\left[ (\boldsymbol{\nabla u})_f \right] \mathbf{I} \right] |\boldsymbol{\Gamma}_f| \end{aligned} \tag{8}$$

where subscript $f$ indicates a quantity at a face centre, for example, $(\boldsymbol{\nabla u})_f$ is the gradient of displacement tensor at the centre of face $f$. The approach used to approximate this face displacement gradient is one of the principal differences between variants of the finite volume method. In addition, polygonal faces may not be flat and approaches have been examined to accommodate this; for example, Tuković et al. [208] proposed decomposing all faces into triangles before evaluating the forces.

As a consequence of the assumed variation (Eq. 2), the gradient of displacement $\boldsymbol{\nabla u}$ is constant within each cell and so the displacement gradient at a face, between two cells, is discontinuous; to resolve this, the standard cell-centred approach expresses the displacement gradient at a face $(\boldsymbol{\nabla u})_f$ as a weighted mean of the displacement gradient at the two adjacent cell-centres:

$$(\boldsymbol{\nabla u})_f \approx \gamma_f (\boldsymbol{\nabla u})_P + (1 - \gamma_f)(\boldsymbol{\nabla u})_{N_f} \tag{9}$$

where subscript $P$ indicates a quantity at the current cell-centre, subscript $N_f$ indicates a quantity at the neighbour cell-centre adjacent to face $f$, and $0 < \gamma_f < 1$ is the

interpolation weight. Typically, the interpolation weight is calculated using an inverse distance method:

$$\gamma_f = \frac{|\boldsymbol{x}_{N_f} - \boldsymbol{x}_f|}{|(\boldsymbol{x}_f - \boldsymbol{x}_P) + (\boldsymbol{x}_{N_f} - \boldsymbol{x}_f)|} \tag{10}$$

In addition to the standard cell-centred method for approximating the face centre displacement gradient given in Eq. (9), a number of alternative methods have also been examined, for example, temporary elements with isoparametric formulations [204] or using a compact stencil for the normal gradient as in the original discretisation of Demirdžić et al. [2]; in this compact stencil form, the normal component is calculated using central differencing:

$$\begin{aligned}(\boldsymbol{\nabla u})_f \approx & \underbrace{\boldsymbol{n}_f \left[ \frac{|\boldsymbol{\Delta}_f|}{|\boldsymbol{\Gamma}_f|} \frac{\boldsymbol{u}_{N_f} - \boldsymbol{u}_P}{|\boldsymbol{d}_f|} + \frac{\boldsymbol{\Gamma}_f - \boldsymbol{\Delta}_f}{|\boldsymbol{\Gamma}_f|} \cdot (\boldsymbol{\nabla u})_f \right]}_{\text{normal component}} \\ & + \underbrace{(\mathbf{I} - \boldsymbol{n}_f \boldsymbol{n}_f) \cdot \left[ \gamma_f (\boldsymbol{\nabla u})_P + (1 - \gamma_f)(\boldsymbol{\nabla u})_{N_f} \right]}_{\text{tangential component}}\end{aligned} \tag{11}$$

where $\boldsymbol{n}_f = \boldsymbol{\Gamma}_f / |\boldsymbol{\Gamma}_f|$ are the face unit normals, and:

$$\boldsymbol{\Delta}_f = \frac{\boldsymbol{d}_f}{\boldsymbol{d}_f \cdot \boldsymbol{n}_f} |\boldsymbol{\Gamma}_f| \tag{12}$$

methods, such as the Gauss divergence method or point Gauss divergence method [208] have also been proposed. With respect to the Gauss divergence method of gradient calculation, this approach stems from the Lawrence Livermore Laboratory 'hydrocodes' of the 1960s developed by Wilkins [399, 400]. Zienkiewicz and Oñate [6, 12] claimed this Gauss divergence cell-gradient method to be "*an early attempt to use FV concepts in CSM*"; this link is, however, tenuous; the Gauss divergence cell-gradient calculation is not a core postulate of the finite volume method and is in fact not required. For descriptions of subsequent finite difference developments based on the original Wilkins [399] approach, the interested reader is referred to [401, 402].

Although the discretisation of the surface force in terms of displacement $\boldsymbol{u}$ is complete, the presented discretisation is unstable and known to suffer from so-called *checker-boarding* errors. Without an appropriate stabilisation term, oscillations in the displacement field, which are twice the period of the cell size, will go unnoticed. These unstable oscillations are analogous to the spurious singular modes that appear in reduced-integration finite element discretisations, also known as zero-energy modes or *hourglassing*. Typically the implicit cell-centred approach adds the so-called Rhie–Chow stabilisation term to the discretised divergence of stress (Eq. 8), as introduced to solid mechanics by Demirdžić and Muzaferija [29]:

$$\begin{aligned}\mathscr{D}_{\text{Rhie-Chow}} &= \sum_{f=1}^{nFaces} \left\{ K_f \left[ |\boldsymbol{\Delta}_f| \frac{\boldsymbol{u}_{N_f} - \boldsymbol{u}_P}{|\boldsymbol{d}_f|} + (\boldsymbol{\Gamma}_f - \boldsymbol{\Delta}_f) \cdot (\boldsymbol{\nabla u})_f \right] - \boldsymbol{\Gamma}_f \cdot \left[ K_f (\boldsymbol{\nabla u})_f \right] \right\} \\ &= \sum_{f=1}^{nFaces} K_f \left[ |\boldsymbol{\Delta}_f| \frac{\boldsymbol{u}_{N_f} - \boldsymbol{u}_P}{|\boldsymbol{d}_f|} - \boldsymbol{\Delta}_f \cdot (\boldsymbol{\nabla u})_f \right]\end{aligned} \tag{14}$$

At this point, it is worth noting the locally conservative nature of the discretisation: adjacent cells share integration points at the face centres, resulting in the force at cell faces being locally and hence globally conserved. This is a characteristic shared by all finite volume methods.

To complete the discretisation of the surface force in terms of displacement $\boldsymbol{u}$, the cell-centred displacement gradients need to be expressed in terms of the cell-centred displacements. For its accuracy on unstructured grids and ease of implementation, the least-squares method is the most popular:

$$(\boldsymbol{\nabla u})_P \approx \left[ \sum_{f=1}^{nFaces} w_f^2 \boldsymbol{d}_f \boldsymbol{d}_f \right]^{-1} \cdot \sum_{f=1}^{nFaces} \left[ w_f^2 \boldsymbol{d}_f \left( \boldsymbol{u}_{N_f} - \boldsymbol{u}_P \right) \right] \tag{13}$$

As shown previously in Fig. 8, vector $\boldsymbol{d}_f$ joins cell-centre $P$ to the neighbour cell-centre $N_f$. The scalar weighting function can be taken as unity ($w_f = 1$) [29] or as the inverse distance ($w_f = 1/|\boldsymbol{d}_f|$) [194]. Alternative gradient calculation

This third-order diffusion term corresponds to the difference between two ways of calculating the normal gradient of displacement at a face, resulting in an ability to 'sense' high-frequency oscillations in $\boldsymbol{u}$. The approach was first proposed by Rhie and Chow [403] in the context of cell-centred finite volume methods for incompressible fluid flow, and is commonly used in cell-centred finite volume fluid formulations. The $K_f$ coefficient controls the magnitude of the smoothing effect and is typically taken as $K_f = \mu$ [29], $K_f = \mu + \lambda$ [194] or $K_f = 2\mu + \lambda$ [30]. The third-order diffusion term also serves a purpose towards choice of implicit components within the segregated solution algorithm: this is discussed further below. Alternative forms of diffusion/smoothing terms have been also been proposed, for example, the fourth-order Jameson–Schmidt–Turkel [404] term employed in Godunov-type approaches [31, 237], which takes the form of a Laplacian of a Laplacian:

$$\mathscr{D}_{\mathrm{JST}} \;=\; \boldsymbol{\nabla}^2\left[K_{\mathrm{JST}}\left(\boldsymbol{\nabla}^2\boldsymbol{u}\right)\right] \tag{15}$$

The scalar coefficient $K_{\mathrm{JST}}$ gives the correct dimension to the dissipation as well as controlling its magnitude.

The final discretised form of the governing momentum equation, employing the Rhie–Chow form of stabilisation and $K_f = 2\mu + \lambda$, is expressed as:

$$\begin{aligned}\rho\,\frac{\boldsymbol{u}_P - 2\boldsymbol{u}_P^{[m-1]} + \boldsymbol{u}_P^{[m-2]}}{\Delta t^2}\,\Omega_P \\ = \sum_{f=1}^{nFaces} \boldsymbol{n}_f \cdot \left[\mu(\boldsymbol{\nabla u})_f + \mu(\boldsymbol{\nabla u})_f^T + \lambda\,\mathrm{tr}\left[(\boldsymbol{\nabla u})_f\right]\mathbf{I}\right]|\boldsymbol{\Gamma}_f| \\ + \sum_{f=1}^{nFaces}(2\mu+\lambda)\left[|\boldsymbol{\Delta}_f|\frac{\boldsymbol{u}_{N_f} - \boldsymbol{u}_P}{|\boldsymbol{d}_f|} - \boldsymbol{\Delta}_f \cdot (\boldsymbol{\nabla u})_f\right] \\ + \rho \boldsymbol{f}_{b_P}\Omega_P\end{aligned} \tag{16}$$

where the face displacement gradients $(\boldsymbol{\nabla u})_f$ are calculated using Eqs. (9), (10) and (13). The primitive unknown variables are the cell-centre displacement vectors $\boldsymbol{u}_P$ at time $t$ (time index $[m]$).

Boundary conditions are incorporated through appropriate modification of the surface force term discretisation at faces coinciding with the boundary of the solution domain. In the case of a displacement condition $\boldsymbol{u}_b$ (Dirichlet boundary condition), the face displacement gradients are calculated at the face, while in the case of a traction condition $\boldsymbol{T}_b$ (Neumann boundary condition), the specified traction directly replaces the surface stress expression. Initial conditions, in the form of the displacement field at $t = 0$, $t = -\Delta t$, and $t = -2\Delta t$, must also be specified.

### 3.2.4 Solution Algorithm

In order to solve the discretised governing equation (Eq. 16) for the unknown displacement vector, the typical cell-centre approach uses a *segregated* solution procedure, where the central-differencing component in Eq. (16), $(2\mu+\lambda)|\boldsymbol{\Delta}_f|(\boldsymbol{u}_{N_f} - \boldsymbol{u}_P)/|\boldsymbol{d}_f|$, and $\rho\left(\boldsymbol{u}_P/\Delta t^2\right)\Omega_P$ within the inertia term are treated implicitly; all other terms are calculated explicitly using the latest available displacement field. The purpose of the segregated approach is to temporarily decouple/segregate the three scalar components of the vector momentum equation so that they can be solved sequentially; outer fixed-point/Gauss–Seidel/Picard iterations provide the necessary coupling, where the displacement gradient terms are explicitly updated each outer iteration using the latest available displacement field. Employing this implicit–explicit split, the discretised equation for each cell can be written in the form of a linear algebraic equation:

$$a_P\,\boldsymbol{u}_P \;-\; \sum_{f=1}^{nFaces} a_{N_f}\boldsymbol{u}_{N_f} \;=\; \boldsymbol{b}_P \tag{17}$$

where

$$a_P = \frac{\rho\Omega_P}{\Delta t^2} + \sum_{f=1}^{nFaces} a_{N_f} \tag{18}$$

$$a_{N_f} = (2\mu+\lambda)\frac{|\boldsymbol{\Delta}_f|}{|\boldsymbol{d}_f|} \tag{19}$$

$$\begin{aligned}\boldsymbol{b}_P = \;& \rho\,\frac{2\boldsymbol{u}_P^{[m-1]} - \boldsymbol{u}_P^{[m-2]}}{\Delta t^2}\,\Omega_P \\ & + \sum_{f=1}^{nFaces} \boldsymbol{n}_f \cdot \left\{\mu(\boldsymbol{\nabla u})_f + \mu(\boldsymbol{\nabla u})_f^T + \lambda\,\mathrm{tr}\left[(\boldsymbol{\nabla u})_f\right]\mathbf{I}\right\}|\boldsymbol{\Gamma}_f| \\ & - \sum_{f=1}^{nFaces}(2\mu+\lambda)\boldsymbol{\Delta}_f \cdot (\boldsymbol{\nabla u})_f \;+\; \rho\boldsymbol{f}_{b_P}\Omega_P\end{aligned} \tag{20}$$

In contrast, typical implicit vertex-centred and implicit finite element solution algorithms treat the entire divergence of stress term implicitly within the linear system matrix, or a linearisation of it when nonlinearities are present. This so-called *block-coupled* approach has also been proposed for the cell-centred approach [25, 59]: in this case, $a_P$ and $a_{N_f}$ in Eq. (17) are second-order tensors.

The algebraic equations (Eq. 17) can be assembled for all $M$ cells in the domain into the form of three decoupled linear systems:

$$[\boldsymbol{K}][\boldsymbol{U}] = [\boldsymbol{F}] \tag{21}$$

where $[\boldsymbol{K}]$ is a $M \times M$ sparse matrix with diagonal coefficients $a_P$ and off-diagonal coefficients $a_{N_f}$, $[\boldsymbol{U}]$ is a vector of the unknown cell-centre displacement vectors, and $[\boldsymbol{F}]$ is the source vector containing contributions from $\boldsymbol{b}_P$. In finite element parlance, $[\boldsymbol{K}]$ is the global stiffness matrix and $[\boldsymbol{F}]$ is the global force vector. The segregated cell-centred discretisation ensures that matrix $[\boldsymbol{K}]$ has the following properties [29]:

- It is sparse with the number of non-zero elements in each row equal to the number of nearest neighbours cells (those sharing a face with the cell) plus one;
- It is symmetric;
- It is positive definite;
- It is diagonally dominant ($|a_P| \geq \sum_{f=1}^{nFaces} |a_{N_f}|$), which makes the linear system efficiently solved by a number of iterative methods, which retain the sparsity of matrix $[\boldsymbol{K}]$: this results in significantly lower memory require-

ments than equivalent direct linear solvers, for example, see [25]. The most common iterative method used is the conjugate gradient method with incomplete Cholesky preconditioning [405].

It is worth noting that the segregated solution algorithm has been shown to suffer from slow convergence for slender geometry undergoing bending [25]; in that case, a block-coupled algorithm is significantly faster [25] and $[\boldsymbol{K}]$ is a $M \times M$ sparse matrix, where each coefficient is a second-order tensor.

For the segregated approach, the linear system (Eq. 21) need not be solved to a tight tolerance as coefficients and source terms are approximated from the previous outer iteration; instead, a reduction in the residuals of one order of magnitude is typically sufficient. Outer iterations are performed until the predefined solution tolerance has been achieved. Under-relaxation of the displacement field and/or the linear system may improve convergence, depending on the boundary conditions and mesh. Acceleration of the approach can be achieved through geometric multi-grid procedures [86, 120, 197], block-coupled algorithms [30, 188, 189, 199], Aitken acceleration [78, 160, 199], and/or parallelisation on distributed memory clusters [88, 194]. A favourable characteristic of the solution procedure is the straightforward extension to nonlinearity: nonlinear terms (material, geometric or boundary conditions) are resolved *on the fly*; after each outer iteration the coefficients and the source terms are updated and the procedure continues as in the linear case, for example, compare the linear elasticity approach of Jasak and Weller [194] with the finite strain elasto-plastic frictional contact procedure of Cardiff et al. [30].

In addition to the displacement-based approach described above, alternative solution algorithms, where pressure and displacement are the primary variables, have been proposed by Bijelonja et al. [95, 97, 100] and Fowler and Yee [200]; the benefit of such approaches is their ability to deal with incompressible and quasi-incompressible solids in a straightforward manner, while avoiding pressure instabilities.

## 3.3 Implicit Vertex-Centred Approach

### 3.3.1 Discretisation of Space

Like the other approaches, the vertex-centred approach divides the spatial domain into a finite number of contiguous cells that do not overlap and fill the space completely. When compared with the *typical* cell-centred approach, there are two key differences related to the mesh arrangement:

- The vertex-centred approach integrates the governing equations over cells in a secondary-grid, with cells that are typically constructed around the vertices/points in the primary grid (Fig. 9). The resulting secondary grid cells may not preserve convexity;
- The primitive unknowns are stored at the vertices/points of the primary grid, corresponding to the approximate, but not necessarily exact, centre of the secondary-grid cells.

However, in essence vertex-centred approaches can be viewed as a form of cell-centred method integrated over a secondary mesh.

In principal, the primary mesh can consist of arbitrary convex polyhedral cells; however, depending on the chosen discretisation (for example, if shape functions are used), the method may be limited to triangular/quadrilateral meshes in 2-D and tetrahedral/hexahedral meshes in 3-D; in fact, no

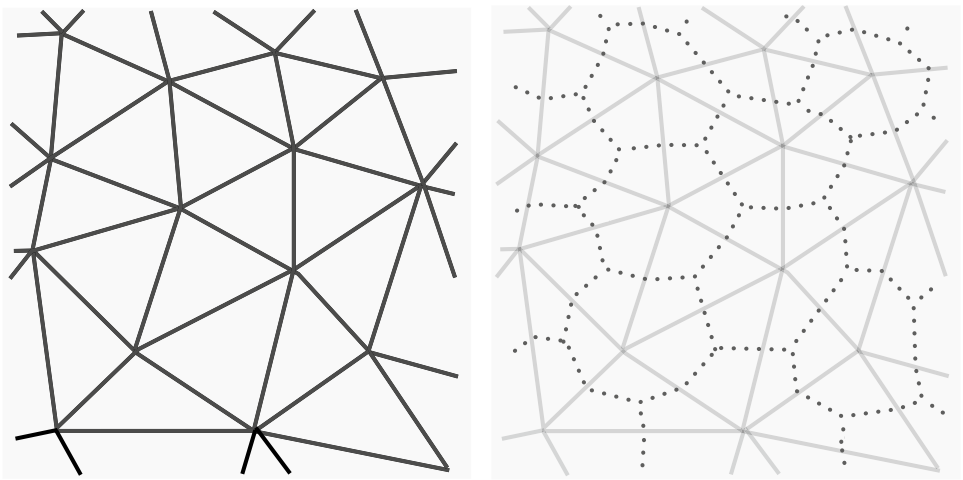

(a) Primary mesh (b) Secondary-grid used to integrate the governing equations

**Fig. 9** 2-D vertex-centred grid showing the (**a**) primary mesh, (**b**) secondary-grid used to integrate the governing equations. Figure adapted from Hassan [406]. (Color figure online)

vertex-centred solid mechanics examples using polyhedral meshes were found when preparing this article.

In addition to this form of the vertex-centred approach, a variant exists where the primary mesh cells around a vertex are used to perform the integration, for example, as discussed by Oñate et al. [12]; this produces overlapping regions of integration, where neighbouring vertices share part of their integrated volume. Secondary-grid cells can also be created by joining the mesh cell centres together [249], rather than joining the cell-centres to the face-centres as per the classic vertex-based method.

### 3.3.2 Discretisation of the Mathematical Model Equations

The vertex-centred approach starts from the strong integral form of the governing momentum equation (Eq. 1), which is integrated over a secondary-grid [5]. The vertex-centred approach discretises each term of the governing equation over the cells in the secondary-grid. An example secondary-grid cell is shown in Fig. 10, where each vertex $i$ in the primary grid is uniquely associated with a cell in the secondary-grid.

As with the cell-centred variant, the discretisation of each of the three terms (inertia, surface forces, body forces) in the governing conservation law (Eq. 1) will now be discussed in turn.

To approximate the volume integral temporal term, the displacement $\boldsymbol{u}$ within each secondary-grid cell is assumed to be constant [24, 240, 273]. Consequently, for a volume about vertex $i$, the term may be approximated in terms of the acceleration at vertex $i$ and the secondary-grid cell volume $\Omega_i$ about vertex $i$:

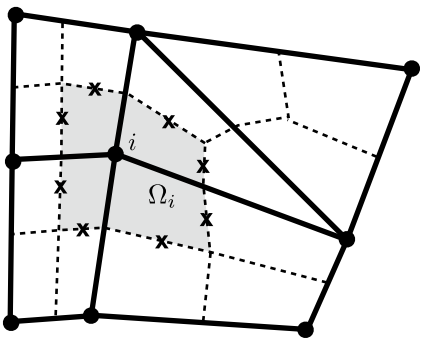


**Fig. 10** A typical control volume constructed around vertex $i$, with a volume $\Omega_i$. The solid lines show the primary grid and the dashed lines show the secondary-grid. When calculating the momentum balance for a secondary-grid cell (shaded), the displacement gradient is calculated at the boundary edge centres (boundary face centres in 3-D) of the secondary-grid cell (marked by "x"). Figure adapted from Bailey and Cross [24]. (Color figure online)

$$\int_{\Omega} \rho \frac{\partial^2 \boldsymbol{u}}{\partial t^2} \, \mathrm{d}\Omega \approx \rho \left( \frac{\partial^2 \boldsymbol{u}}{\partial t^2} \right)_i \Omega_i \tag{22}$$

As with other finite volume approaches, the acceleration term $\partial^2 \boldsymbol{u}/\partial t^2$ may be discretised in time using any appropriate finite difference scheme. For example, Slone et al. [273] employed the Newmark finite difference scheme, which is popular in the finite element community. For ease of comparison with the cell-centred approach (Eq. 5), a first-order Euler scheme is assumed here, giving the final discretised term as:

$$\int_{\Omega} \rho \frac{\partial^2 \boldsymbol{u}}{\partial t^2} \, \mathrm{d}\Omega \approx \rho \, \frac{\boldsymbol{u}_i - 2\boldsymbol{u}_i^{[m-1]} + \boldsymbol{u}_i^{[m-2]}}{\Delta t^2} \, \Omega_i \tag{23}$$

Comparing this expression with the equivalent cell-centred expression (Eq. 5), the only difference is the mesh location where the unknown displacement is stored. A conceptual difference comes from the fact that vertex $i$ is not in general situated at the centre of the secondary-grid cell volume $\Omega_i$; consequently, in the approximation of the inertia term, the cell-centred approach allows a local linear displacement distribution, whereas the vertex-centred approach requires a constant displacement distribution.

The volume integral body force term is discretised in a similar manner to the temporal term, where the body force $\boldsymbol{f}_b$ is assumed to be constant within each secondary-grid cell and equal to the value at vertex $i$:

$$\int_{\Omega} \rho \boldsymbol{f}_b \, \mathrm{d}\Omega \approx \rho \boldsymbol{f}_{b_i} \Omega_i \tag{24}$$

Once again the discretised term differs from the the equivalent cell-centred term in that a constant rather than a linear local variation is assumed. In the case that vertex $i$ does lie at the centroid of the control volume, then the vertex-centred and cell-centred terms are the same.

To discretise the surface force term, the closed surface integral in Eq. (1) is converted into a sum of surface integrals over the faces of the secondary-grid cell, taking the same form as Eq. (7). Approximation of the stress term at each face requires an assumption about the local displacement distribution. In contrast to the standard cell-centred approach, *most* vertex-centred approaches explicitly use shape functions to describe the local displacement field variation. Following the standard finite element notation, these shape (or interpolation) functions refer to the displacement within each cell of the primary mesh:

$$\boldsymbol{u}(\boldsymbol{x}) = \sum_{i=1}^{nVertices} N_i(\boldsymbol{x}) \boldsymbol{u}_i = [\boldsymbol{N}][\boldsymbol{u}] \tag{25}$$

where $nVertices$ is the number of vertices in the primary mesh cell of interest, $N_i(\boldsymbol{x})$ is the shape function associated

with vertex $i$ within the cell, $\boldsymbol{u}_i$ is the displacement at vertex $i$, and $[\boldsymbol{N}]$ and $[\boldsymbol{u}]$ represent a vector of all shape functions and nodal displacements within the cell respectively. It should be emphasised that these shape functions refer to the vertices and cells of the primary mesh, as opposed to of the secondary mesh cells.

As is standard in the conventional continuous Bubnov–Galerkin finite element method, the shape functions, which are defined in the reference domain and mapped to the physical domain, approximate the displacement field as a continuous piecewise distribution. As the shape functions describe the displacement distribution between the vertices on the primary mesh, this allows convenient calculation of the displacement gradients at the secondary-grid cell boundaries when applying the momentum balance (Fig. 10). Although shape functions are a key characteristic of the vertex-centred approaches presented in literature, they are *not* essential. As shown by Tsui et al. [249], it is possible to develop a vertex-centred finite volume approach that does not directly use shape functions; similar to many cell-centred approaches, Tsui et al. [249] applied the Gauss divergence theorem to calculate secondary-grid cell displacement gradients; these gradients were then interpolated to secondary-grid cell faces. In the cell-centred approach, the truncated Taylor series expansion about the cell centres (Eq. 2) fulfills the role of shape functions. As shape functions are specific to the cell geometry (e.g. triangle, quadrilateral, tetrahedral), shape function based approaches are limited in their choice of element shape, whereas all convex polyhedral meshes are valid for cell-centred approaches.

To approximate the stress at the faces of a secondary-grid cell, the gradient of displacement must be calculated. The use of shape functions allows this spatial gradient of displacement to be conveniently calculated as:

$$\boldsymbol{\nabla u} \approx \sum_{i=1}^{nVertices} \boldsymbol{\nabla} N_i(\boldsymbol{x}) \boldsymbol{u}_i = [\boldsymbol{B}][\boldsymbol{u}] \tag{26}$$

where $[\boldsymbol{B}]$ is a vector of the shape functions gradients. Substituting Eq. (26) into Eq. (7) allows the surface force term to be expressed in terms of the unknown displacements at the primary mesh vertices:

$$\begin{aligned} &\sum_{f=1}^{nFaces} \int_{\Gamma_i} \boldsymbol{n} \cdot \left[\mu \boldsymbol{\nabla u} + \mu (\boldsymbol{\nabla u})^T + \lambda \operatorname{tr}(\boldsymbol{\nabla u}) \mathbf{I}\right] \mathrm{d}\Gamma \\ &\quad \approx \sum_{f=1}^{nFaces} \sum_{v=1}^{nVertices} \boldsymbol{n}_f \cdot \left[\mu \boldsymbol{\nabla} N_{vf} \boldsymbol{u}_v + \mu \boldsymbol{u}_v \boldsymbol{\nabla} N_{vf} + \lambda \operatorname{tr}(\boldsymbol{\nabla} N_{vf} \boldsymbol{u}_v) \mathbf{I}\right] \end{aligned} \tag{27}$$

where *nVertices* refers to the number of vertices in the primary-grid cell in which the secondary-grid face $f$ is situated; $N_{vf}$ refers to the corresponding shape function for vertex $v$ within the primary-gird cell. Consequently, the surface force term for a secondary-grid cell surrounding vertex $v$ will be a function of the displacement at vertex $v$ as well as the displacement at all vertices that share a primary-grid cell with vertex $v$. For example, for the secondary-grid cell shown in Fig. 10, the surface force term will be a function of the displacements at all vertices shown except for the vertex in the top-right.

The final discretised form of the governing momentum equation for the vertex-centred approach is expressed for a secondary-grid cell as:

$$\begin{aligned} &\rho \frac{\boldsymbol{u}_i - 2\boldsymbol{u}_i^{[m-1]} + \boldsymbol{u}_i^{[m-2]}}{\Delta t^2} \Omega_i \\ &\quad = \sum_{f=1}^{nFaces} \sum_{v=1}^{nVertices} \boldsymbol{n}_f \\ &\qquad \cdot \left[\mu \boldsymbol{\nabla} N_{vf} \boldsymbol{u}_v + \mu \boldsymbol{u}_v \boldsymbol{\nabla} N_{vf} + \lambda \operatorname{tr}(\boldsymbol{\nabla} N_{vf} \boldsymbol{u}_v) \mathbf{I}\right] \\ &\qquad + \rho \boldsymbol{f}_{b_v} \Omega_v \end{aligned} \tag{28}$$

As with the other finite volume approaches, boundary conditions are incorporated through appropriate modification of the surface force term, and initial conditions must be specified for dynamic cases.

### 3.3.3 Solution Algorithm

The discretised equation for each secondary-grid cell can be written in the form of an algebraic equation:

$$\boldsymbol{A}_i \cdot \boldsymbol{u}_i - \sum_{v=1}^{nVertices} \boldsymbol{A}_v \cdot \boldsymbol{u}_v = \boldsymbol{b}_i \tag{29}$$

where $\boldsymbol{u}_i$ is the displacement at the primary-grid vertex associated with the secondary-grid cell, and *nVertices* indicates all vertices which share a primary-grid cell with vertex $i$. $\boldsymbol{A}_i$ and $\boldsymbol{A}_v$ are the corresponding block coefficients (second-order tensors in 3-D).

In earlier publications [5], the vertex-centred approach followed a similar solution algorithm to the standard cell-centred approach, where the surface force term was partitioned into *implicit* and *explicit* components and a segregated solution algorithm was employed. In later publications [24], a block-coupled solution procedure is used, where the entire surface force term is discretised implicitly. As noted previously, similar coupled solution algorithms were later proposed for the cell-centred variant by Das et al. [188] and Cardiff et al. [25].

Following the block-coupled approach, the algebraic equations (Eq. 29) can be assembled for all $M$ secondary-grid cells (primary-grid vertices) in the domain to form a system of linear equations:

$$[\boldsymbol{K}][\boldsymbol{U}] = [\boldsymbol{F}] \tag{30}$$

where the $M \times M$ global stiffness matrix $[\boldsymbol{K}]$ is sparse with block diagonal coefficients $\boldsymbol{A}_i$ and off-diagonal block coefficients $\boldsymbol{A}_\nu$, $[\boldsymbol{U}]$ is a vector of the unknown primary-grid vertex displacement vectors, and the global force source vector $[\boldsymbol{F}]$ contains contributions from $\boldsymbol{b}_i$.

This linear system can then be solved using direct or iterative linear solvers, where iterative conjugate gradient solvers with diagonal/Jacobi scaling have been favoured in literature, for example, [5, 24]. Parallelisation on distributed memory supercomputers has been addressed by McManus et al. [303, 304], and mixed displacement-rotation approaches have also been employed [300–302].

### 3.4 Explicit Cell-Centred Godunov-Type Approach

Godunov-type procedures are specialised approaches for analysis of problems that involve wave propagation, shocks and solution discontinuities. Features that distinguish this variant of finite volume approach from the others are the use of acoustic Riemann solvers, solution reconstruction procedures, slope limiters for gradient calculations, occasionally nodal integration, as well as representing the governing equations as a coupled system of first-order equations; in addition, explicit time marching solution algorithms are employed.

#### 3.4.1 Discretisation of Space

The majority of Godunov-type approaches are spatially discretised using cell-centred approaches, for example, [26–28, 196, 220, 222, 223, 225–229, 231–236]; consequently, this section will focus on such approaches; however, Godunov-type approaches have also used vertex-centred [31, 237], staggered grid [224, 228] and face-centred [20, 21] formulations. To-date, many of the developments have been limited to one and two dimensions, but in general the procedures can be extended to three dimensions. Like the *implicit* cell-centred approach described in Sect. 3.2, the solution spatial domain is divided into a finite number of contiguous convex polyhedral cells bounded by polygonal faces that do not overlap and fill the space completely.

#### 3.4.2 Discretisation of the Mathematical Model Equations

In a notable deviation from the other finite volume variants, Godunov-type approaches portray the second-order governing momentum equation (Eq. 1) as a coupled system of first-order equations:

$$\int_\Omega \rho \frac{\partial \boldsymbol{v}}{\partial t}\, \mathrm{d}\Omega = \oint_\Gamma \boldsymbol{n} \cdot \boldsymbol{\sigma}\, \mathrm{d}\boldsymbol{\Gamma} + \int_\Omega \rho \boldsymbol{f}_b\, \mathrm{d}\Omega \tag{31}$$

$$\int_\Omega \frac{\partial \boldsymbol{F}}{\partial t}\, \mathrm{d}\Omega = \oint_\Gamma \boldsymbol{v}\boldsymbol{n}\, \mathrm{d}\boldsymbol{\Gamma} \tag{32}$$

where $\boldsymbol{v}$ is the velocity vector and the deformation gradient, $\boldsymbol{F}$, defines the local deformation as:

$$\boldsymbol{F} = \mathbf{I} + (\boldsymbol{\nabla u})^T \tag{33}$$

Equation (32) is obtained by taking the time-derivative of Eq. (33) and employing the Gauss divergence theorem.

To ensure the compatibility conditions are satisfied, the deformation gradient at the initial time should be curl free:

$$\boldsymbol{\nabla} \times \boldsymbol{F}^{[m=0]} = \mathbf{0} \tag{34}$$

In addition, the discrete evolution of $\boldsymbol{F}$ (or $\boldsymbol{\nabla u}$) should not allow curl errors to escalate. For further discussion of this point, see [27, 28, 40, 214, 225]. It is also possible to employ the evolution of the displacement gradient $\boldsymbol{\nabla u}$ directly rather than the deformation gradient, as shown by Trangenstein and Colella [40]; however, this is less popular in literature.

The governing system of coupled first-order equations (Eqs. 31, 32) can be expressed concisely as:

$$\int_\Omega \frac{\partial \boldsymbol{\mathcal{U}}}{\partial t}\, \mathrm{d}\Omega = \oint_\Gamma \boldsymbol{\mathcal{F}}_n\, \mathrm{d}\boldsymbol{\Gamma} + \int_\Omega \boldsymbol{\mathcal{S}}\, \mathrm{d}\Omega \tag{35}$$

where $\boldsymbol{\mathcal{U}}$ is the primary unknown vector, $\boldsymbol{\mathcal{F}}_n$ is the flux vector, and $\boldsymbol{\mathcal{S}}$ is the source vector, given as:

$$\boldsymbol{\mathcal{U}} = \begin{pmatrix} \boldsymbol{v} \\ \boldsymbol{F} \end{pmatrix}, \quad \boldsymbol{\mathcal{F}}_n = \begin{pmatrix} {}^{\boldsymbol{t}}/_{\rho} \\ \boldsymbol{v}\boldsymbol{n} \end{pmatrix}, \quad \boldsymbol{\mathcal{S}} = \begin{pmatrix} \boldsymbol{f}_b \\ \mathbf{0} \end{pmatrix} \tag{36}$$

and the traction vector, $\boldsymbol{t}$, gives the stress on a plane as $\boldsymbol{t} = \boldsymbol{n} \cdot \boldsymbol{\sigma}$. To close the system, we give the constitutive relation (Hooke's law) in terms of the deformation gradient:

$$\boldsymbol{\sigma} = \mu \boldsymbol{F}^T + \mu \boldsymbol{F} + \lambda\, \mathrm{tr}(\boldsymbol{F})\mathbf{I} - (2\mu + 3\lambda)\mathbf{I} \tag{37}$$

We next describe the discretisation of the three terms in Eq. (35): the time derivative term, the diffusion term and the body force term.

Assuming the primary unknowns ($\boldsymbol{v}$ and $\boldsymbol{F}$) vary linearly within each cell according to Eq. (2), the volume integrals can be expressed in terms of the cell-centre values (subscript $P$) and the surface integral becomes a sum over the face-centre values (subscript $f$); consequently, Eq. (35) becomes:

$$\frac{\partial \boldsymbol{\mathcal{U}}_P}{\partial t}\Omega_P = \sum_{f=1}^{nFaces} \boldsymbol{\mathcal{F}}_{n_f} |\boldsymbol{\Gamma}_f| \;+\; \boldsymbol{\mathcal{S}}_P \Omega_P \tag{38}$$

Similar to the other approaches, discretisation of the time-rate term can be achieved using a variety of finite difference methods. Here we assume a first-order *forward* Euler

discretisation to allow straight-forward comparison with the other methods:

$$\frac{\mathcal{U}_P - \mathcal{U}_P^{[m-1]}}{\Delta t}\Omega_P = \sum_{f=1}^{nFaces} \mathcal{F}_{n_f}^{[m-1]}|\mathbf{\Gamma}_f| \quad + \quad \mathcal{S}_P\Omega_P \tag{39}$$

where, as before, $m$ is the time-step counter, which for brevity has been dropped on the unknown current time value. Of course, as an explicit time-marching solution algorithm will be employed, the time step size is limited by the Courant–Friedrichs–Lewy constraint [34]; this condition is necessary for stability but is not sufficient. It is also necessary that the time integrator avoids the creation of new local extrema, known as the total variation diminishing property or the local maximum principle; the first-order forward Euler approach is one such method that obeys this condition.

Alternatively, the flux calculation in Eq. (39), which sums over the cell faces, can be expressed as a sum over the cell points/vertices according to:

$$\frac{\mathcal{U}_P - \mathcal{U}_P^{[m-1]}}{\Delta t}\Omega_P = \sum_{v=1}^{nVertices} \mathcal{F}_{n_v}^{[m-1]}|\boldsymbol{C}_v| \quad + \quad \mathcal{S}_P\Omega_P \tag{40}$$

where the calculation of the point/vertex/nodal area vector, $\boldsymbol{C}_v$, is given in Carré et al. [221] and Kluth and Després [26] or equivalently in Maire et al. [222].

Up to this point, the presented discretisation coincides with the cell-centred approach described in Sect. 3.2, apart from the introduction of a system of first-order conservation equation and the use of the forward Euler method as opposed to the backward Euler method; however, in the discretisation of the face flux, $\mathcal{F}_n$, Godunov-type methods deviate from the other approaches. As a result of the assumed piecewise linear distribution (Eq. 2), there is a discontinuity at the cell internal faces. A distinguishing characteristic of Godunov-type methods is the acknowledgement of this discontinuity in the solution field, known as a Riemann problem, and the development of appropriate methods (Riemann solvers) to deal with the propagation of this discontinuity. Accordingly, the face flux, $\mathcal{F}_n$, is defined as a function of the solution variable at either side of the interface:

$$\mathcal{F}_{n_f} = f(\mathcal{U}_{Pf}, \mathcal{U}_{Nf}) \tag{41}$$

The solution at either side of the interface ($\mathcal{U}_{P_f}$ and $\mathcal{U}_{N_f}$) is determined via extrapolation from the adjacent cell centres:

$$\begin{aligned} \mathcal{U}_{P_f} &= \mathcal{U}_P + \boldsymbol{G}_P \cdot (\boldsymbol{x}_f - \boldsymbol{x}_P) \\ \mathcal{U}_{N_f} &= \mathcal{U}_N + \boldsymbol{G}_N \cdot (\boldsymbol{x}_f - \boldsymbol{x}_N) \end{aligned} \tag{42}$$

where $\boldsymbol{G}_P$ is the gradient of $\mathcal{U}$ within cell $P$, and $\boldsymbol{G}_N$ is the gradient within cell $N$. A critical component of Godunov-type methods is the definition of this solution *reconstruction*, such that the local maximum principle is preserved i.e. the value of $\mathcal{U}$ at face $f$ should not be greater than the value at adjacent cell centres $P$ and $N$. There are a number of ways to define such discrete gradients; here, as a typical example, the monotone upstream scheme for conservation law (MUSCL) scheme is described [27]. The MUSCL approach consists of two steps: first, the gradient is predicted based on local neighbouring values, then this gradient is corrected/limited to respect the local maximum principle.

To predict the gradient, the second-order least-squares method described in Sect. 3.2 can be used; this approach does not prohibit overshoots and undershoots at the faces, and hence does not satisfy the local maximum principle. To remedy this, a so-called *slope limiter* is used to restrict the value of the gradient, $\boldsymbol{G}$. The slope limiter is included through modification of the reconstruction expression (Eq. 42):

$$\begin{aligned} \mathcal{U}_{P_f} &= \mathcal{U}_P + \phi_P \boldsymbol{G}_P \cdot (\boldsymbol{x}_f - \boldsymbol{x}_P) \\ \mathcal{U}_{N_f} &= \mathcal{U}_N + \phi_N \boldsymbol{G}_N \cdot (\boldsymbol{x}_f - \boldsymbol{x}_N) \end{aligned} \tag{43}$$

where $0 \leq \phi \leq 1$ is a scalar slope limiter. When $\phi = 1$, no limiting is applied, whereas when $\phi = 0$, full limiting is applied and the value near the face is assumed equal to the cell-centre value. Choosing the value of $\phi$ is a balance between stability (lower value of $\phi$) and accuracy (higher value of $\phi$). For the MUSCL procedure, $\phi$ is determined as described by Lee et al. [27]:

1. Find the smallest and largest values among the current and adjacent cells:

$$\mathcal{U}^{\min} = \min(\mathcal{U}_P, \mathcal{U}_{Ni}), \quad \mathcal{U}^{\max} = \max(\mathcal{U}_P, \mathcal{U}_{Ni}) \tag{44}$$

   where $\mathcal{U}_{Ni}$ represents the values at neighbour cells, which share an internal face with cell $P$.
2. Calculate the un-restricted reconstructed value $\mathcal{U}_{Pf}$ with $\phi_P = 1$ at each internal face within cell $P$.
3. Find the maximum allowable value of $\phi_{Pf}$ for each face in cell $P$:

$$\phi_{Pf} = \begin{cases} \min\left(1, \frac{\mathcal{U}^{\max} - \mathcal{U}_P}{\mathcal{U}_{P_f} - \mathcal{U}_P}\right), & \text{if} \quad \mathcal{U}_{P_f} - \mathcal{U}_P > 0 \\ \min\left(1, \frac{\mathcal{U}^{\min} - \mathcal{U}_P}{\mathcal{U}_{P_f} - \mathcal{U}_P}\right), & \text{if} \quad \mathcal{U}_{P_f} - \mathcal{U}_P < 0 \\ 1, & \text{if} \quad \mathcal{U}_{P_f} - \mathcal{U}_P = 0 \end{cases}$$

4. Select $\phi_P = \min_f(\phi_{Pf})$
5. Calculate the reconstructed value at each internal face using $\phi_P$ determined in step 4 and Eq. 43.

To complete the discretisation, all that remains is to express the flux vector, $\mathcal{F}_{n_f}$, in terms of the solution vector, $\mathcal{U}$. To

achieve this, the Rankine–Hugoniot jump conditions [32] are employed. These jump conditions describe the relationship between the states on both sides of a shock wave. The jump conditions corresponding to Eqs. 31 and 32 are [27]:

$$U[\![\boldsymbol{v}]\!] = -(1/\rho)\boldsymbol{n} \cdot [\![\boldsymbol{\sigma}]\!] \tag{45}$$

$$U[\![\boldsymbol{F}]\!] = -[\![\boldsymbol{v}]\!]\boldsymbol{n} \tag{46}$$

where the operator $[\![\cdot]\!]$ represents the jump across the shock, for example, $[\![\boldsymbol{\mathcal{U}}_f]\!] = \boldsymbol{\mathcal{U}}_{N_f} - \boldsymbol{\mathcal{U}}_{P_f}$. The wave speed is indicated by $U$. Using Eqs. (45) and (46) and assuming a constant wave speed, the face flux can be expressed as the sum of an average flux and a stabilisation flux [27, 28]:

$$\boldsymbol{\mathcal{F}}_{n_f} = \boldsymbol{\mathcal{F}}^{\text{average}}_{n_f} + \boldsymbol{\mathcal{F}}^{\text{stab}}_{n_f} \tag{47}$$

where the average flux is:

$$\boldsymbol{\mathcal{F}}^{\text{average}}_{n_f} = \frac{1}{2}\left[\boldsymbol{\mathcal{F}}_n(\boldsymbol{\mathcal{U}}_{P_f}) + \boldsymbol{\mathcal{F}}_n(\boldsymbol{\mathcal{U}}_{N_f})\right] \tag{48}$$

and the so-called upwinding stabilisation term is:

$$\boldsymbol{\mathcal{F}}^{\text{stab}}_{n_f} = \begin{bmatrix} \frac{\rho}{2}\left[c_s\mathbf{I} + (c_p - c_s)\boldsymbol{n}_f\boldsymbol{n}_f\right] \cdot \left(\boldsymbol{v}_{N_f} - \boldsymbol{v}_{P_f}\right) \\ \frac{1}{2}\left[\frac{1}{c_s}\mathbf{I} + \left(\frac{1}{c_p} - \frac{1}{c_s}\right)\boldsymbol{n}_f\boldsymbol{n}_f\right] \cdot \left(\boldsymbol{n}_f \cdot \left[\boldsymbol{\sigma}_{N_f} - \boldsymbol{\sigma}_{P_f}\right]\right) \end{bmatrix} \tag{49}$$

The volumetric and shear wave speeds are indicated by $c_p$ and $c_s$. Jameson–Schmidt–Turkel stabilisation has been used as an alternative to this upwinding stabilisation, and in principle Rhie–Chow stabilisation could also be used.

The final discretised governing equations, given in terms of unknowns $\boldsymbol{v}_P^{[m]}$ and $\boldsymbol{F}_P^{[m]}$ at time-step $m$, are expressed as:

$$\begin{aligned} &\frac{\boldsymbol{v}_P^{[m]} - \boldsymbol{v}_P}{\Delta t}\Omega_P \\ &= \sum_{f=1}^{nFaces} \frac{1}{2\rho}\boldsymbol{n}_f \cdot \left[\mu\boldsymbol{F}_{P_f}^T + \mu\boldsymbol{F}_{P_f} + \lambda\,\mathrm{tr}\left(\boldsymbol{F}_{P_f}\right)\mathbf{I} - (2\mu + 3\lambda)\mathbf{I}\right]|\Gamma_f| \\ &\quad + \sum_{f=1}^{nFaces} \frac{1}{2\rho}\boldsymbol{n}_f \cdot \left[\mu\boldsymbol{F}_{N_f}^T + \mu\boldsymbol{F}_{N_f} + \lambda\,\mathrm{tr}\left(\boldsymbol{F}_{N_f}\right)\mathbf{I} - (2\mu + 3\lambda)\mathbf{I}\right]|\Gamma_f| \\ &\quad + \sum_{f=1}^{nFaces} \frac{1}{2}\left[c_s\mathbf{I} + (c_p - c_s)\boldsymbol{n}_f\boldsymbol{n}_f\right] \cdot \left(\boldsymbol{v}_{N_f} - \boldsymbol{v}_{P_f}\right)|\Gamma_f| \\ &\quad + \boldsymbol{f}_{b_P}\,\Omega_P \end{aligned} \tag{50}$$

$$\begin{aligned} &\frac{\boldsymbol{F}_P^{[m]} - \boldsymbol{F}_P}{\Delta t}\Omega_P \\ &= \sum_{f=1}^{nFaces} \frac{1}{2}\left(\boldsymbol{v}_{P_f}\boldsymbol{n}_f + \boldsymbol{v}_{N_f}\boldsymbol{n}_f\right)|\Gamma_f| \\ &\quad + \sum_{f=1}^{nFaces} \frac{1}{2}\left[\frac{1}{c_s}\mathbf{I} + (\frac{1}{c_p} - \frac{1}{c_s})\boldsymbol{n}_f\boldsymbol{n}_f\right] \cdot \left[\boldsymbol{n}_f \cdot \left(\boldsymbol{\sigma}_{N_f} - \boldsymbol{\sigma}_{P_f}\right)\right]|\Gamma_f| \end{aligned} \tag{51}$$

where the $m-1$ time index on $\boldsymbol{F}$ and $\boldsymbol{v}$ has been omitted for brevity i.e. $\boldsymbol{F} \equiv \boldsymbol{F}^{[m-1]}$ and $\boldsymbol{v} \equiv \boldsymbol{v}^{[m-1]}$. The stress either side of a face is calculated according to Eq. (37).

### 3.4.3 Solution Algorithm

The solution of the governing discretised equations (Eqs. 50, 51) proceeds in an explicit manner as follows:

1. Increase the total time by $\Delta t = \alpha_{\text{CFL}}\frac{h_{\min}}{c_p}$, according to the Courant–Friedrichs–Lewy [34] condition, where $h_{\min}$ is the shortest length within the mesh and $\alpha_{\text{CFL}}$ is typically chosen to be less than 1/2
2. Store the old-time solution values: $\boldsymbol{v}^{[m-1]} \leftarrow \boldsymbol{v}^{[m]}$ and $\boldsymbol{F}^{[m-1]} \leftarrow \boldsymbol{F}^{[m]}$
3. Calculate the reconstructed solution values, $\boldsymbol{v}_{N_f}$, $\boldsymbol{v}_{P_f}$, $\boldsymbol{F}_{N_f}$ and $\boldsymbol{F}_{P_f}$, at each cell face according to Eq. (43)
4. Solve Eq. (50) for $\boldsymbol{v}^{[m]}$
5. Solve Eq. (51) for $\boldsymbol{F}^{[m]}$
6. Repeat steps 1–5 until the end time has been reached

Like all explicit methods, this approach does not require the solution of an implicit linear system of equations and hence each time-step can be evaluated more rapidly than in the previously discussed implicit methods; however, the time-step size limit essentially restricts explicit methods to hyperbolic-style problems. Finally, the explicit nature of the algorithm allows straight-forward and efficient parallelisation on distributed memory supercomputers.

## 3.5 Discussion

The field of finite volume solid mechanics comprises more approaches than those presented above, however, the selected three variants capture the primary differences in the approaches. It can be seen that the distinction between the variants can be narrowed down to four components:

1. Control volume construction;
2. Face gradient calculation;
3. Stabilisation approach;
4. Solution methodology.

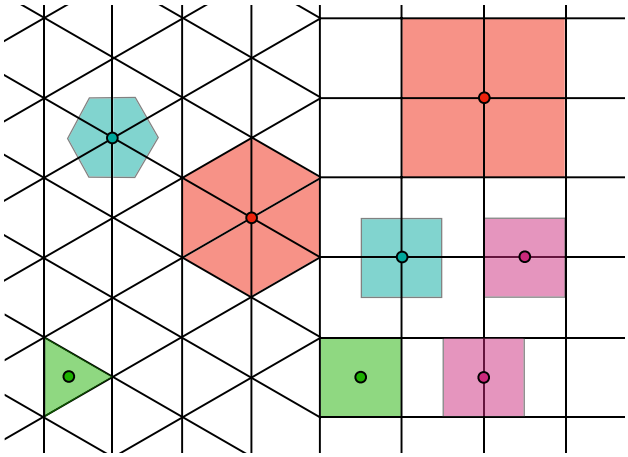

**Fig. 11** Illustration of the four ways to construct control volumes on a primary mesh: (1) cell-centred (green); (2) vertex-centred with non-overlapping control volumes (blue); (3) vertex-centred with overlapping control volumes (red); and (4) staggered-grid (purple). The nodal locations are indicated by filled circles. (Color figure online)

Each of these components is briefly reviewed below, followed by the natural definition of a unified approach linking all variants.

#### 3.5.1 Control Volume Construction

There are predominantly four ways to construct control volumes (Fig. 11): (1) cell-centred, (2) vertex-centred with non-overlapping volumes; (3) vertex-centred with overlapping control volumes, (4) and a staggered-grid. In terms of the relative merits of the different approaches, a number of observations can be made:

1. The staggered-grid is restricted to structured quadrilateral/hexahedral meshes in 2-D/3-D;
2. The vertex-centred approach with non-overlapping control volumes requires the construction and storage of a second mesh;
3. The vertex-centred approach has nodes on the boundary, whereas the cell-centre approach typically does not;
4. The cell-centred approach allows convenient approximation of the face normal gradients but requires interpolation to approximate the tangential gradients;
5. In contrast, the vertex-centred approach with overlapping volumes allows convenient approximation of the tangential gradients but requires interpolation to approximate the normal gradients.

#### 3.5.2 Face Gradient Calculation

Once the control volume is constructed, all approaches must approximate the traction at each control volume face. To achieve this, the gradient of displacement at the face $(\boldsymbol{\nabla u})_f$ is approximated in terms of the nodal displacement values. Neglecting any additional stabilisation terms (addressed in the next section), the most common approaches are:

1. Interpolate the gradient from the adjacent cell-centres:

$$(\boldsymbol{\nabla u})_f = \frac{|\boldsymbol{d}_{Pf}|(\boldsymbol{\nabla u})_P + |\boldsymbol{d}_{Nf}|(\boldsymbol{\nabla u})_N}{|\boldsymbol{d}_f|} \tag{52}$$

   where $\boldsymbol{d}_f$ is the vector from the centre of cell $P$ to the centre of cell $N$, $\boldsymbol{d}_{Pf}$ is the vector from the centre of cell $P$ to the centre of face $f$, and $\boldsymbol{d}_{Nf}$ is the vector from the centre of cell $N$ to the centre of face $f$. These interpolation weights may differ depending on the specific approach.
2. Calculate the normal gradient using central-differencing, and interpolate the tangential gradient from the adjacent cell-centres:

$$(\boldsymbol{\nabla u})_f = \boldsymbol{n}_f \frac{\boldsymbol{u}_N - \boldsymbol{u}_P}{|\boldsymbol{d}_f|} + \left(\mathbf{I} - \boldsymbol{n}_f \boldsymbol{n}_f\right) \cdot \frac{|\boldsymbol{d}_{Pf}|(\boldsymbol{\nabla u})_P + |\boldsymbol{d}_{Nf}|(\boldsymbol{\nabla u})_N}{|\boldsymbol{d}_f|} \tag{53}$$

3. Calculate the normal gradient using central-differencing, and calculate the tangential gradient using the point or edge values. In the case of a staggered-grid, these point or edge values correspond to nodes and no interpolation is necessary. For the cell-centred approach, these point or edge values are interpolated from the cell-centred nodes, and an appropriate face tangential gradient calculation method used; for example, the face-Gauss method [25, 208] is a generalisation of the approach used in the original Demirdžić et al. [2] approach:

$$(\boldsymbol{\nabla u})_f = \boldsymbol{n}_f \frac{\boldsymbol{u}_N - \boldsymbol{u}_P}{|\boldsymbol{d}|_f} + \sum_{e=1}^{nEdges} \boldsymbol{m}_e \boldsymbol{u}_e L_e \tag{54}$$

   where $\boldsymbol{m}_e$ is the outward-facing bi-normal at edge $e$, $L_e$ is the length of edge $e$, and $\boldsymbol{u}_e$ is the displacement at the centre of edge $e$, which has been interpolated from adjacent cell-centres.
4. Extrapolate the gradient from each adjacent cell-centre, and take the average:

$$(\boldsymbol{\nabla u})_f = \frac{(\boldsymbol{\nabla u})_P + \boldsymbol{d}_{Pf} \cdot \boldsymbol{\nabla}(\boldsymbol{\nabla u})_P + (\boldsymbol{\nabla u})_N + \boldsymbol{d}_{Nf} \cdot \boldsymbol{\nabla}(\boldsymbol{\nabla u})_N}{2} \tag{55}$$

5. For each of the previous face gradient calculation methods, a limiter can be applied to preserve the local maximum principle, as discussed in Sect. 3.4.
6. Use shape functions to evaluate the face gradient. As an example, taking a vertex-based method and a 2-D triangular grid with linear shape functions, the face gradient is given in Voigt notation as:

$$\left[(\boldsymbol{\nabla u})_f\right] = \begin{bmatrix} \partial u_x/\partial x \\ \partial u_y/\partial y \\ \partial u_x/\partial y \\ \partial u_y/\partial x \end{bmatrix} = \underbrace{\frac{1}{x_{13}y_{23} - x_{23}y_{13}} \begin{bmatrix} y_{23} & 0 & y_{31} & 0 & y_{12} & 0 \\ 0 & x_{32} & 0 & x_{13} & 0 & x_{21} \\ x_{32} & 0 & x_{13} & 0 & x_{21} & 0 \\ 0 & y_{23} & 0 & y_{31} & 0 & y_{12} \end{bmatrix}}_{\text{Derivative of shape functions}} \cdot \begin{bmatrix} u_{x_1} \\ u_{y_1} \\ u_{x_2} \\ u_{y_2} \\ u_{x_3} \\ u_{y_3} \end{bmatrix} \tag{56}$$

   where subscripts 1, 2 and 3 refer to the three nodes in the triangle, and the relative coordinates are given as $x_{ab} = x_a - x_b$. Here we are referring to the vertex-centred method, however, shape functions could in principle be used with any control volume construction.
7. Use a higher-order approach, for example, the fourth-order approach proposed by Demirdžić [203].

To provide additional insight, let us consider the face gradient calculations on a simple grid. Taking a uniform quadrilateral mesh (Fig. 12), we will calculate the gradient at a face using the most popular of the methods above. The discretised governing equation for the cell in Fig. 12 can be written in the form of a tensor algebraic equation:

$$\sum_{i=1}^{i=13} \boldsymbol{A}_i \cdot \boldsymbol{u}_i = \boldsymbol{0} \tag{57}$$

which corresponds to a block row in the resulting stiffness matrix, assuming a block-coupled solution methodology is used. It is possible to present the coefficients $\boldsymbol{A}_i$ of this equation graphically to allow direct comparison between the different face gradient calculation approaches: Fig. 13 compares the resulting coefficients from using methods 1, 2, 3 and 6, neglecting any stabilisation terms. Noting that boundary conditions have not been considered, a number of observations can be made:

- Methods 2, 3 and 6 employ the same compact computational stencil, whereas method 1 (interpolated gradient) uses a larger stencil, including second face-neighbours;
- All coefficients are symmetric;
- All methods show geometric symmetries, for example, the top-right coefficient is equal to the bottom-left coefficient; this is a consequence of the momentum/force being conserved between nodes;
- In methods 1, 2, and 3, the normal forces are calculated entirely from the central cell displacement as well as the left, right, top and bottom cell displacements (far-left/right/top/bottom cells in the case of method 1). Similarly, the shear forces are calculated entirely from the top-left, top-right, bottom-left and bottom-right cell displacements;
- Methods 2 (interpolated tangential gradient) and 3 (tangential gradient calculated at the face) are equivalent for this simple grid. For meshes including skewness and non-orthogonality, this may not be the case;
- Method 1 differs from methods 2 and 3 in only one way: the left, right, top and bottom cell coefficients have been moved to a more distant neighbour and scaled in magni-

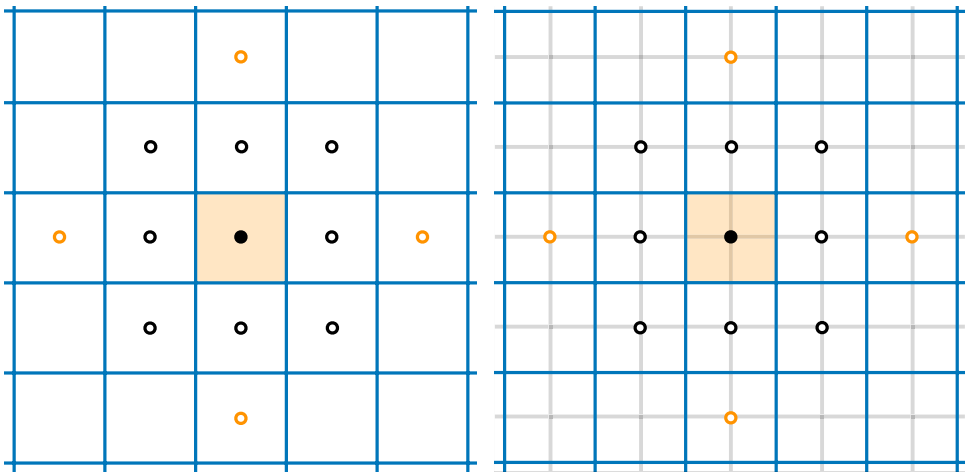

(a) Mesh over which the equations are integrated

(b) Mesh over which the equations are integrated, as well as the primary mesh where the shape functions are defined (in gray)

**Fig. 12** Local integration domain (shaded orange) and computational stencil (white-filled dots) for a node (black-filled dot) in a 2-D quadrilateral mesh. All methods include close neighbours (white-filled dots with black border) within their stencil, while method 1 additionally includes distant neighbours (white-filled dots with orange border). (Color figure online)

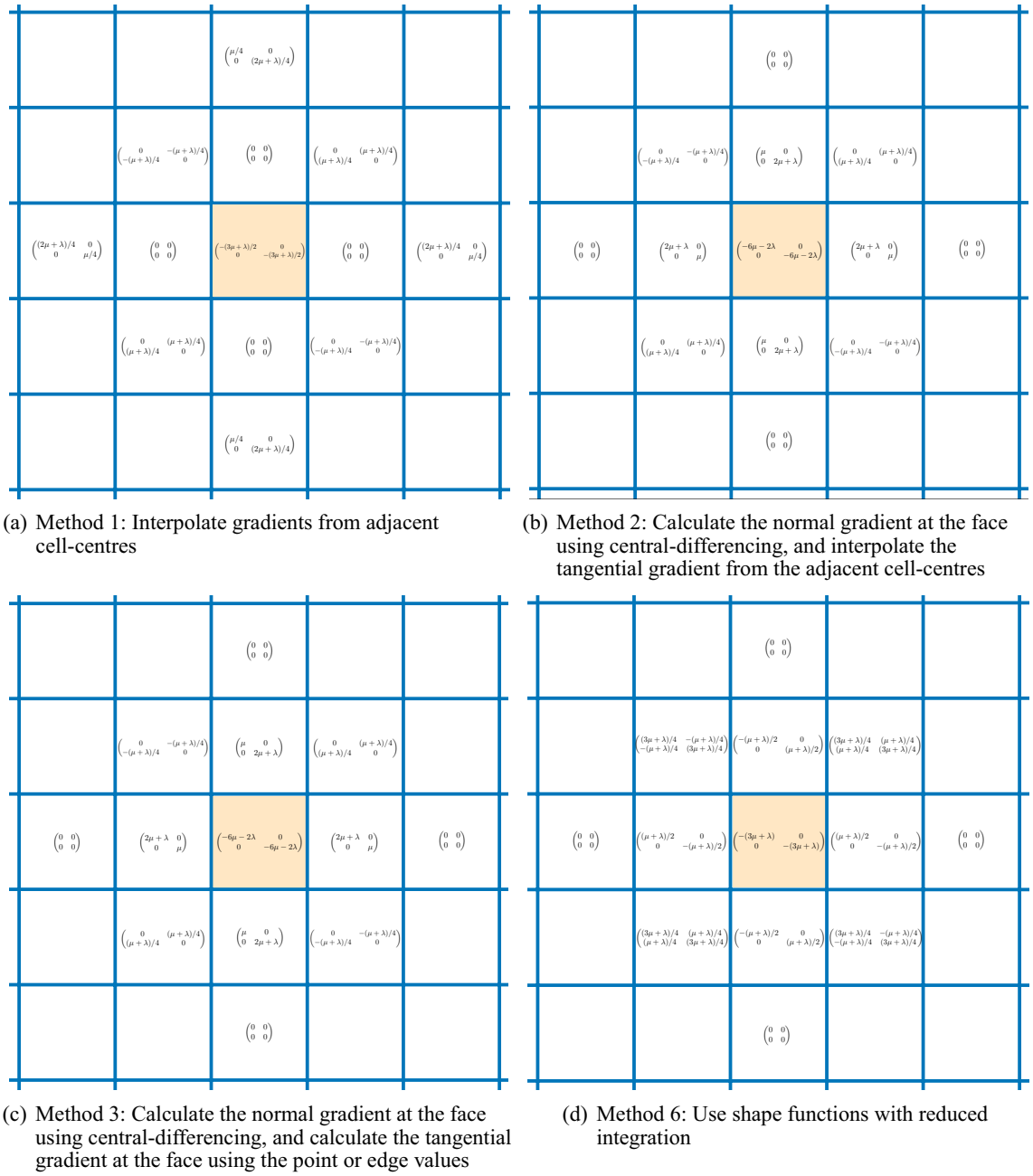

(a) Method 1: Interpolate gradients from adjacent cell-centres

(b) Method 2: Calculate the normal gradient at the face using central-differencing, and interpolate the tangential gradient from the adjacent cell-centres

(c) Method 3: Calculate the normal gradient at the face using central-differencing, and calculate the tangential gradient at the face using the point or edge values

(d) Method 6: Use shape functions with reduced integration

**Fig. 13** A comparison of the block coefficients in the stiffness matrix for the centre node/cell, where different face gradient calculation methods are employed. A unit thickness is assumed and stabilisation terms have been disregarded. (Color figure online)

tude; in addition, the central coefficient has been scaled in magnitude. This corresponds to the normal component being calculated using a larger stencil (interpolated gradient) in method 1 vs. methods 2 and 3 (central differencing at the face);

- Method 6 (shape functions) requires the force to be integrated over 8 faces compared with 4 faces for methods 1, 2 and 3; this comes from the way in which the mesh is constructed from a primary mesh;
- Half the components of the corner coefficients are zero for methods 1, 2 and 3, while they are all non-zero for method 6.

It should be noted that the coefficients that appear in the linear system matrix depend on the chosen solution algorithm; for block-coupled approaches, the coefficients will be as shown, whereas for segregated approaches, the

coefficients will be more sparse and will not contain inter-component couplings (the off-diagonal components of the coefficients will be zero). For example, the matrix coefficients corresponding to method 2 (and equivalently method 3) are given for the segregated approach in Fig. 14. In contrast to the coefficients given in Fig. 13b, the segregated coefficients (Fig. 14) differ in the following ways:

- As noted, all inter-component coupling is zero i.e. all block off-diagonal coefficients are zero; this allows the two scalar displacement equations to be solved separately;
- The matrix has greater sparsity that the other approaches, leading to reduced memory requirements;
- The coefficients produce a matrix which is *weakly* diagonally dominant: the magnitude of the centre node coefficient is equal to the sum of the magnitudes of the other nodes. Such a weakly diagonally dominant system (which becomes strongly diagonally dominant with the inclusion of Dirichlet/essential boundary conditions) promotes the convergence of iterative linear solvers.

### 3.5.3 Stabilisation Approach

For the discretisations that require stabilisation, three distinct forms of stabilisation term can be found; these can be expressed as a stabilisation traction $\boldsymbol{t}^{\text{stab}}$ applied at the control volume face:

$$\boldsymbol{t}^{\text{stab}} = \begin{cases} \alpha^{\text{stab}} K_f \left( \dfrac{\boldsymbol{u}_N - \boldsymbol{u}_P}{|\boldsymbol{d}_f|} - \boldsymbol{n}_f \cdot \dfrac{|\boldsymbol{d}_{Nf}| \nabla \boldsymbol{u}_N + |\boldsymbol{d}_{Pf}| \nabla \boldsymbol{u}_P}{|\boldsymbol{d}_f|} \right) |\boldsymbol{\Gamma}_f| & \text{Rhie–Chow} \\ -\alpha^{\text{stab}} \rho \, c_p \, |\boldsymbol{d}_f|^2 \left( \nabla^2 \boldsymbol{v}_N - \nabla^2 \boldsymbol{v}_P \right) |\boldsymbol{\Gamma}_f| & \text{Jameson–Schmidt–Turkel} \\ \rho \left[ c_s \mathbf{I} + (c_p - c_s) \boldsymbol{n}_f \boldsymbol{n}_f \right] \cdot \dfrac{\boldsymbol{v}_N + \boldsymbol{d}_{Nf} \cdot \nabla \boldsymbol{v}_N - \boldsymbol{v}_P - \boldsymbol{d}_{Pf} \cdot \nabla \boldsymbol{v}_P}{2} |\boldsymbol{\Gamma}_f| & \text{Godunov upwinding} \end{cases} \tag{58}$$

where $\alpha^{\text{stab}}$ is a user-defined scaling factor, the pressure wave speed of sound is $c_p = \sqrt{\frac{2\mu+\lambda}{\rho}}$, and the shear wave speed of sound is $c_s = \sqrt{\frac{\mu}{\rho}}$.

In Eq. (58), Jameson–Schmidt–Turkel and Godunov-upwinding terms are given in a form that is only suitable for dynamic problems; however, it is possible to define similar stabilisation terms for quasi-static analyses:

$$\boldsymbol{t}^{\text{stab}} = \begin{cases} \alpha^{\text{stab}} K_f \left( \dfrac{\boldsymbol{u}_N - \boldsymbol{u}_P}{|\boldsymbol{d}_f|} - \boldsymbol{n}_f \cdot \dfrac{|\boldsymbol{d}_{Nf}| \nabla \boldsymbol{u}_N + |\boldsymbol{d}_{Pf}| \nabla \boldsymbol{u}_P}{|\boldsymbol{d}_f|} \right) |\boldsymbol{\Gamma}_f| & \text{Rhie–Chow} \\ -\alpha^{\text{stab}} K_f \, |\boldsymbol{d}_f| \left( \nabla^2 \boldsymbol{u}_N - \nabla^2 \boldsymbol{u}_P \right) |\boldsymbol{\Gamma}_f| & \text{Jameson–Schmidt–Turkel} \\ \alpha^{\text{stab}} \dfrac{K_f}{2} \dfrac{\boldsymbol{u}_N + \boldsymbol{d}_{Nf} \cdot \nabla \boldsymbol{u}_N - \boldsymbol{u}_P - \boldsymbol{d}_{Pf} \cdot \nabla \boldsymbol{u}_P}{|\boldsymbol{d}_f|} |\boldsymbol{\Gamma}_f| & \text{Godunov upwinding} \end{cases} \tag{59}$$

where the Rhie–Chow term is given for comparison. A user-defined scaling factor $\alpha^{\text{stab}}$ is added to the Godunov-type term in 59, as this form of the term does not have the same physical significance as the dynamic term in Eq. (58). After some algebraic manipulation, where we include the $(1/2)$ factor in $\alpha^{\text{stab}}$ and note that $\boldsymbol{d}_{Nf} = -|\boldsymbol{d}_{Nf}| \boldsymbol{n}_f$, the Godunov upwinding-type stabilisation term is seen to be identical to Rhie–Chow stabilisation. This shows that even in its original dynamic form (Eq. 58), it is in fact just a scaled version of Rhie–Chow stabilisation, and is equivalent for a specific choice of scaling parameters.

Using the 2-D square grid (Fig. 12) as before, the computational stencil and coefficients resulting from the Rhie–Chow and Jameson–Schmidt–Turkel stabilisation terms can be graphed (Fig. 15). Scale factors of $\alpha^{\text{stab}} = (1/4)$ for the Jameson–Schmidt–Turkel term and $\alpha^{\text{stab}} = 1$ for the Rhie–Chow term are chosen so that the magnitude of the terms are similar. For this grid, both approaches produce similar coefficients, however, the Jameson–Schmidt–Turkel approach differs in that it includes additional coupling in the corner coefficients. It can also be seen that both approaches require a large computational stencil, in that second face-neighbours are needed. When either of these stabilisation approaches are combined with one of the face gradient calculations methods discussed above, the stencil of coefficients are summed. For example, the computational stencil and coefficients from face gradient calculation method 1 with Rhie–Chow stabilisation are shown in Fig. 16a, and from face gradient calculation method 2 with Jameson–Schmidt–Turkel stabilisation in Fig. 16b.

Within literature, a number of authors have described stabilisation techniques, however, stability analysis of finite volume discretisations for solid mechanics is not common. Of course, the stability of a formulation quickly becomes apparent in use, however, we can also take inspiration from finite element approaches [407] and analyse the stiffness matrix eigenvalues. Taking a single unconstrained finite element, the number of zero eigenvalues of the stiffness matrix indicates the number

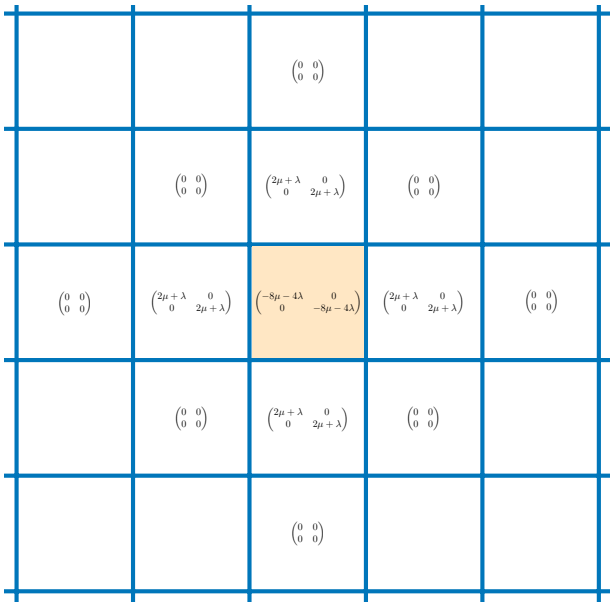


**Fig. 14** Stiffness matrix coefficients for methods 2 and 3 when a segregated solution algorithm is used; the inter-component coupling terms are included via the source vector in a deferred correction manner. (Color figure online)

of zero energy modes. For a stable formulation, the number of zero valued eigenvalues is equal to the number of rigid degrees of freedom; in 3-D, there are three rigid translations and three rigid rotations, whereas in 2-D there are two rigid translations and one rigid rotation. For an unstable formulation, there will be additional zero valued eigenvalues, where the corresponding eigenvector indicates the unstable mode. For the finite volume method, an equivalent analysis of an individual cell/element is less obvious. One such approach is to consider a periodic patch of finite volume cells, containing a central cell and all neighbour cells within its computational stencil (Fig. 17), and analyse the eigenvalues of its (block-coupled) global stiffness matrix. In this case, as there are 9 cells, each with 2 degrees of freedom, the global stiffness matrix is $18 \times 18$. As each cell contains all eight other cells in their stencil (due to the periodic conditions), the stiffness matrix is fully dense (no zero block entries). In this case, using face gradient calculation method 2, the stiffness matrix contains 2 zero eigenvalues, corresponding to the two rigid translation directions; the periodic conditions prohibit rigid rotation; this indicates that the discretisation is stable in this configuration. In addition to analysing a periodic patch of *internal* cells, it may also be necessary to examine a patch of cells adjacent to a boundary. The discretisation at boundary faces is typically different than at internal faces, and so boundaries may quell or excite spatial instabilities.

### 3.5.4 Solution Methodology

Like other popular numerical methods, the finite volume method can employ implicit or explicit solution algorithms. The relative merits of implicit vs explicit approaches are independent of the finite volume method; the interested reader can find numerous textbooks addressing this topic, for example, [407–409].

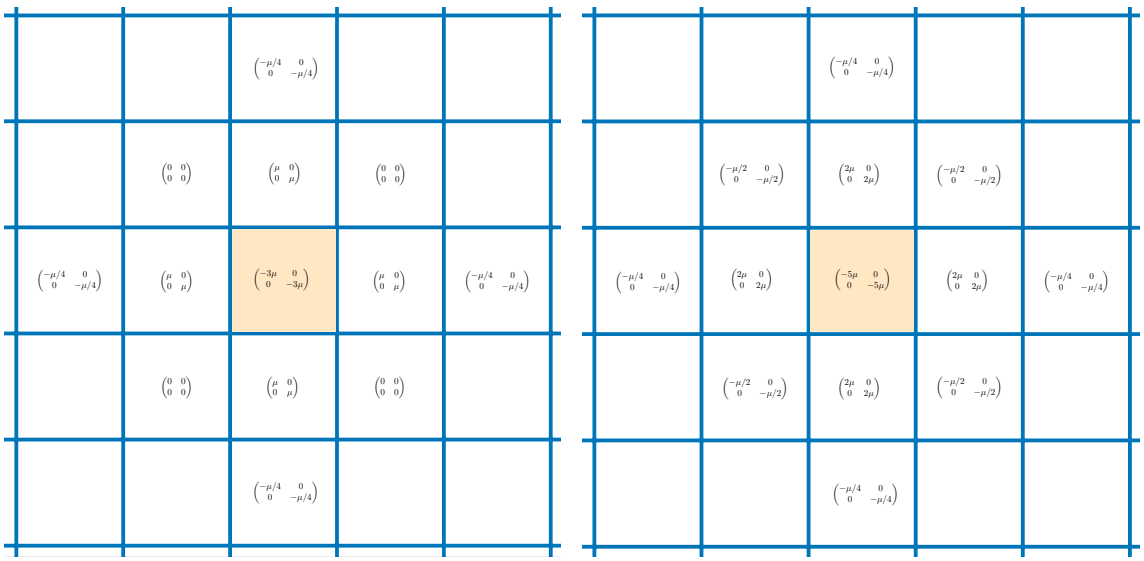


(a) Rhie-Chow with a scale factor $\alpha^{\text{stab}} = 1$

(b) Jameson-Schmidt-Turkel with a scale factor $\alpha^{\text{stab}} = (1/4)$

**Fig. 15** A comparison of the block coefficients in the stiffness matrix for the centre node/cell for two styles of stabilisation term: Rhie–Chow and Jameson–Schmidt–Turkel. (Color figure online)

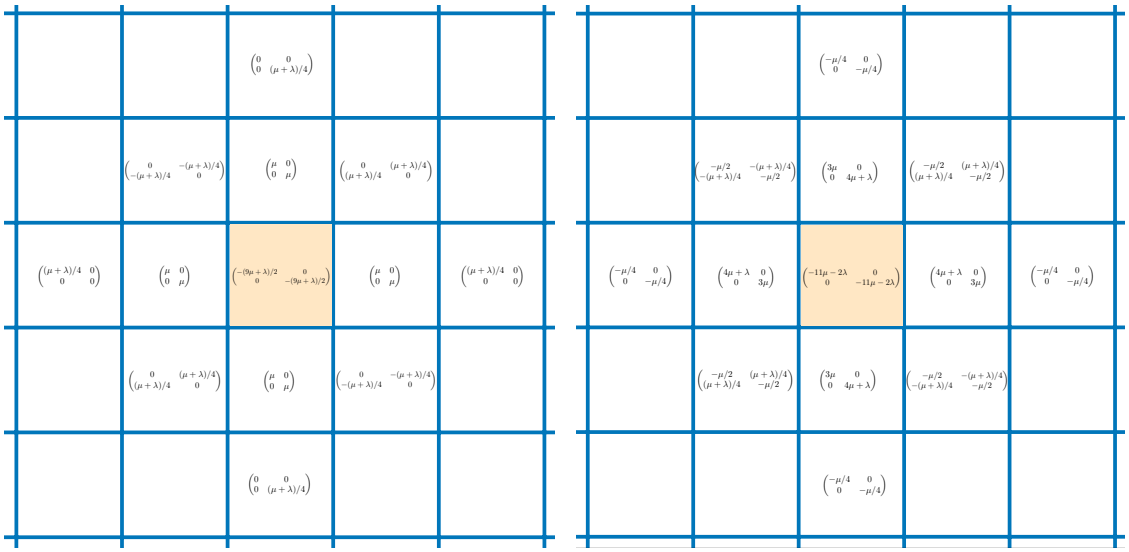

(a) Face gradient calculation method 1 with Rhie-Chow stabilisation, to be compared with Figure 13(a)

(b) Face gradient calculation method 2 with Jameson-Schmidt-Turkel stabilisation, to be compared with Figure 13(b)

**Fig. 16** The effect on the stiffness matrix coefficients by including stabilisation terms. (Color figure online)

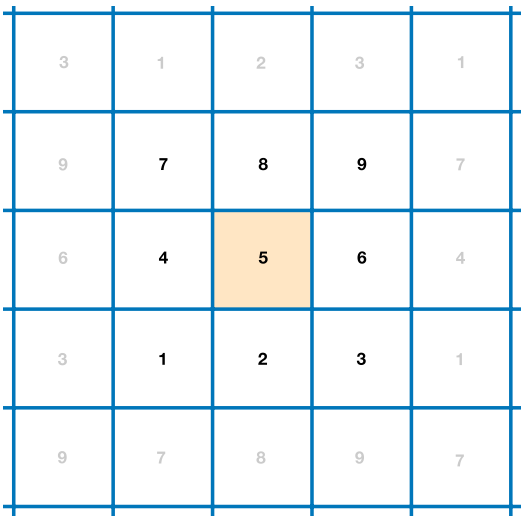


**Fig. 17** A periodic patch of finite volume cells, containing a central cell (cell 5) and all neighbour cells within its computational stencil. The periodic/cyclic neighbours are indicated as cells in grey numbering. (Color figure online)

#### 3.5.5 A Generalised Finite Volume Method for Solid Mechanics

Based on these four components, it is possible to describe a generalised approach encompassing all individual variants, as shown in Fig. 18. Common approaches are indicated by the coloured lines: implicit cell-centred (green), implicit vertex-centred (blue), explicit Godunov-type (red), and staggered-grid (purple). This figure allows the relationship between the variants to be concisely expressed. What is also apparent from this figure is that there are avenues that have yet to be fully explored.

## 4 Comparing of the Finite Volume Method for Computational Solid Mechanics with the Finite Element Method

Within this section, the finite volume method for solids mechanics is compared with the "standard" continuous Bubnov–Galerkin finite element method, for example, as described by Bathe [408], Zienkiewicz and Taylor [410], and Belytschko et al. [407]. Following the approach taken in the previous section, the finite element method will be compared to the finite volume method in terms of: (a) discretisation of space and time; (b) discretisation of the mathematical model equations; and (c) solution algorithm.

### 4.1 Discretisation of Time and Space

Like the finite volume method, the finite element method follows the standard time-marching temporal discretisation approach. Similarly, the solution domain space is divided into a finite number of convex cells (or elements) that do not overlap and fill the space completely. With regard to the mesh, the following differences can be noted between the finite element method and each of the finite volume variants:

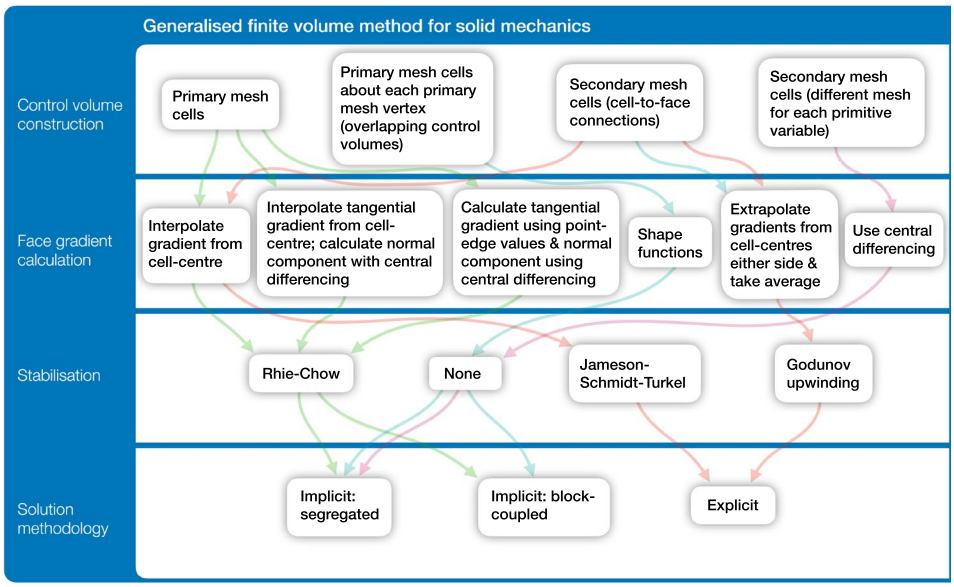


**Fig. 18** Generalisation of the finite volume method for solid mechanics, allowing the creation of any scheme through appropriate selection of four key components: (1) control volume construction method, (2) face gradient calculation approach, (3) stabilisation technique, and (4) solution methodology. Common approaches are indicated by the coloured lines: implicit cell-centred (green), implicit vertex-centred (blue), explicit Godunov-type (red), and staggered-grid (purple). (Color figure online)

- The cell-centred approach and vertex-centred approaches which *do not* use shape functions are applicable to general convex polyhedra in 3-D and general polygons in 2-D, whereas the standard finite element method is limited to standard element shapes, such as hexahedra/tetrahedra in 3-D and quadrilaterals/triangles in 2-D. A consequence of this it that 'hanging nodes' (Fig. 19) are common in finite volume analyses but not directly possible with the standard finite element method;
- The vertex-centred (and hypothetically cell-centred) approaches which *do* use shape function are limited to the same types of meshes used by the standard finite element method.

## 4.2 Discretisation of the Mathematical Model Equations

In Sect. 3.1, the conservation of linear momentum in strong integral form (Eq. 1) was taken as the starting point for the finite volume discretisation. In contrast, the finite element method requires the weak form of the governing equation, and hence begins with the strong differential form:

$$\rho\frac{\partial^2\boldsymbol{u}}{\partial t^2} = \boldsymbol{\nabla}\cdot\left[\mu\boldsymbol{\nabla u} + \mu(\boldsymbol{\nabla u})^T + \lambda\,\mathrm{tr}(\boldsymbol{\nabla u})\mathbf{I}\right] + \rho\boldsymbol{f}_b \tag{60}$$

This form is then multiplied by an arbitrary continuous weighting function $\boldsymbol{\omega}$ and integrated over the material volume to give the conservation of momentum in weak form:

$$\int_\Omega \boldsymbol{\omega}\cdot\left\{\rho\frac{\partial^2\boldsymbol{u}}{\partial t^2} - \boldsymbol{\nabla}\cdot\left[\mu\boldsymbol{\nabla u} + \mu(\boldsymbol{\nabla u})^T + \lambda\,\mathrm{tr}(\boldsymbol{\nabla u})\mathbf{I}\right] - \rho\boldsymbol{f}_b\right\}\mathrm{d}\Omega = \mathbf{0} \tag{61}$$

Unsurprisingly a finite volume method is recovered if the weighting functions $\boldsymbol{\omega}$ are taken as unity within the control volumes and zero elsewhere.

To derive the finite element method, the weak form (Eq. 61) is rearranged using integration by parts combined with the Gauss divergence theorem:

$$\int_\Omega \rho\boldsymbol{\omega}\cdot\frac{\partial^2\boldsymbol{u}}{\partial t^2}\,\mathrm{d}\Omega + \int_\Omega \boldsymbol{\nabla\omega} : \overbrace{\left[\mu\boldsymbol{\nabla u} + \mu(\boldsymbol{\nabla u})^T + \lambda\,\mathrm{tr}(\boldsymbol{\nabla u})\mathbf{I}\right]}^{\sigma}\mathrm{d}\Omega = \oint_{\Gamma_T}\boldsymbol{\omega}\cdot\boldsymbol{T}_\Gamma\,\mathrm{d}\Gamma + \int_\Omega \rho\boldsymbol{\omega}\cdot\boldsymbol{f}_b\,\mathrm{d}\Omega \tag{62}$$

where $\Gamma_T$ is the region of the domain boundary where tractions $\boldsymbol{T}_\Gamma$ are applied. In the second term on the left-hand side of Eq. (62), the differential operator now acts on the

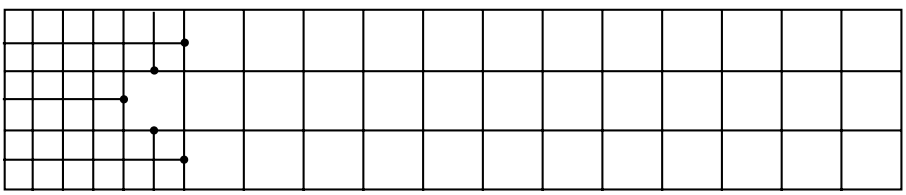

**Fig. 19** 2-D quadrilateral mesh of a beam, where 'hanging nodes' are shown as black dots. (Color figure online)

weighting function $\boldsymbol{\omega}$, in contrast to Eq. (1) where it acts on the stress tensor $\boldsymbol{\sigma}$. It is assumed that the weighting functions, also known as test functions, satisfy the following requirements [407]:

- They are *not* functions of time;
- They are $C^0$ continuous;
- They vanish on displacement boundaries.

Interpreting the weighting functions $\boldsymbol{\omega}$ as *virtual displacements* allows Eq. (62) to be viewed as the principle of virtual work. In this way, the original problem of trying to find a displacement field which satisfies the conservation of linear momentum can be reinterpreted as trying to find a displacement field which minimises the total energy.

The finite element method then assumes the displacement $\boldsymbol{u}$ within each mesh element to vary according to *shape functions*, as presented previously in Eq. (25). The standard *Bubnov–Galerkin* form of the finite element method is achieved by assuming that the weighting functions $\boldsymbol{\omega}$ in Eq. (62) are approximated using the same shape functions as the displacement field:

$$\boldsymbol{\omega} = \sum_{A=1}^{nVertices} N_A \bar{\boldsymbol{\omega}}_A \tag{63}$$

where $\bar{\boldsymbol{\omega}}_A$ represents the discrete weighting function value at vertex $A$; uppercase letter $A$ is used as an index for vertices to avoid confusion with index notation $i, j$ and $k$.

Combining Eqs. 25 (displacement shape functions), 63 and 62, the finite element equations are expressed as [411]:

$$\underbrace{\int_\Omega \rho \sum_{A=1}^{nVertices} N_A \bar{\boldsymbol{\omega}}_A \cdot \sum_{B=1}^{nVertices} N_B \frac{\partial^2 \boldsymbol{u}_B}{\partial t^2} \, \mathrm{d}\Omega}_{\text{Inertial force term}}$$
$$+ \underbrace{\int_\Omega \sum_{A=1}^{nVertices} \nabla N_A \bar{\boldsymbol{\omega}}_A : \left[ \mu \sum_{B=1}^{nVertices} \nabla N_B \boldsymbol{u}_B + \mu \sum_{B=1}^{nVertices} \boldsymbol{u}_B \nabla N_B + \lambda \, \mathrm{tr}\left( \sum_{B=1}^{nVertices} \nabla N_B \boldsymbol{u}_B \right) \mathbf{I} \right] \mathrm{d}\Omega}_{\text{Internal force term}}$$
$$= \underbrace{\oint_{\Gamma_T} \sum_{A=1}^{nVertices} N_A \bar{\boldsymbol{\omega}}_A \cdot \boldsymbol{T}_\Gamma \, \mathrm{d}\Gamma}_{\text{External (surface) force term}} + \underbrace{\int_\Omega \sum_{A=1}^{nVertices} N_A \bar{\boldsymbol{\omega}}_A \cdot \rho \boldsymbol{f}_b \, \mathrm{d}\Omega}_{\text{External (body) force term}} \tag{64}$$

To proceed, we will switch to index notation, not referring to spatial directions $i$ and $j$ or nodes $A$ and $B$, but instead to the degrees of freedom [411]. For this, the index for a global degree of freedom $P$ can be given uniquely in terms of the spatial index and node index:

$$P = f(i, A) \tag{65}$$

Examining Eq. (64) term by term and using both index notation and degree of freedom notation, the inertial force term can be expanded as:

$$\begin{aligned}
&\int_\Omega \rho \sum_{A=1}^{nVertices} N_A \bar{\boldsymbol{\omega}}_A \cdot \sum_{B=1}^{nVertices} N_B \frac{\partial^2 \boldsymbol{u}_B}{\partial t^2} \, \mathrm{d}\Omega \\
&= \sum_{A=1}^{nVertices} \sum_{i=1}^{nDims} \int_\Omega \rho N_A \bar{\omega}_{iA} \sum_{B=1}^{nVertices} N_B \frac{\partial^2 U_{iB}}{\partial t^2} \, \mathrm{d}\Omega \\
&= \sum_{A=1}^{nVertices} \sum_{i=1}^{nDims} \bar{\omega}_{iA} \sum_{B=1}^{nVertices} \sum_{j=1}^{nDims} \int_\Omega \rho N_A \delta_{ij} N_B \frac{\partial^2 U_{iB}}{\partial t^2} \, \mathrm{d}\Omega \\
&= \sum_{P=1}^{nDoF} \bar{\omega}_P \sum_{Q=1}^{nDoF} M_{PQ} \frac{\partial^2 U_Q}{\partial t^2} \, \mathrm{d}\Omega
\end{aligned} \tag{66}$$

where $nDims$ is the number of spatial dimensions, $\delta_{ij}$ is the Kronecker delta, and $nDoF = nDims \times nVertices$ is the number of global degrees of freedom. Matrix $M_{PQ}$ is known as the mass matrix and is given as:

$$M_{PQ} = \int_\Omega \rho N_A \delta_{ij} N_B \, \mathrm{d}\Omega \tag{67}$$

The volume integral can be calculated (or approximated) using Gaussian/numerical quadrature:

$$M_{PQ} \approx \sum_{p=1}^{nQuadPoints} w_p \, \rho(\xi_p) \, N_A(\xi_p) \, \delta_{ij} \, N_B(\xi_p) \tag{68}$$

where *nQuadPoints* is the number of quadrature points, $w$ is the quadrature weight, and $\xi$ is the quadrature location within the element. For example, using one-point quadrature, the quadrature locations are situated at the centroids of the elements; in that case, the density and the derivative of the shape functions are evaluated at element centroids.

Unlike finite volume approaches, the resulting mass matrix will not in general be diagonal; however, diagonalisation or *lumping* of the mass matrix is common, although often ad hoc [407]; for example, the row-sum technique calculates the diagonal elements as the sum of the coefficients for that row.

The internal force term in Eq. (64) can be simplified as:

$$\begin{aligned}
&\int_\Omega \sum_{A=1}^{nVertices} \boldsymbol{\nabla} N_A \bar{\boldsymbol{\omega}}_A \; : \; \left[ \mu \sum_{B=1}^{nVertices} \boldsymbol{\nabla} N_B \boldsymbol{u}_B + \mu \sum_{B=1}^{nVertices} \boldsymbol{u}_B \boldsymbol{\nabla} N_B + \lambda \, \mathrm{tr}\left( \sum_{B=1}^{nVertices} \boldsymbol{\nabla} N_B \boldsymbol{u}_B \right) \mathbf{I} \right] \mathrm{d}\Omega \\
&= \int_\Omega \sum_{A=1}^{nVertices} \sum_{i=1}^{nDims} \sum_{j=1}^{nDims} N_{A,j} \bar{\omega}_{iA} \left( \mu N_{B,j} U_{iB} + \mu N_{B,i} U_{jB} + \lambda N_{B,k} U_{kB} \delta_{ij} \right) \mathrm{d}\Omega \\
&= \sum_{P=1}^{nDoF} \bar{\omega}_P K_{PQ} U_Q
\end{aligned} \tag{69}$$

where matrix $K_{PQ}$ is known as the stiffness matrix:

$$K_{PQ} = \int_\Omega \sum_{j=1}^{nDims} N_{A,j} \left[ \mu N_{B,j} + \mu N_{B,i} + \lambda N_{B,i} \delta_{ij} \right] \mathrm{d}\Omega \tag{70}$$

The integral can once again be evaluated using Gaussian/numerical quadrature:

$$K_{PQ} \approx \sum_{p=1}^{nQuadPoints} \sum_{j=1}^{nDims} w_p \, N_{A,j}(\xi_p) \left[ \mu(\xi_p) N_{B,j}(\xi_p) + \mu(\xi_p) N_{B,i}(\xi_p) + \lambda(\xi_p) N_{B,i}(\xi_p) \, \delta_{ij} \right] \tag{71}$$

Evaluating this integral exactly (using sufficient quadrature points) would naively appear to be the best approach; however, formulations that use *full* integration tend to suffer from locking [407], which can be described as an overly stiff behaviour in bending. Consequently, *reduced* integration is often favoured, where the local field is under-integrated. This reduced integration has the benefit of relieving this locking phenomena as well as reducing the computational time, due to the lower number of integration points.

A downside of reduced integration is the introduction of spatial instabilities into the discretisation. In essence, the element is capable of deforming in certain *modes* which offer no resistance. These spurious singular or zero energy modes produce an accordion-like deformation pattern known as hourglassing. Similar to the finite volume method, a stabilisation term is included in the formulation to suppress such spatial instabilities. For the finite element method, this hourglass stabilisation is incorporated through the inclusion of a stabilisation stiffness within the element stiffness matrix, or a viscous stabilisation term for dynamic problems [407]. For static problems a variety of stabilisation methods have been proposed, but typically a *stabilisation stiffness* term $K^{\mathrm{stab}}_{PQ}$ is added to the element stiffness matrix of the form [407, 412]:

$$K^{\mathrm{stab}}_{PQ} = \alpha_{\mathrm{stab}} \, \mu \, N^{\mathrm{stab}}_{A,j} \, N^{\mathrm{stab}}_{B,j} \, \Omega \tag{72}$$

where $N^{\mathrm{stab}}_{A/B,j}$ represents the gradient interpolators used to define the hourglass deformation modes. The $\alpha_{\mathrm{stab}}$ is a scaling factor typically set between 0.005 and 0.1 [407, 412], depending on the form of $N^{\mathrm{stab}}_{A,j}$. For volumetric spatial instabilities, $\mu$ is replaced by the bulk modulus, $\kappa = (2/3)\mu + \lambda$, and $N^{\mathrm{stab}}_{A,j}$ represents the gradient interpolators for the volumetric/pressure hourglass mode.

Finally, the two external force terms in Eq. (64) are expressed as:

$$\oint_{\Gamma_T} \sum_{A=1}^{nVertices} N_A \bar{\boldsymbol{\omega}}_A \cdot \boldsymbol{T}_\Gamma \, \mathrm{d}\Gamma + \int_\Omega \sum_{A=1}^{nVertices} N_A \bar{\boldsymbol{\omega}}_A \cdot \rho \boldsymbol{f}_b \, \mathrm{d}\Omega = \sum_{P=1}^{nDoF} \bar{\omega}_P F_P \tag{73}$$

where vector $F_P$ is known as the global force vector:

$$F_P = \oint_{\Gamma_T} \sum_{A=1}^{nVertices} N_A T_{i\Gamma} \, \mathrm{d}\Gamma + \int_{\Omega} \sum_{A=1}^{nVertices} \rho N_A f_{ib} \, \mathrm{d}\Omega \tag{74}$$

and once again the integrals are evaluated using quadrature.

Equation (64) can now be expressed as:

$$\bar{\boldsymbol{\omega}}^T \left( \boldsymbol{M} \frac{\partial^2 \boldsymbol{U}}{\partial t^2} + \boldsymbol{K}\boldsymbol{U} - \boldsymbol{F} \right) = \boldsymbol{0} \tag{75}$$

where the global vectors of dimension $nDoF \times 1$ are:

$$\bar{\boldsymbol{\omega}} = [\bar{\omega}_P], \quad \boldsymbol{U} = [U_P], \quad \boldsymbol{F} = [F_P] \tag{76}$$

and global matrices of dimension $nDoF \times nDoF$ are:

$$\boldsymbol{M} = [M_P], \quad \boldsymbol{K} = [K_P] \tag{77}$$

As Eq. (75) is satisfied for all values of $\bar{\boldsymbol{\omega}}$, this requires that the bracketed term is equal to zero. This gives the semi-discrete form (discrete in space, not in time) of the finite element equations:

$$\boldsymbol{M} \frac{\partial^2 \boldsymbol{U}}{\partial t^2} + \boldsymbol{K}\boldsymbol{U} = \boldsymbol{F} \tag{78}$$

To complete the discretisation, the acceleration term $\frac{\partial^2 \boldsymbol{U}}{\partial t^2}$ is discretised using a finite difference scheme. Similar to the finite volume approaches, many finite difference schemes can be used, where Newmark schemes are popular. The simple Euler backward scheme is given here for comparative purposes:

$$\boldsymbol{M} \frac{\boldsymbol{U} - 2\boldsymbol{U}^{[m-1]} + \boldsymbol{U}^{[m-2]}}{\Delta t^2} + \boldsymbol{K}\boldsymbol{U} = \boldsymbol{F} \tag{79}$$

Boundary tractions/forces have already been included in $\boldsymbol{F}$ via the external (surface) force term in Eq. (64). For the incorporation of displacement conditions, this signifies that some of the degrees of freedom in $\boldsymbol{U}$ are known; these equations can hence be disregarded. As in the case with the finite volume methods, initial conditions, in the form of the displacement field at $t = 0$, $t = -\Delta t$, and $t = -2\Delta t$, must also be specified.

## 4.3 Solution Algorithm

Once known degrees of freedom have been incorporated, Eq. (79) represents a system of $nDoF - nKnownDof$ linear algebraic equations, where $nKnownDof$ is the number of known degrees of freedom. Similar to the analogous matrices in the finite volume method, the mass matrix is a function of the density and element geometry; the stiffness matrix is a function of the mechanical properties and element geometry; and the force vector $\boldsymbol{F}$ contains surface and body force contributions as well as inertial terms and non-zero known degree of freedom contributions. Like the finite volume approaches, this system of algebraic equations can be solved using either an implicit or explicit time marching procedure.

For implicit approaches, Eq. (79) can be rearranged and solved for $\boldsymbol{U}$:

$$\left( \frac{1}{\Delta t^2} \boldsymbol{M} + \boldsymbol{K} \right) \boldsymbol{U} = \boldsymbol{F} + \boldsymbol{M} \frac{2\boldsymbol{U}^{[m-1]} - \boldsymbol{U}^{[m-2]}}{\Delta t^2} \tag{80}$$

Assuming a stable discretisation, the matrix of the linear system $\left( \frac{1}{\Delta t^2} \boldsymbol{M} + \boldsymbol{K} \right)$ (or $\boldsymbol{K}$ for quasi-static) has the following properties:

- It is sparse with the number of non-zero elements in each row equal to the number of vertices which share an element with the current vertex, plus one;
- It is symmetric;
- It is positive definite;
- In general, unlike for the cell-centred finite volume approaches where a segregated algorithm is used, it is not diagonally dominant; however, finite volume discretisations that employed block-coupled solution methodologies will produce a similar non-diagonally dominant matrix.

To solve Eq. (80), typically a direct linear solver is employed, for example, Gaussian elimination, LU decomposition or multi-frontal methods; however, iterative methods such as preconditioned conjugate gradient are also possible [408].

## 4.4 Discussion

### 4.4.1 Overview

Given the close relationship between the finite volume and finite element methods, it is not surprising that both have been compared previously: some notable dissections include those from Oñate, Zienkiewicz, Idelsohn [6, 8, 11, 12, 413–416], Lahrmann [417], Perré and Passard [293], Harrild and Henriquez [418], Zarrabi and Basu [55], Fang et al. [419], Yamamoto et al. [420], Jacquemet and Henriquez [421, 422], Vaz Jr. et al. [37], Filippini et al. [423], and recently Demirdžić [424]. The general consensus is that both methods share the same data structure and general strategy to assemble the corresponding characteristic matrices, with the main conceptual difference being in the local integration domain and local integration method. Although a number of authors have claimed superior accuracy of one method over the other [37, 417, 418], the majority of authors have found both methods to produce similar predictions with no significant differences [293, 419, 420, 422].

One generally accepted appeal of the finite volume method is the ease with which it can be followed and implemented: the finite volume method is simply based on balancing forces acting on a volume, requiring no knowledge of advanced mathematical frameworks. Comparing the derivations in Sects. 3.2 and 4.2, the finite element approach would appear to be more mathematically involved; however, proponents of the finite element method claim that the principle of virtual work and energy minimisation techniques are as equally interpretable as the balance equation form.

#### 4.4.2 Weak Vs. Strong Forms of the Conservation Law and the Implications

As discussed, finite volume and finite element methods differ is their philosophy: where the finite volume method deals with the strong balance form of the governing law, the finite element method deals with the equivalent weak virtual energy form. One consequence of this is the manner in which local conservation is enforced. As finite volume approaches discretise surface integrals at the (typically non-overlapping) control volume boundaries, strong local conservation is achieved: forces are equal and opposite at cell boundaries. As a consequence of this local conservation, global conservation within the domain is automatically achieved. In contrast, finite element methods discretise the surface force term as a volume integral using locally overlapping integration domains: this results in local conservation in an average sense, rather than directly for each element. Global conservation is ensured in an average sense, assuming there are sufficient numbers of elements. An additional consequence of these contrasting approaches is how each method treats Neumann/natural boundary conditions: considering traction conditions, finite volume methods satisfy these conditions exactly regardless of the mesh density; whereas finite element approaches satisfy them in an approximate sense, and as the mesh is refined strong enforcement is approached.

As noted by a number of authors, for example, [11, 12, 24], by choosing unity weighting functions in the weak form of the governing equation (Eq. 62), it is possible to recover the finite volume method. Spalding [321] alludes to this point by referring to finite volume approaches as *unity-weighting function methods* and to finite element approaches as *non-unity weighting function methods*.

#### 4.4.3 Geometric Flexibility

As *standard* finite element methods use shape functions to define a continuous displacement distribution, this limits their application to meshes containing *standard* element shapes. Concretely, only standard shapes such as triangles and quadrilaterals are allowed in 2-D, and tetrahedra and hexahedra in 3-D. Similarly, finite volume approaches that explicitly use shape functions are constrained in the same way. More commonly finite volume methods describe the local solution distribution using a truncated Taylor expansion, resulting in discontinuous jumps at the cell interfaces. An outcome of this is the ability of finite volume approaches to deal with general convex polyhedral meshes. In this way, finite volume approaches are more flexible in terms of mesh generation and dynamic remeshing. In addition to hanging nodes, typical finite volume discretisations can deal with overset/*chimera* and immersed boundary meshes in a straight-forward manner.

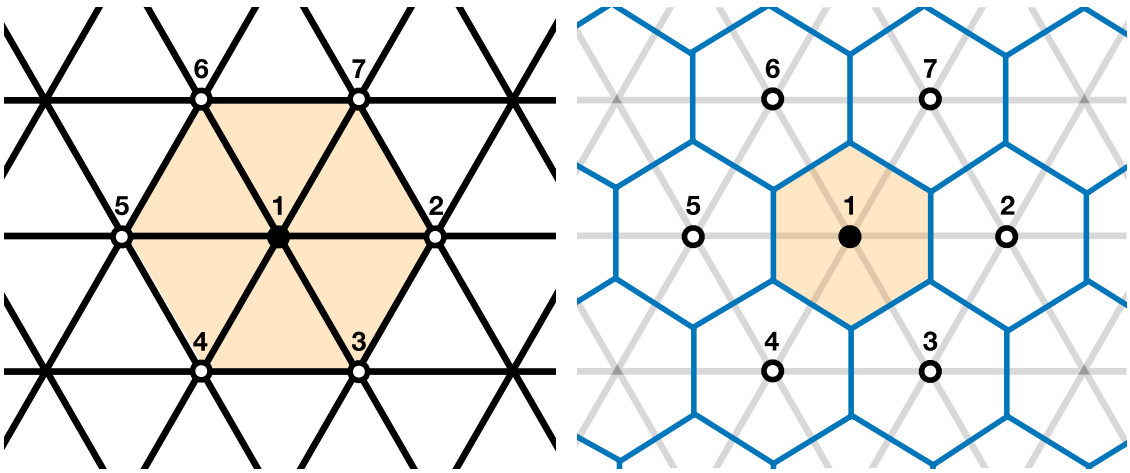


(a) Local integration domain around a vertex in the finite element method

(b) Local integration domain for a cell in the finite volume method

**Fig. 20** Uniform 2-D triangular grid showing the local integration domains and computational stencils for the finite element and finite volume methods. The centre node is shown as a black dot and all neighbouring nodes are shown as white-filled dots, where nodes are vertices in the finite element method, and are cell-centres in the finite volume method. (Color figure online)

#### 4.4.4 Mass Matrix and Stiffness Matrix Properties

A desirable property of final volume methods for explicit implementation and parallelisation is that the mass matrix is automatically diagonal. For finite element methods, the lack of a diagonal consistent mass matrix results in the use of so-called *mass lumping* approaches, which are often ad-hoc, as noted previously. The stiffness matrix, however, bares many similarities between the methods.

To allow direct comparison, let us consider finite volume and finite element discretisations on a uniform equilateral-triangular grid (Fig. 20). We will consider a typical domain of integration around a node, where a node represents a vertex in the finite element method and a cell-centre in the finite volume method. For ease of comparison, the dual mesh is used for the finite volume method. In the finite element case (Fig. 20a), the local integration domain (shaded in orange) consists of all elements adjacent to the centre node (black-filled dot). Consequently, the computational stencil for the centre vertex consists of the six neighbouring vertices (indicated by white-filled dots), which share an element with the centre node. In the finite volume case (Fig. 20b), the local integration domain (shaded in orange) is the cell itself containing the node at its centre (black-filled dot); the computational stencil includes all neighbouring cell-centres (white-filled dots). In this case, as both methods share the same computational stencil, the resulting stiffness matrices will share the same structure and sparsity, *assuming* that the same solution strategy is used, for example, block-coupled or segregated. For a triangular grid, *either* the nodal locations *or* the orientation of the local integration domains can be aligned between the methods, but not both; as such, the comparison of coefficients from both methods is not entirely direct, however, it does still provide insight. Here it was

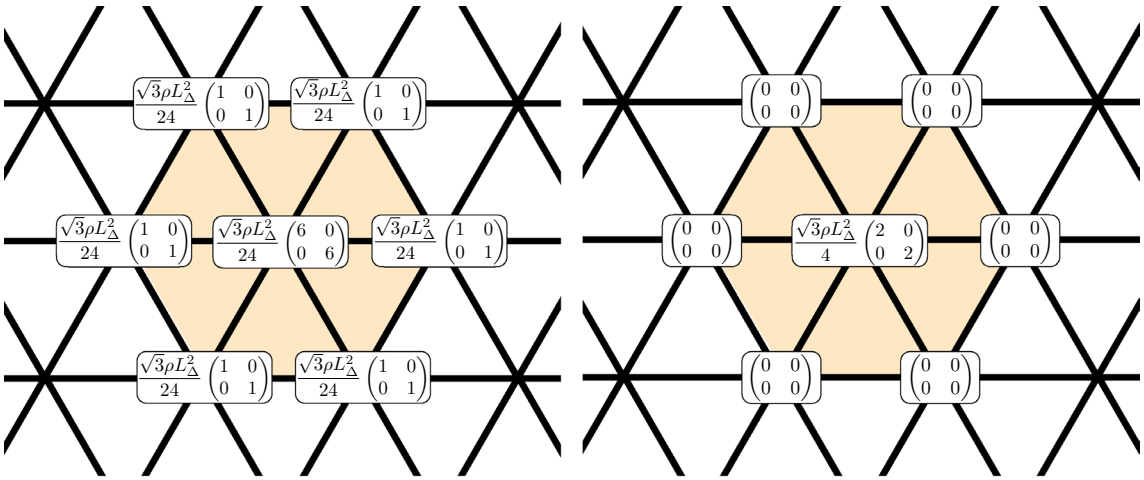


(a) Finite element method *consistent* mass matrix

(b) Finite element method *lumped* mass matrix

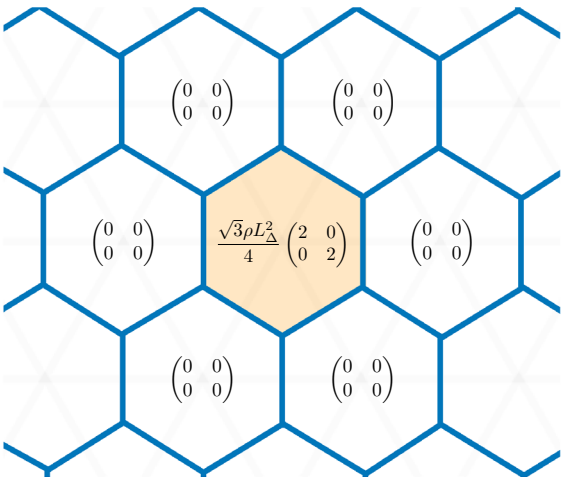


(c) Finite volume method

**Fig. 21** Block coefficients for a row in the mass matrix corresponding to the centre node, where $L_\Delta$ is the triangle side-length, a unit thickness is assumed, and $\frac{\sqrt{3}}{4}L_\Delta^2$ is the area of a triangular element. The area of the hexagonal finite volume cell is equal to $\frac{\sqrt{3}}{2}L_\Delta^2$. (Color figure online)

chosen to align the nodal locations rather than the local integration domains: the finite volume cell can be seen to be rotated 90° relative to the finite element cell, as well as being one third the area.

It is important to mention that the size and shape of the computational stencil in the finite volume method depend on the approach used to calculate the displacement gradients at the cell faces. Here face gradient calculation method 2 in Sect. 3.5 has been employed. Alternative face gradient calculation methods can result in the *second cell-neighbours* being included in the stencil; in contrast, a characteristic of the finite element method is that the integration domain is fixed regardless of local discretisation.

An additional observation is that the local integration domains overlap in the finite element method, but do not in the typical finite volume method i.e. integration domains for neighbouring finite element nodes overlap. An overlapping version of the vertex-centred finite volume method has been considered by Oñate et al. [12] but has not received significant attention.

Referring to the node numbering given in Fig. 20, the block row for the centre node in the global mass matrix is given for the finite element method [407], consistent and lumped, as well as the finite volume method in Fig. 21. The finite element mass-lumped approach can be seen to coincide with the finite volume approach; from this, we can see that the finite element lumped approach is essentially assigning the mass of the hexagon surrounding a node to the node itself, corresponding with the integration domain of the finite volume approach.

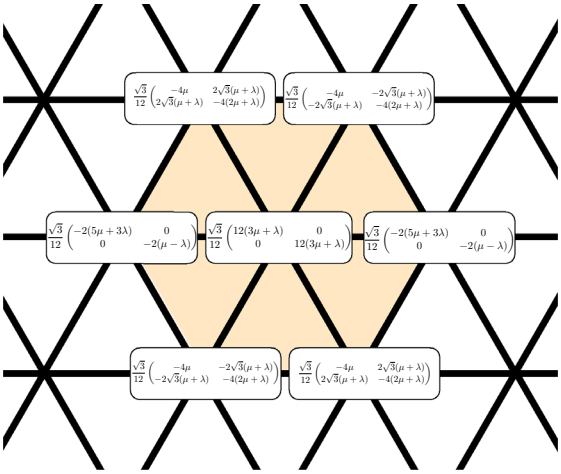

(a) Finite element method stiffness matrix

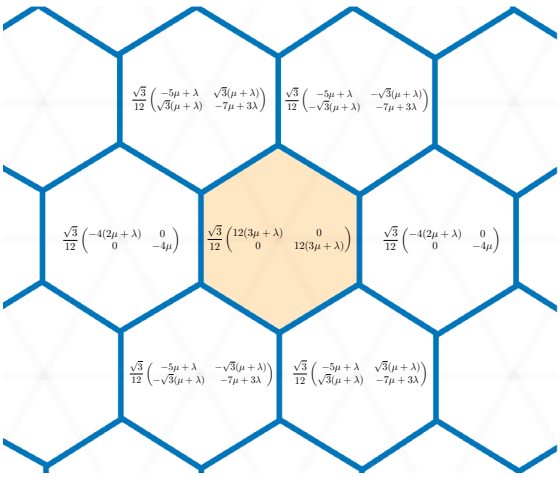

(b) Finite volume method stiffness matrix with a *coupled* solution algorithm

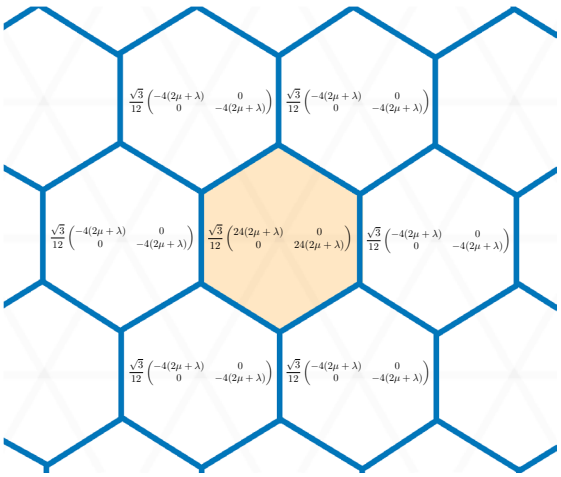

(c) Finite volume method stiffness matrix with a *segregated* solution algorithm

**Fig. 22** Block coefficients for a row in the stiffness matrix corresponding to the centre node, where $L_\Delta$ is the triangle side-length and a unit thickness is assumed. (Color figure online)

Considering next the stiffness matrix. Once again taking the same uniform 2-D triangular grid given in Fig. 20, the block row for the centre node in the global stiffness matrix for the finite element method [407] is compared with the equivalent row from the finite volume method in Fig. 22. For the finite volume method, the matrix using a block-coupled solution algorithm is given, as well as for the segregated approach. Examining the general structure of the coefficients for all three methods (Fig. 22a–c), the following observations can be made:

- All three methods employ the same computational stencil;
- The coefficients are symmetric in all three cases, albeit the effect of boundary conditions has not been considered here;
- As expected, all three methods show geometric symmetries, for example, the top-right coefficient is equal to the bottom-left coefficient;
- The finite element and coupled finite volume approaches show the same sparsity structure i.e. there are zeros in the same locations; in addition, the coefficients have the same signs and show similar magnitudes, but do not have the same value, apart from for the central node;
- The segregated finite volume approach differs from the others by removing all inter-component coupling from the coefficients, as discussed in Sect. 3.5;
- The segregated finite volume approach produces a row of coefficients which is weakly diagonally dominant, also discussed in Sect. 3.5;
- The momentum/force *between nodes* is conserved for all three methods (based on the symmetry of the coefficients), however, conservation of momentum/force *between elements/cells* is *not* directly enforced for the finite element method, whereas it *is* for the finite volume method.

#### 4.4.5 Discretisation Stabilisation

As described in Sect. 4.2, finite element formulations which under-integrate the local domain require the inclusion of a stabilisation term, in the same way one is required in many finite volume formulations. In the finite element method, these spurious singular, zero energy modes produce an accordion-like deformation pattern known as hourglassing (Fig. 23a), named due to its visual similarity to an hourglass timing device. These spatial instabilities are equivalent to checkerboarding instabilities that occur in finite volume formulations (Fig. 23b); these checkerboarding pressure-type instabilities are also possible in finite element formulations. The origin of these spatial instabilities in both finite element and finite volume formulations is a *rank deficiency* in their respective stiffness matrices. Essentially, a stable discretisation should not support any deformation modes which do not offer resistance, apart from rigid body translations and rotations. More precisely, rank deficiency refers to the fact that the discretised stiffness matrix has zero-valued eigenvalues which are not related to rigid body motions (as discussed in Sect. 3.5). For example, considering a 3-D element/cell, the stiffness matrix for a *full rank* formulation has six zero valued eigenvalues: three rigid translations and three rigid rotations; for a rank deficient formulation, additional zero valued eigenvalues are present corresponding to zero energy instability modes.

To address these spatial instabilities, both finite element and finite volume approaches add a stabilisation term to the discretised governing equations. In both cases, there are two primary constraints on the form of this stabilisation term [407]:

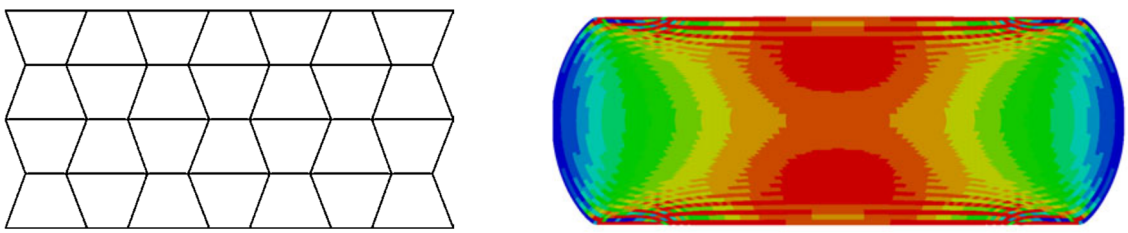

**(a)** Example of the *hourglassing* spatial instabilities in reduced integration finite element formulations (taken from [408])

**(b)** Example of the *checkboarding* spatial instabilities (hydrostatic pressure field) in cell-centred finite volume formulations (taken from [30])

**Fig. 23** The equivalence of spatial instabilities in finite element and finite volume formulations. (Color figure online)

- It should not significantly affect the accuracy of the discretisation, and
- It should not affect the linear completeness of the discretisation; in other terms, the discretisation should still be able capable of describing a linear solution field exactly after the inclusion of the stabilisation term.

For both methods, a variety of techniques exist and the stabilisation *force* often takes a similar form:

$$
\begin{aligned}
\boldsymbol{lf}^{\text{stab}} &= l\alpha^{\text{stab}} C^{\text{stab}} \Omega \left( \boldsymbol{\nabla}^2 \boldsymbol{u} - \boldsymbol{\nabla} \cdot \boldsymbol{\nabla} \boldsymbol{u} \right) l && \text{Rhie–Chow stabilisation} \\
&\quad - \alpha^{\text{stab}} C^{\text{stab}} \Omega \, \boldsymbol{\nabla}^2 \left( \boldsymbol{\nabla}^2 \boldsymbol{u} \right) && \text{Jameson–Schmidt–Turkel stabilisation} \\
f_P^{\text{stab}} &= \alpha^{\text{stab}} C^{\text{stab}} \Omega \, N_{A,j} N_{B,j} U_Q && \text{Hourglass stabilisation}
\end{aligned}
\tag{81}
$$

where $C^{\text{stab}}$ is some measure of mechanical property that gives an appropriate dimension to the dissipation, such as $\mu$, $2\mu + \lambda$, $\mu + \lambda$, or $\kappa$, for quasi-static analyses, or a function of the speed of sound for dynamic analyses. The $\alpha^{\text{stab}}$ factor allows the magnitude of the stabilisation to be scaled.

#### 4.4.6 Performance of the Methods

The differences in local integration domain and local integration method between the finite volume and finite element methods has consequences for the robustness, accuracy and efficiency of the resulting methods. Particularly for nonlinear analysis, the ideal discretisation is unclear due to a variety of numerical challenges which are yet to be fully resolved, including [425]: (1) spurious hourglassing and pressure checker-boarding, (2) bending difficulties, (3) shear and volumetric locking, (4) high frequency noise in the vicinity of shocks, (5) lower order of convergence for strains and stresses in comparison with displacements, and (6) sensitivity to mesh distortions. It is these challenges that finite volume discretisations can potentially solve in a novel way.

Apart from this, a major motivation for finite volume solid mechanics schemes is the challenge of multi-physics problems. As long as the finite volume method is prominent in the world of computational fluid mechanics, there will be a demand for straight-forward finite volume solid mechanics implementations. These solid mechanics implementations can share the same computational framework, discretisation and solution methodologies as their fluid counterparts and can be integrated seamlessly into the code base.

Regarding accuracy and overly stiff behaviour, finite volume methods have not shown the same locking behaviour typical in fully integrated finite element methods. Given their similarity with reduced integrated finite elements, it is perhaps not surprising that this is the case; however, like finite elements, the absolute accuracy depends on the details of the formulation. Concerning order of accuracy, an attractive property of most finite volume methods is that the error in the strain and stress reduces at a second-order rate, like the displacement [37, 208]; this may not be the case for many finite element schemes, where the error in the strain and stress reduce at a rate closer to first order.

As models become larger and the availability of supercomputers and cloud computing increases, code parallelisation is becoming critical. Due to the widespread use of iterative linear solvers, finite volume methods (fluid and solid) commonly exploit hundreds or thousands of CPU cores, for example, the OpenFOAM software. In contrast, as direct linear solvers have often been the chosen solution approach for finite element schemes, parallel efficiency is inherently limited (relative to iterative solvers) and the use of large numbers of CPU cores has been less common; however, there are a number of projects focussed on the application of finite element methods to supercomputers using iterative solvers, for example, ParaFEM [426]. Apart from the choice between direct and iterative linear solver, cell-centred finite volume approaches possess a convenient advantage over vertex-centred methods (such as the finite element method) when it comes to domain decomposition parallelisation: each node (cell-centre) is uniquely located on one CPU core domain. As a result, duplication of nodal data at processor-to-processor boundaries is not required. In contrast, in the finite element method, nodes (vertices) that lie on a processor-to-processor boundary are present on at least two processor domains, requiring the use of *ghost elements* or similar data duplication techniques. A final point related to parallelisation is the debate around open-source vs. commercial software, which equally affects both finite volume and finite element methods. For many, the current *per-CPU-core* pricing of some well known commercial codes may in fact be the greatest practical obstacle to parallel efficiency.

#### 4.4.7 Higher Order Discretisations

Apart from the size of the finite element solid mechanics community, arguably the next greatest advantage of the finite element method over the finite volume method is its straight-forward extension to higher-order discretisation. A key feature of the finite element method is that an element

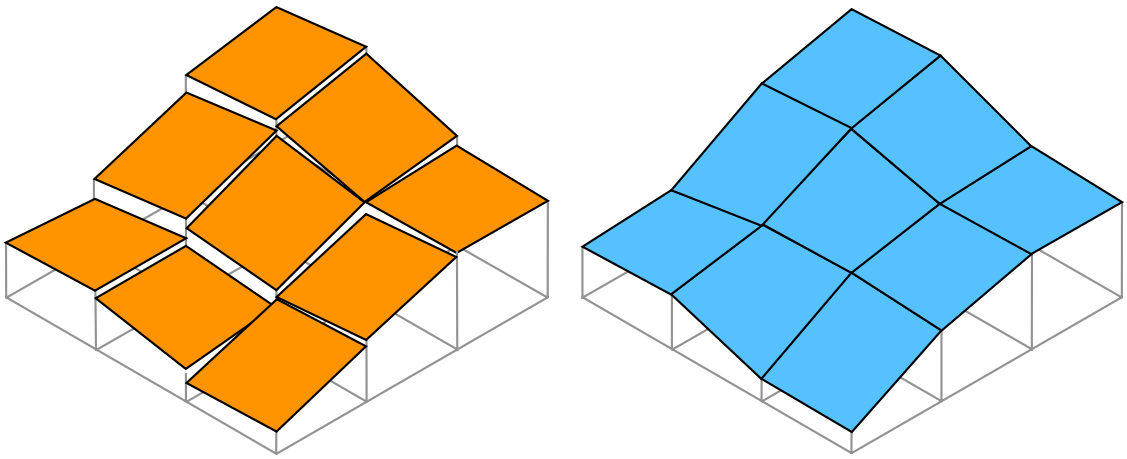

(a) Discontinuous field representation within the finite volume method and discontinuous Galerkin finite element method

(b) Continuous field representation within the finite element method

**Fig. 24** A comparison between the representation of the displacement field in the finite volume method (and discontinuous Galerkin finite element method) and the finite element method. Adapted from Lee et al. [27]. (Color figure online)

is completely characterised by the coordinates and degrees of freedom associated with its nodes/vertices [411]. This compact computational stencil allows uncomplicated inclusion of higher-order local distributions. As noted previously, higher-order finite volume approaches have been developed for solid mechanics [203], however, as the order increases, so does the size of the computational stencil; this introduces significant challenges for unstructured polyhedral grids, and as such, higher-order schemes are not as common as in the finite element field.

For linear analyses, the power of higher-order schemes is undeniable, notwithstanding challenges with locking behaviour, however, for nonlinear analysis such higher order schemes are not commonly used in practice. For example, considering an elasto-plastic analysis, as noted by Belytschko et al. [407], the stress may have discontinuous derivatives at the surface separating elastic and plastic material. In this case, the errors in Gaussian quadrature of an element that contains an elastic–plastic interface are likely to be large; higher-order quadrature is not a solution as it often leads to stiff behaviour or locking. Additionally, finite element users are typically recommended to use lower order formulations for problems that include either contact, large strains or plasticity [412].

#### 4.4.8 Discontinuous Galerkin Methods

The standard *continuous* Bubnov–Galerkin finite element method, as presented above, assumes a continuous distribution of the displacement between elements. In contrast, as shown in Fig. 24, the finite volume method *typically* assumes discontinuous jumps in the displacement field at the interfaces between cells (although it does not have to). There is, however, a class of finite element approaches known as discontinuous Galerkin methods, introduced by Reed and Hill [427], which assume similar jumps in the solution field across element boundaries. In this way, the local integration method adopted by the discontinuous Galerkin method combines features of the finite volume and finite element methods. In particular, discontinuous Galerkin schemes bare the following desirable finite volume properties [428]:

- They produce mass matrices that are block-diagonal;
- They easily handle irregular meshes with hanging nodes;
- They are locally conservative, which is a critical property for computational fluid dynamics.

In addition, a potential advantage of discontinuous Galerkin schemes over finite volume schemes is their ease of extension to higher orders, and the mixing of lower and higher order elements.

Discontinuous Galerkin methods are, however, typically implemented using explicit solution algorithms. The reason they are less suitable for implicit implementations (and analysis of quasi-static type problems) is they possess large numbers of globally-coupled degrees of freedom. To overcome this disadvantage, the so-called *hybridisable* discontinuous Galerkin (HDG) method was introduced by Cockburn et al. [429]. The key characteristic of the hybridisable form was defining *traces* of field variables as single values at cell interfaces, allowing a significant reduction in the number of global unknowns. Detailed analysis of the

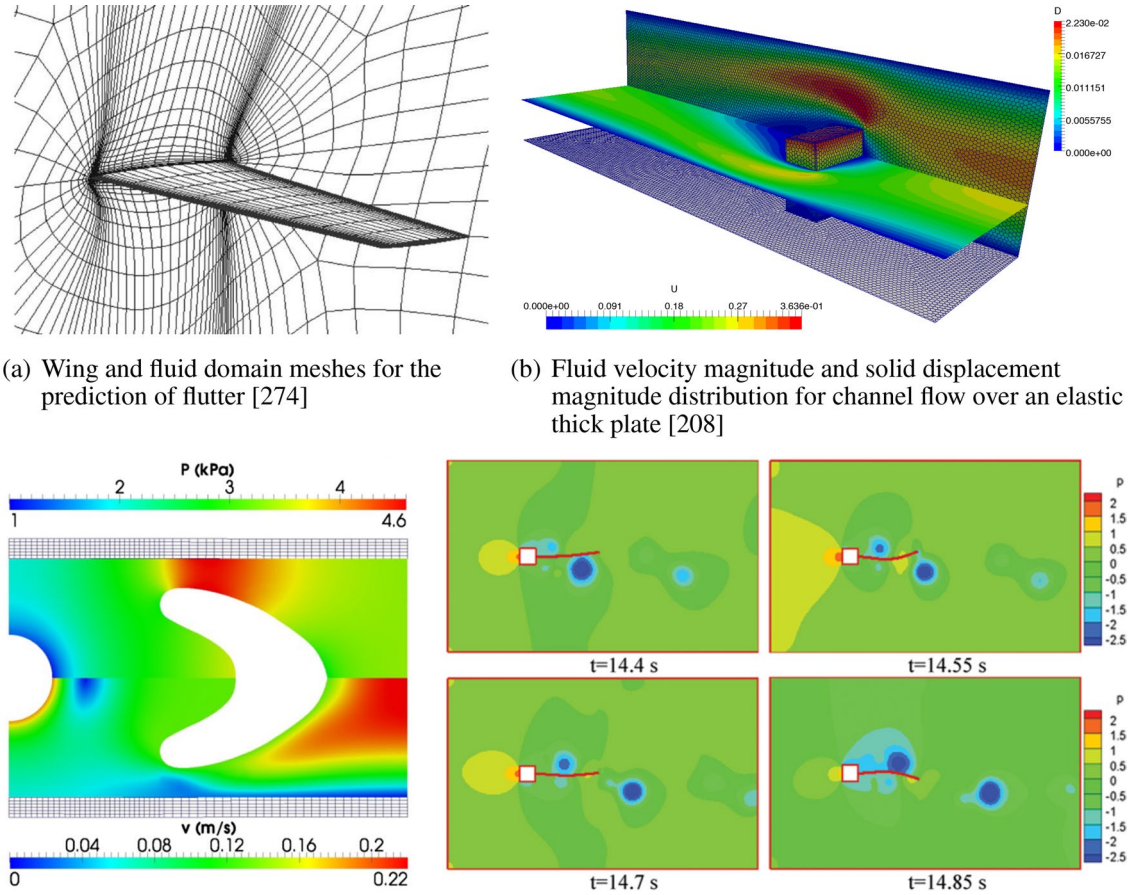


(a) Wing and fluid domain meshes for the prediction of flutter [274]

(b) Fluid velocity magnitude and solid displacement magnitude distribution for channel flow over an elastic thick plate [208]

(c) Pressure (top) and velocity (bottom) distribution around a red blood cell [158]

(d) Pressure field for flow over a rigid square with a thin flexible plate attached [249]

**Fig. 25** Fluid–solid interaction examples. (Color figure online)

HDG method is outside the scope of the current article and readers are referred to recent articles on the application of HDG to solid mechanics [430–433].

## 5 Applications of the Finite Volume Method for Computational Solid Mechanics

Some of the main areas where finite volume methods have been applied to solid mechanics are summarised below, including example images.

### 5.1 Fluid–Solid Interaction

Example cases are shown in Fig. 25, and examples references include: [29, 94, 96, 98, 99, 113, 120, 121, 138–140, 142–145, 147, 149, 152–160, 162, 164, 199, 208, 216, 239, 249, 268, 271, 272, 274–277, 277–280, 309, 434–467].

### 5.2 Fracture and Adhesive Joints

Example cases are shown in Fig. 26, and examples references include: [84, 119–132, 140, 380, 446, 457, 468–500].

### 5.3 Microstructure Analysis

Example cases are shown in Fig. 27, and examples references include: [38, 49, 339–345, 347–354, 492–494, 496, 497, 501–558].

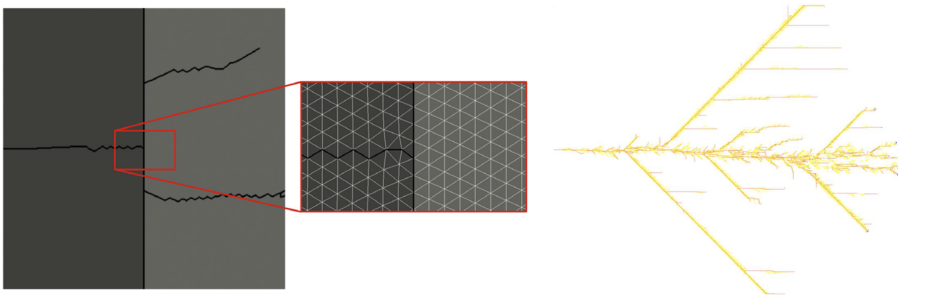

(a) Crack path predictions through a material interface [91] (b) Dynamic crack path predictions in PMMA [129]

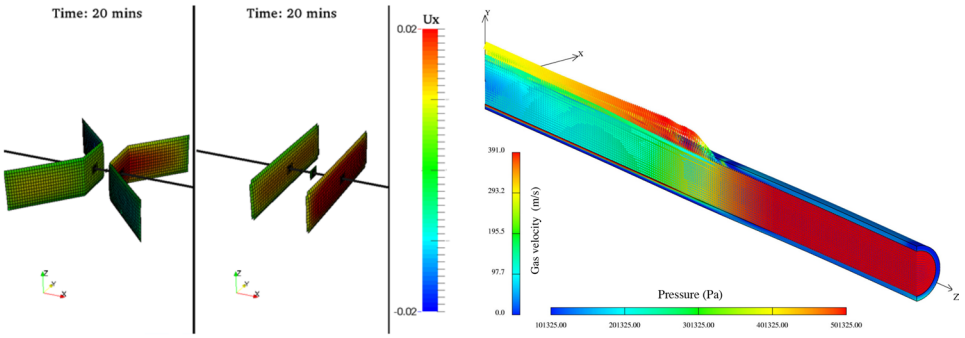


(c) Crack path predictions during hydraulic fracturing [84] (d) Predicting rapid crack propagation in gas-pressurised pipes [477]

**Fig. 26** Fracture and adhesive joint examples. (Color figure online)

### 5.4 Metal Forming and Casting

Example cases are shown in Fig. 28, and examples references include: [30, 44, 46, 47, 50, 51, 51–54, 110, 135–137, 276, 281, 285–287, 331, 334, 336, 385, 386, 388, 389, 391, 559–567].

### 5.5 Biomechanics

Example cases are shown in Fig. 29, and examples references include: [60, 102, 105, 138, 156, 158, 196, 259, 278, 337, 418, 421, 455, 458, 464, 465, 568–587].

### 5.6 Screw Compressors

Example cases are shown in Fig. 30, and examples references include: [147, 148, 151–153, 161, 588–594];

### 5.7 Geomechanics and Poroelasticity

Example cases are shown in Fig. 31, and examples references include: [78, 80–82, 84, 149, 307–313, 595].

## 6 Softwares Employing the Finite Volume Method for Solid Mechanics

A number of software have, or previously have, implemented versions of the finite volume method for solid mechanics; these software, in alphabetical order, include:

- COMET/STAR-CD (commercial software) [29, 41, 44, 46, 57, 58, 95, 97, 100, 120, 136, 137, 147, 148, 151–153, 161, 197, 201, 588–593, 596, 597];
- FOAM/OpenFOAM (open-source software) [25, 28, 30, 77, 78, 80, 83, 84, 88, 91, 94, 96, 98, 99, 101, 104, 105, 113, 140, 155, 156, 158–160, 162, 164, 193, 194, 196, 208, 446, 450, 451, 457, 461, 462, 466, 467, 487, 489–493, 496, 553, 582];
- GTEA (in-house software) [297];
- MulPhys (in-house software) [260];
- NASIR (in-house software) [500, 598–606];
- PHOENICS (commercial software) [13–15, 17, 315–321];
- PHYSICA (in-house software) [241, 265–267, 607];
- TRANSPORE (in-house software) [293].

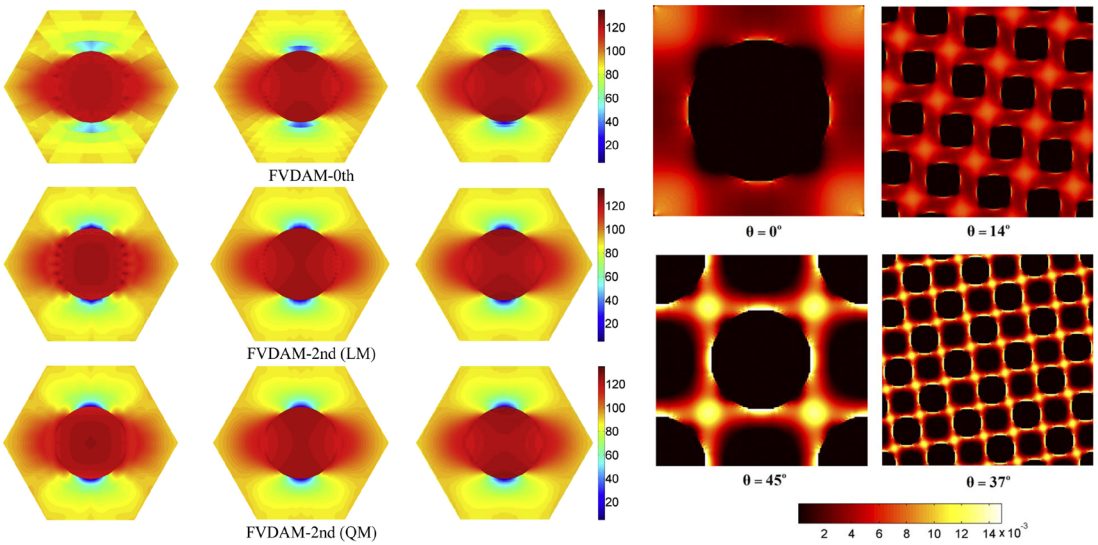


(a) Stress predictions for a hexagonal array of cylindrical inclusions in a boron/aluminum composite [350]

(b) Effective plastic strain distributions for a boron/aluminium unidirectional composite with an applied average transverse shear strain [346]

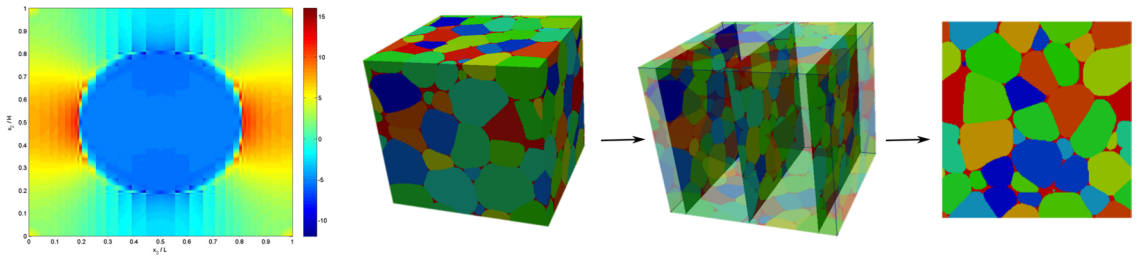

(c) Transverse stress distribution in the repeating unit cell of a carbon/aluminium composite loaded by a longitudinal uniaxial stress [539]

(d) Micro-structural analysis of advanced ceramics [495]

**Fig. 27** Microstructure analysis examples. (Color figure online)

## 7 Conclusions and Challenges

The various finite volume approaches to solid mechanics can be seen to share many similarities, and in fact can all be described in a general unified manner (Sect. 3.5). When comparing the finite volume approach with the finite element approach, the likenesses are clear: both approaches adopt the same general strategy to discretise space into cells/elements, both use similar data storage structures, and both follow similar approaches to assemble their corresponding characteristic matrices. The main differences lie in how the local integration domains are constructed, how the local integration is performed, and their fundamental philosophy: finite volume approaches are rooted in balance laws, where the governing equation is enforced by summing forces/fluxes acting on a control volume; in contrast, finite element methods adopt a more mathematical approach, based on variational methods, where the weak form of the governing equation is imposed in a volumetrically-averaged sense.

To end this article, we state three main challenges we see for the development of finite volume solid mechanics, such that its strengths and weaknesses may be rigorously explored in the context of solid mechanics, and its merits, relative to other similar approaches, may become clear to the computational solid mechanics community at large:

1. Awareness:

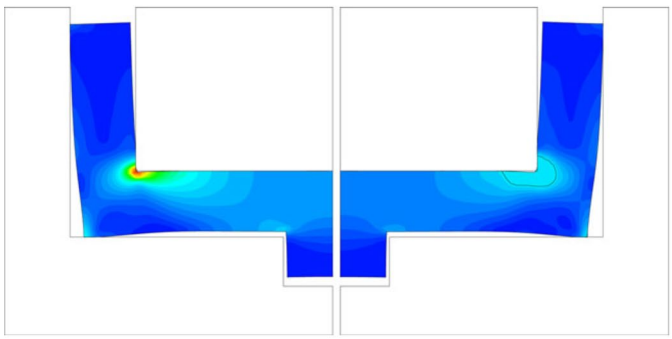

(a) Shape and effective stress predictions in a cast part [137]

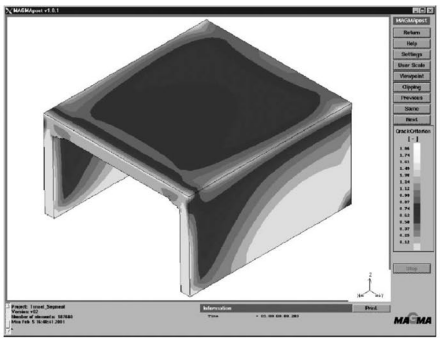

(b) Casting of a tunnel section showing the *crack criterion* distribution [336]

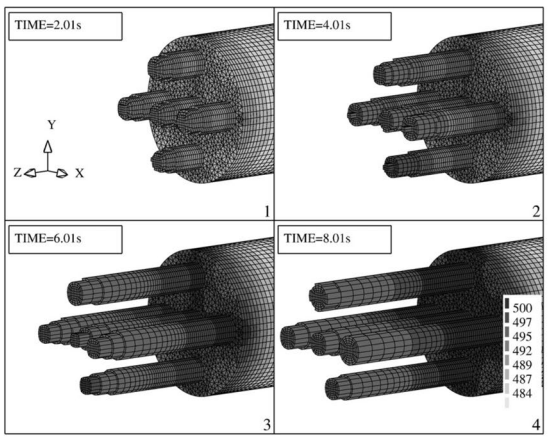


(c) Temperature distribution during extrusion [287]

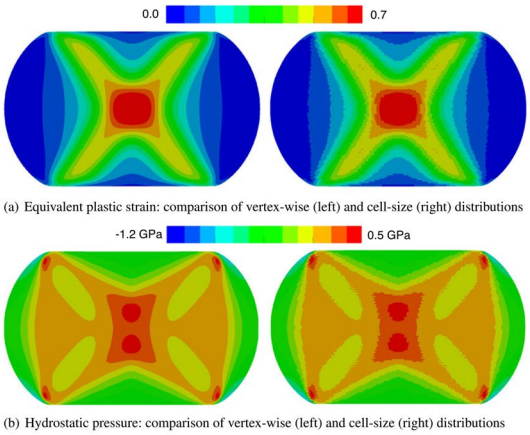


(d) Predicted geometry, equivalent plastic strain and hydrostatic pressure distributions in flat wire rolling [30]

**Fig. 28** Metal forming and casting examples. (Color figure online)

Three decades after the first contributions to the field, there is still a general lack of awareness around the capabilities of the finite volume method in the sphere of solid mechanics; consequently, in the worst case, prestigious journals inadvertently assign inappropriate reviewers, reviewers who, having only limited knowledge of the area, accept poor or reject good articles, for example, see [35], and authors are unaware of major developments in the field when surveying the literature.

2. Benchmarking:

   As should be clear from this review, numerous differing finite volume formulations are possible; although some variants have been developed specifically for specialised applications, the comparison of the differing approaches on standard benchmarks is rare. Without such comparisons, in terms of efficiency, accuracy and robustness, it will not be possible to determine which approaches are optimal for certain classes of problems. Furthermore, given the trends in modern computing, the suitability of proposed approaches for execution on large-scale distributed memory clusters ($> 1000$ s CPU cores) should be further explored. Simulations using hundreds of millions of cells are commonplace at CFD conferences: clearly finite volume-based solid mechanics procedures have great potential. Similarly, finite volume variants should be benchmarked against alternative approaches, such as the finite element method, to determine relative merits, not just on academic standard cases but on complex industrial cases to test robustness. Processes such as *round robin* benchmarking series, for example [608], may offer one solution.

3. Code dissemination:

   Where possible, code for published procedures should be shared for academic scrutiny: such distribution has the potential to: (a) accelerate academic progress, as

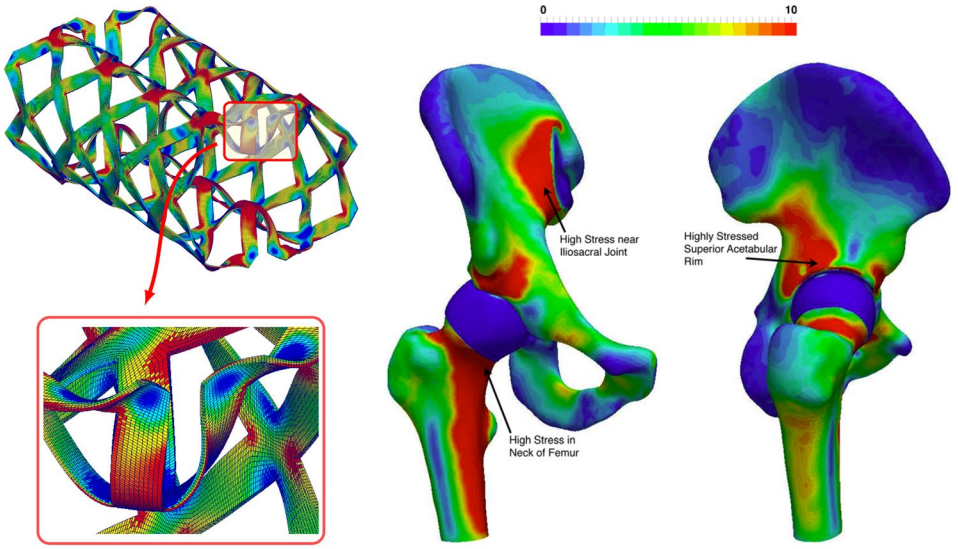


(a) Pressure distribution in a loaded stent-like structure [196]

(b) Von Mises stress distribution in the natural hip joint during stance [105]

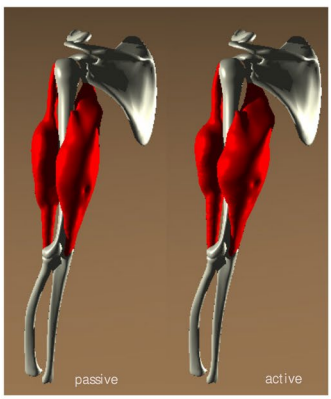


(c) Simulation of isometric contraction in the triceps and biceps muscles [259]

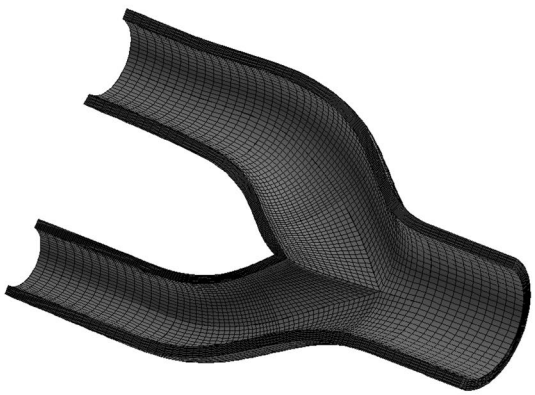

(d) Mesh of an idealised carotid artery wall [577]

**Fig. 29** Biomechanics examples. (Color figure online)

others learn from and build on methods, as well as aiding in the discovery and resolution of errors; (b) facilitate ease of understanding and ease of implementation; (c) allow direct comparison of methods; (d) provide insight into the algorithm intricacies that may not be clear from academic articles; and (e) allow faster integration into commercial software and industrial use.

## Appendix 1: Table of Most Cited Articles Related to the Finite Volume Method for Solid Mechanics

Table 1 lists the most cited articles related to the finite volume method for solid mechanics; the references have been listed in order of decreasing number of citations, and only articles with greater than fifty citations have been included, according to Google Scholar citations on 25th August 2018. As noted in the body of the article, care should be taken when interpreting the data, as the number of citations may not be directly proportional to impact on the field; for example, Weller et al. [193] has by far the greatest number of citations; however, a significant percentage of its received citations are related to its computational fluid mechanics developments, rather than its solid mechanics contributions.

## Appendix 2: Overview of the Discretisation Used in HOTFGM/HFGMC/FVDAM Approaches

There are a variety of related methods with finite volume attributes which have been designed for the analysis of heterogenous microstructures. The related methods include the *higher-order theory for functionally graded material*

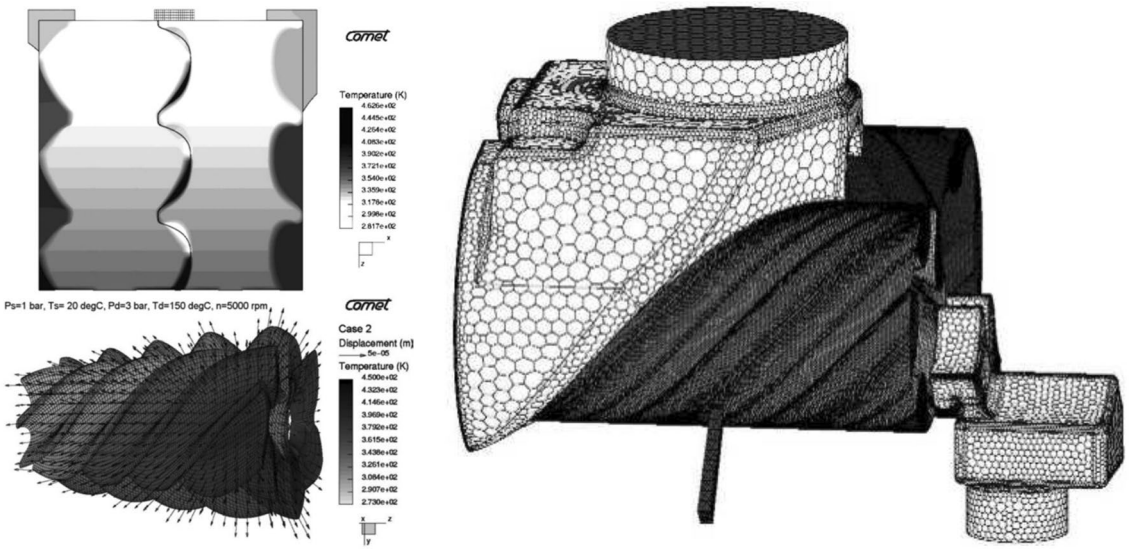


(a) Displacement and temperature distribution of a rotor in an oil-free compressor [147]

(b) Mesh of screw compressor [152]

**Fig. 30** Screw compressor examples. (Color figure online)

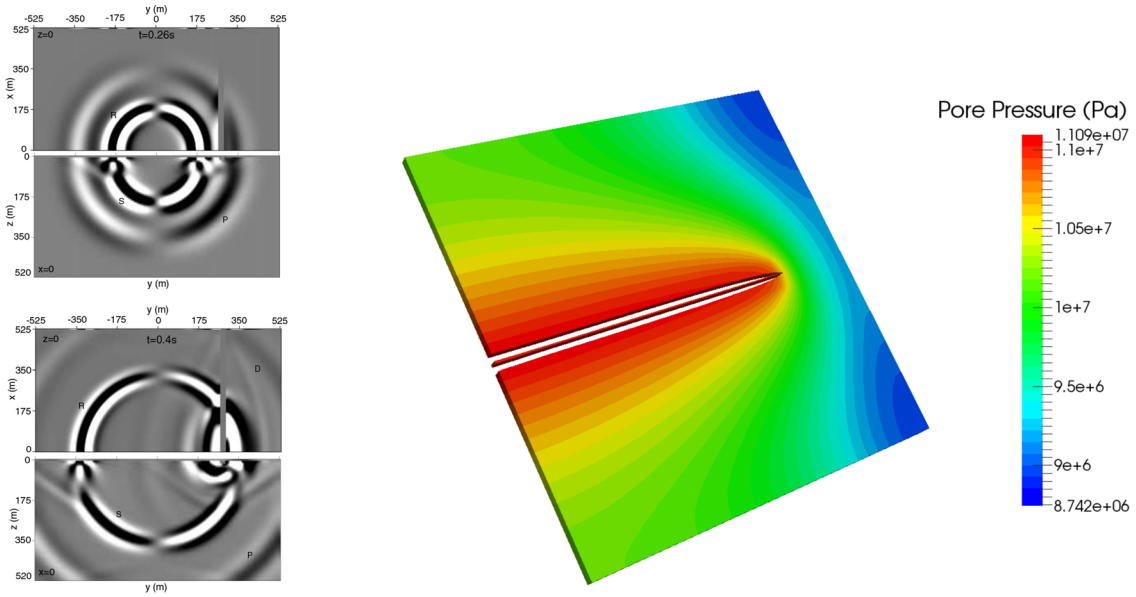


(a) Elastic waves in a heterogenous medium [309]

(b) Pore-pressure predictions near a hydraulic fracture [82]

**Fig. 31** Geomechanics and poroelasticity examples. (Color figure online)

(HOTFGM) [339], the *high-fidelity generalised method of cells* (HFGMC) [340–343], and the *finite volume direct averaging micromechanics* (FVDAM) theory [344, 345]. A brief summary of the methods is given here, and readers are referred to Aboudi et al. [339], Bansal and Pindera [345] and Cavalcante et al. [38] for further details.

The HOTFGM and HFGMC approaches start by spatially discretising the solution domain into rectangular

**Table 1** Most cited articles related to the finite volume method for solid mechanics from Google Scholar citations on 25th August 2018

| Reference | Formulation-type | Number of citations |
|---|---|---|
| Weller et al. [193] | Cell-centred | 1988 |
| Demirdžić and Muzaferija [29] | Cell-centred | 408 |
| Idelsohn and Oñate [11] | Vertex-centred and cell-centred | 221 |
| Demirdžić and Muzaferija [41] | Cell-centred | 189 |
| Jasak and Weller [194] | Cell-centred | 185 |
| Pindera et al. [351] | HFGMC/HOTFGM/FVDAM | 185 |
| Demirdžić and Martinović [3] | Cell-centred | 172 |
| Bailey and Cross [24] | Vertex-centred | 143 |
| Oñate et al. [12] | Vertex-centred and cell-centred | 128 |
| Fryer et al. [5] | Vertex-centred | 103 |
| Slone et al. [272] | Vertex-centred | 101 |
| Slone et al. [273] | Vertex-centred | 97 |
| Bansal and Pindera [345] | HFGMC/HOTFGM/FVDAM | 94 |
| Voller [609] | Vertex-centred | 91 |
| Bijelonja et al. [97] | Cell-centred | 87 |
| Taylor et al. [251] | Vertex-centred | 86 |
| Cavalcante et al. [518] | HFGMC/HOTFGM/FVDAM | 80 |
| Taylor et al. [241] | Vertex-centred | 70 |
| Khatam and Pindera [530] | HFGMC/HOTFGM/FVDAM | 70 |
| Fallah et al. [255] | Vertex-centred | 64 |
| Ivanković et al. [119] | Cell-centred | 61 |
| Karač et al. [132] | Cell-centred | 59 |
| Taylor et al. [] | Vertex-centred | 58 |
| Bailey et al. [267] | Vertex-centred | 57 |
| Slone et al. [274] | Vertex-centred | 56 |
| Murphy and Ivanković [128] | Cell-centred | 55 |
| Tuković and Jasak [112] | Cell-centred | 54 |
| Demirdžić et al. [197] | Cell-centred | 52 |
| Bailey et al. [264] | Vertex-centred | 51 |

Approaches for heterogeneous periodic microstructures are indicated by HFGMC/HOTFGM/FVDAM

so-called *generic cells*, which are further split into a second discretisation level containing four rectangular sub-cells (Fig. 32); for brevity and clarity, the description here has been limited to two dimensions; however, the approaches have been extended to three dimensions, as described in Aboudi et al. [339]. As a consequence of the assumed orthogonal Cartesian mesh, curved interfaces between material phases are approximated in a castellated *staircase* manner, as shown in Fig. 32; this limitation was later removed by the FVDAM approach with extension to unstructured quadrilateral meshes. By considering the unit cell of a periodic material, the displacement field can be decomposed into average and fluctuating components, $\boldsymbol{u} = \bar{\boldsymbol{u}} + \boldsymbol{u}'$, where the average displacement is determined from the specified macroscopic average strains, $\bar{\boldsymbol{u}} = \bar{\boldsymbol{\varepsilon}}\boldsymbol{x}$. Within each sub-cell, the fluctuating displacement is then assumed to vary quadratically as a function of the local coordinates, $\bar{y}_2$ and $\bar{y}_3$:

$$\boldsymbol{u}'(\bar{y}_2,\bar{y}_3) = \boldsymbol{W}_{00} + \bar{y}_2\boldsymbol{W}_{10} + \bar{y}_3\boldsymbol{W}_{01} + \frac{1}{2}\left(3\bar{y}_2^2 - \frac{h^2}{4}\right)\boldsymbol{W}_{20} + \frac{1}{2}\left(3\bar{y}_3^2 - \frac{l^2}{4}\right)\boldsymbol{W}_{02} \quad (82)$$

where $h$ and $l$ are the width and height respectively of the sub-cell; $\boldsymbol{W}_{00}$, $\boldsymbol{W}_{10}$, $\boldsymbol{W}_{01}$, $\boldsymbol{W}_{20}$, and $\boldsymbol{W}_{02}$ are unknown vector displacement coefficients, each with three components; the $\boldsymbol{W}_{00}$ component corresponds to the unknown displacement at the centre of the sub-cell, while the remaining coefficients correspond to higher-order displacement contributions within the sub-cell. Accordingly, there are $5 \times 3 = 15$ unknown displacement coefficients within each sub-cell and hence $4 \times 15 = 60$ within each generic cell; in three dimensions, there are 168 unknown quantities. For brevity here, the $(\gamma)$ and $(\beta)$ superscripts indicating the sub-cell have been dropped i.e. $\bar{y}_2 = \bar{y}_2^{(\beta)}$, $\bar{y}_3 = \bar{y}_3^{(\gamma)}$, etc. It is also worth pointing out that although the approach has been developed for

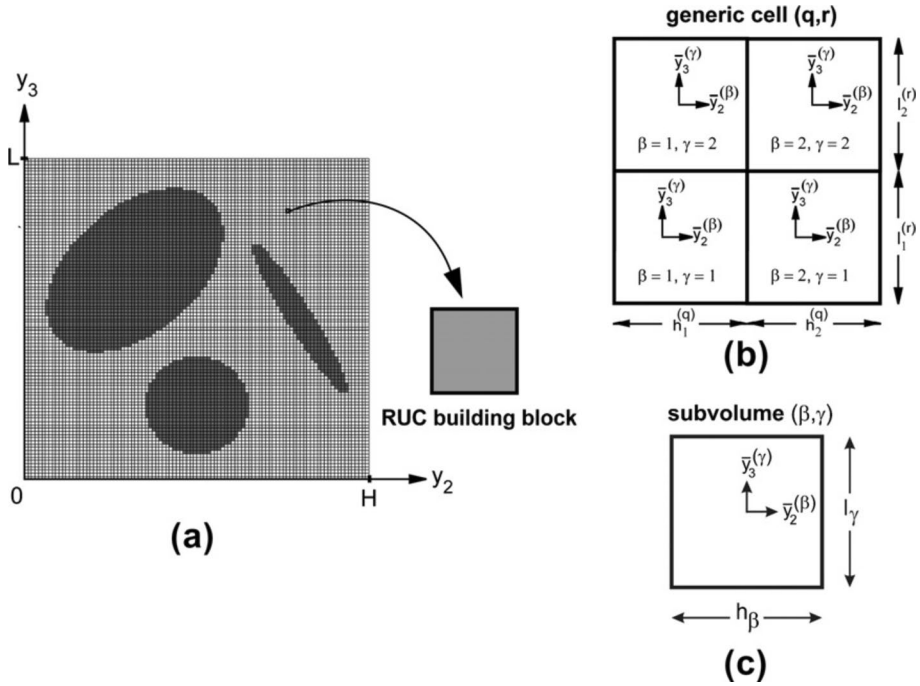


**Fig. 32** **a** Unit cell of a periodic material with microstructure discretised into rectangular building blocks. **b** Two-level discretisation employed by HFGMC into ($q$, $r$) generic cells further subdivided into four ($b$, $c$) subcells. **c** Single-level discretisation employed in the FVDAM theory into stand-alone ($b$, $c$) sub-volumes. Figure taken from Cavalcante et al. [38]. (Color figure online)

periodic microstructures, the method can also be used for general structural stress analysis by assuming the average displacement $\bar{\boldsymbol{u}}$ to be zero.

To determine the unknown displacement coefficients, the 0th, 1st and 2nd *moments* of momentum conservation are applied to each sub-cell, in addition to the enforcement of traction and displacement continuity between sub-cells and generic cells, and inclusion of boundary conditions. A characteristic of the method, which is not possessed by the other finite volume variants, is the enforcement of these so-called *moments* of the governing equation. To achieve this, the governing equation (Eq. 1), where temporal and body force terms have been neglected, is written in terms of a so-called stress moment $\boldsymbol{S}$:

$$\oint_{\Gamma} \boldsymbol{n} \cdot \boldsymbol{S} \, \mathrm{d}\Gamma = \boldsymbol{0} \tag{83}$$

with the stress moment defined as:

$$\boldsymbol{S} = \frac{1}{hl} \int_{-\frac{h}{2}}^{\frac{h}{2}} \int_{-\frac{l}{2}}^{\frac{l}{2}} \left[ \boldsymbol{\sigma} \, \bar{y}_2^m \, \bar{y}_3^n \right] \mathrm{d}\bar{y}_2 \, \mathrm{d}\bar{y}_3 \tag{84}$$

The exponents $m$ and $n$ indicate the order of the equation; for example, when $m = n = 0$, the relation reduces to conservation of force; when $m = 1$ and $n = 1$ the relation represents conservation of angular momentum; while for $m > 1$ and $n > 1$ the relation represents conservation of higher stress moments. Note: $m$ is not related to the time-step counter in Eq. (4).

In this way, it is possible to assemble a system of $60N$ algebraic equations of the standard form, $[\boldsymbol{K}][\boldsymbol{U}] = [\boldsymbol{F}]$, where $N$ is the number of generic cells in the solution domain, $[\boldsymbol{U}]$ is a vector of unknown displacement coefficients $\boldsymbol{W}$, the global stiffness matrix $[\boldsymbol{K}]$ is a function of the sub-cell dimensions and mechanical properties, and the global force vector $[\boldsymbol{F}]$ contains contributions from boundary conditions and nonlinear material stresses. The linear system is inverted to give the displacements distributions within the sub-cells.

The HOTFGM and HFGMC approaches described above provide the basis for the subsequent FVDAM approach; the FVDAM approach differs from the HOTFGM and HFGMC methods in a number of ways:

(a) The two-level spatial domain decomposition (generic cells and sub-cells) of the HOTFGM/HFGMC methods is replaced by one-level of discretisation/cells;
(b) The displacement coefficients within each cell $\boldsymbol{W}$ are expressed in terms of surface-averaged displacements i.e. displacement averaged at each cell surface;
(c) Higher order moments of the equilibrium equation are not used;
(d) In the parametric form of the FVDAM, the use of parametric mapping with a parent/reference cell allows the use of an unstructured mesh (similar to the finite element method), instead of the orthogonal Cartesian mesh of the HOTFGM/HFGMC approaches (see Fig. 32);
(e) In the assembled system of algebraic equations $[\boldsymbol{K}][\boldsymbol{U}] = [\boldsymbol{F}]$, the solution vector $[\boldsymbol{U}]$ contains cell sur-

face-averaged displacements, as opposed to sub-cell displacement coefficients.

Further technicals details of the HOTFGM, HFGMC and FVDAM methods can be found in Cavalcante et al. [38], Aboudi et al. [339], Aboudi [340], Aboudi et al. [341], Haj-Ali and Aboudi [342, 343], Bansal and Pindera [344, 345] and Cavalcante and Pindera [349].

**Acknowledgements** The first author gratefully acknowledges financial support from Bekaert through the University Technology Centre (UTC), and from the Irish Composites Centre (IComp). In addition, this publication has emanated from research supported in part by the Irish Research Council through the Laureate programme, grant number IRCLA/2017/45, and I-Form, via a research grant from Science Foundation Ireland (SFI) under Grant No. 16/RC/3872 and is co-funded under the European Regional Development Fund. Furthermore, the valuable comments of Prof. Alojz Ivanković (University College Dublin), Prof. Aleksandar Karač (University of Zenica), Prof. Mark Cross (Swansea University), as well as a number of journal reviewers are gratefully acknowledged.

**Authors' contribution** Both authors contributed to the article concept and design, as well as performing the literature review and data analysis. The first draft of the manuscript was written by Philip Cardiff and both authors commented on and critically revised versions of the manuscript. Both authors read and approved the final manuscript.

**Funding** The first author gratefully acknowledges financial support from Bekaert through the University Technology Centre (UTC), and from the Irish Composites Centre (IComp). In addition, this publication has emanated from research supported in part by the Irish Research Council through the Laureate programme, grant number IRCLA/2017/45, and I-Form, via a research grant from Science Foundation Ireland (SFI) under Grant No. 16/RC/3872 and is co-funded under the European Regional Development Fund.

## Compliance with ethical standards

**Conflict of interest** All authors declare that they have no conflict of interest.

## References

1. Runchal AK (2017) Tributes to an exceptional life: D. Brian Spalding, 9 January 1923–27 November 2016. Available at https://www.astfe.org/doc/Brian_Spalding-Tributes_to_an_Exceptional_Life.pdf
2. Demirdžić I, Martinović D, Ivanković A (1988) Numerical simulation of thermal deformation in welded workpiece. Zavarivanje, 31:209–219 (in Croatian). English translation available at https://www.researchgate.net/profile/Alojz_Ivankovic/publication/296148474_Numerical_simulation_of_thermal_deformation_in_welded_workpiece/links/5d07642ba6fdcc39f12219eb/Numerical-simulation-of-thermal-deformation-in-welded-workpiece.pdf
3. Demirdžić I, Martinović D (1993) Finite volume method for thermo-elasto-plastic stress analysis. Comput Methods Appl Mech Eng 109:331–349
4. Bailey C, Fryer YD, Cross M, Chow P (1991) Predicting the deformation of castings in moulds using a control volume approach on unstructured meshes. In: Cross M, Pittman JFT, Wood RD (eds) Mathematical modelling for materials processing: based on the proceedings of a conference on mathematical modelling of materials processing, organized by the Institute of Mathematics and its Applications, University of Bristol, September, 1991
5. Fryer YD, Bailey C, Cross M, Lai C-H (1991) A control volume procedure for solving the elastic stress–strain equations on an unstructured mesh. Appl Math Model 15:639–645
6. Zienkiewicz OC, Oñate E (1991) Finite volumes vs finite elements: is there really a choice? Nonlinear Computational Mechanics. State of the Art, pp 240–254
7. Cross M, Bailey C, Chow P, Peircleous K (1992) Towards an integrated control volume unstructured mesh code for the simulation of all macroscopic processes involved in shape casting. In: Wood Chenot RD, Zienkiewicz OC (eds) Numerical methods in industrial processes NUMIFORM 92. Belkema, Rotterdam, pp 787–792
8. Oñate E, Cervera M, Zienkiewicz OC (1992) A study of the finite volume format for structural mechanics. Technical report, Internal Report Publication No. 15, CIMNE, Barcelona
9. Cross M (1993) Development of novel computational technique for the next generation of software tools for casting simulation. In: Katgerman L, Piwonka TS, Voler VR (eds) Modelling of casting, welding and advanced solidification processes VI, TMS, pp 115–126
10. Fryer YD, Bailey C, Cross M, Chow P (1993) Predicting micro-porosity in shape casting using an integrated control volume unstructured mesh framework. In: Voler VR, Piwonka TS, Katgerman L (eds) Modelling of casting, welding and advanced solidification processes VI, pp 143–152
11. Idelsohn SR, Oñate E (1994) Finite volumes and finite elements: two 'good friends'. Int J Numer Methods Eng 37:3323–3341
12. Oñate E, Cervera M, Zienkiewicz OC (1994) A finite volume format for structural mechanics. Int J Numer Methods Eng 37:181–201
13. Beale SB, Elias SR (1990) Numerical solution of two-dimensional elasticity problems by means of a SIMPLE-based finite-difference scheme. Technical report, Institute for Mechanical Engineering, National Research Council, Ottawa, Ont. TR-LT-020 (NRC No. 32090)
14. Beale SB, Elias SR (1990) Stress distribution in a plate subject to uniaxial loading. PHOENICS J Comput Fluid Dyn 3(3):255–287
15. Bukhari KM, Qin HQ, Spalding DB (1990) Progress report (to Rolls-Royce Ltd) on the calculation of thermal stresses in bodies of revolution. Technical report, CHAM Ltd
16. Hattel JH, Hansen PN (1990) FDM solutions of the thermoelastic equations using a staggered grid. In: Danish–German–Polish workshop on application of computer methods in practice, Warsaw, Poland
17. Bukhari KM, Hamill IS, Qin HQ, Spalding DB (1991) Stress-analysis simulations in PHOENICS. Technical report, CHAM Ltd
18. Hattel JH (1992) Analysis of thermal induced stresses in die molds. In: Lacaze J, Cross JT, Rappaz M, Sciama G, Svensson I (eds) Examples of European expertise in the computer simulation of solidification and casting. B-18, Ecole de Mines, Nancy, France
19. Hattel JH, Hansen PN, Hansen LF (1993) Analysis of thermal induced stresses in die casting using a novel control volume technique. In: Voller VR, Piwonka TS, Katgerman L (eds) Modelling of casting, welding and advanced solidification processes VI, TMS, Palm Coast, Florida, USA, pp 585–592

20. Sevilla R, Giacomini M, Huerta A (2018) A face-centred finite volume method for second-order elliptic problems. Int J Numer Methods Eng https://doi.org/10.1002/nme.5833
21. Sevilla R, Giacomini M, Huerta A (2018) A locking-free face-centred finite volume (FCFV) method for linear elasticity. Preprint arXiv:1806.07500v1 [math.NA]
22. Ebrahimnejad M, Fallah N, Khoei AR (2014) New approximation functions in the meshless finite volume method for 2D elasticity problems. Eng Anal Boundary Elem 46:10–22
23. Fallah N, Delzendeh M (2018) Free vibration analysis of laminated composite plates using meshless finite volume method. Eng Anal Boundary Elem 88:132–144
24. Bailey C, Cross M (1995) A finite volume procedure to solve elastic solid mechanics problems in three dimensions on an unstructured mesh. Int J Numer Methods Eng 38:1757–1776
25. Cardiff P, Tuković Ž, Jasak H, Ivanković A (2016) A block-coupled finite volume methodology for linear elasticity and unstructured meshes. Comput Struct 17:100–122. https://doi.org/10.1016/j.compstruc.2016.07.004
26. Kluth G, Després B (2010) Discretization of hyperelasticity on unstructured mesh with a cell-centered Lagrangian scheme. J Comput Phys 229:9092–9118
27. Lee CH, Gil AJ, Bonet J (2013) Development of a cell centred upwind finite volume algorithm for a new conservation law formulation in structural dynamics. Comput Struct 118:13–38
28. Haider J, Lee CH, Gil AJ, Bonet J (2017) A first order hyperbolic framework for large strain computational solid dynamics: an upwind cell centred total Lagrangian scheme. Int J Numer Methods Eng 109:407–456
29. Demirdžić I, Muzaferija S (1995) Numerical method for coupled fluid flow, heat transfer and stress analysis using unstructured moving meshes with cells of arbitrary topology. Comput Methods Appl Mech Eng 125:235–255
30. Cardiff P, Tuković Ž, De Jaeger P, Clancy M, Ivanković A (2016) A Lagrangian cell-centred finite volume method for metal forming simulation. Int J Numer Methods Eng 109(13:1777–1803. https://doi.org/10.1002/nme.5345
31. Aguirre M, Gil AJ, Bonet J, Carre AA (2014) A vertex centred finite volume Jameson–Schmidt–Turkel (JST) algorithm for a mixed conservation formulation in solid dynamics. J Comput Phys 259:672–699
32. LeVeque R (2004) Finite volume methods for hyperbolic problems. Cambridge University Press, Cambridge
33. Baliga BR, Atabaki N (2009) Control-volume-based finite-difference and finite-element methods. In: Handbook of numerical heat transfer, vol 22, pp 191–224
34. Courant R, Friedrichs K, Lewy H (1928) On the partial difference equations of mathematical physics. Math Annal 100:32–74
35. Demirdžić I (2015) On the discretization of the diffusion term in finite-volume continuum mechanics. Numer Heat Transf Part B Fundam Int J Comput Methodol 68(1):1–10. https://doi.org/10.1080/10407790.2014.985992
36. Maneeratana K (2000) Development of the finite volume method for non-linear structural applications. PhD thesis, Imperial College, London
37. Vaz M Jr, Mu noz Rojas PA, Filippini G (2009) On the accuracy of nodal stress computation in plane elasticity using finite volumes and finite elements. Comput Struct 87:1044–1057
38. Cavalcante MAA, Pindera M-J, Khatam H (2012) Finite-volume micromechanics of periodic materials: past, present and future. Compos B Eng 43:2521–2543
39. Van Eck NJ, Waltman L (2007) VOS: a new method for visualizing similarities between objects. In: Advances in data analysis: proceedings of the 30th annual conference of the German classification society. Springer, Berlin, pp 299–306
40. Trangenstein JA, Colella P (1991) A higher-order Godunov method for modeling finite deformation in elastic–plastic solids. Commun Pure Appl Math 44:41–100
41. Demirdžić I, Muzaferija S (1994) Finite volume method for stress analysis in complex domains. Int J Numer Methods Eng 37:3751–3766
42. Dioh N, Ivanković A, Leevers P, Williams JG (1994) The high strain rate behaviour of polymers. J Phys IV, 04 (C8). https://doi.org/10.1051/jp4:1994818
43. Rente CJ, Oliveira PJ (2000) Extension of a finite volume method in solid stress analysis to cater for non-linear elasto-plastic effects. In: Tassoulas JL (ed) Proceedings of EM 14th engineering mechanics conference. University of Texas at Austin, USA
44. Teskeredžić A, Demirdžić I, Muzaferija S (2002) Numerical method for heat transfer, fluid flow, and stress analysis in phase-change problems. Numer Heat Transf Part B Fundam 42:437–459
45. Teskeredžić A (2004) Application of the finite volume method to casting problems. PhD thesis, University of Sarajevo
46. Bašić H, Demirdžić I, Muzaferija S (2005) Finite volume method for simulation of extrusion processes. Int J Numer Methods Eng 62:475–494
47. Martins MM, Bressan JD, Button ST, Ivanković A (2010) Extrusion process by finite volume method using OpenFOAM software. In: Chastel Chinesta Y, El Mansori M (eds) International conference on advances in material and processing technologies—AMPT2010. American Institute of Physics, Paris, France, pp 1461–1466
48. Bressan JD, Martins MM, Vaz M Jr (2010) Stress evolution and thermal shock computation using the finite volume method. J Therm Stresses 33:533–558
49. Leonard M, Murphy N, Karač A, Ivanković A (2012) A numerical investigation of spherical void growth in an elastic–plastic continuum. Comput Mater Sci 64:38–40
50. Bressan JD, Martins MM, Button ST (2015) Analysis of aluminium hot extrusion by finite volume method. Mater Today Proc 2(10, Part A):4740–4747
51. Martins MM, Bressan JD, Button ST (2016) Analysis of aluminum extrusion in a 90° die by finite volume method. Adv Mater Res 1135:153–160
52. Martins MM, Bressan JD, Button ST (2017) Finite volume analysis with the maccormack method applied to metal flow in forward extrusion. Univ J Mech Eng 5:1–8
53. Cardiff P, Tang T, Tukovic Z, Jasak H, Ivankovic A, De Jaeger P (2017) An Eulerian-inspired Lagrangian finite volume method for wire drawing simulations. In: IUTAM symposium on multi-scale fatigue, fracture and damage of materials in harsh environments, Galway, Ireland. National University of Ireland Galway
54. Bressan JD, Martins MM, Button ST (2017) Analysis of metal extrusion by the finite volume method. Proc Eng 207:425–430
55. Zarrabi K, Basu A (1999) An axisymmetric finite volume formulation for creep analysis. J Mech Behav Mater 10:325–340
56. Zarrabi K, Basu A (2000) A finite volume element formulation for solution of elastic axisymmetric pressurized components. Int J Press Vessels Pip 77:479–484
57. Džaferović E, Ivanković A, Demirdžić I (2000) Finite volume modelling of linear viscoelastic deformation. In: Proceedings of 3rd congress of Croatian society of mechanics, Dubrovnik, Croatia
58. Demirdžić I, Džaferović E, Ivanković A (2005) Finite-volume approach to thermoviscoelasticity. Numer Heat Transf Part B Fundam 47:213–237
59. Das S, Mathur SR, Murthy JY (2012) Finite-volume method for creep analysis of thin RF MEMS devices using the theory of plates. Numer Heat Transf Part B Fundam 61:71–90

60. Safari A, Tuković Ž, Cardiff P, Walter M, Casey E, Ivanković A (2016) Interfacial separation of a mature biofilm from a glass surface—a combined experimental and cohesive zone modelling approach. J Mech Behav Biomed Mater 54:205–218
61. Demirdžić I, Ivanković A, Martinović D, Muzaferija S (1994) Numerical method for solving linear and non-linear solid body problems. In: Proceedings of 1st Congress of Croatian Society of Mechanics, Pula, Croatia
62. Demirdžić I (1996) Finite volumes in solid mechanics. In: NAFEMS ASME Seminar—alternative strategies in computational mechanics, London
63. Osman H, Ahmad S, Arshad KA (2011) A one-dimensional simulation of an electrofusion welding process. In: International conference on modeling, simulation and applied optimization (ICMSAO), vol 4, pp 1–5 (2011)
64. Junior HGD, Xavier CR, de Castro JA, Campos MF, Palmeira AA, Habibe AF (2013) Mathematical modeling and experimental investigation of the stress evolution at the steel welding. Cadernos UniFOA 8:59–66
65. Bibin KS, Ramarajan A (2013) Unstructured finite volume approach for 3-D unsteady thermo-structural analysis using biconjugate gradient stabilized method. In J Innov Res Sci Eng Technol 2:1389–1400
66. Martinović D, Horman I (1998) Numerical simulation of clay bricks drying process. In: II Medjunarodni naučno-stručni skup Proizvodnja i prerada nemetalnih mineralnih sirovina i njihova primjena u industriji, Zenica, Bosnia and Herzegovina (in Bosnian)
67. Demirdžić I, Horman I, Martinović D (2000) Finite volume analysis of stress and deformation in hygro-thermo-elastic orthotropic body. Comput Methods Appl Mech Eng 190:1221–1232
68. Martinović D, Horman I (2000) Drying induced stresses in clay bricks an hygro-thermo-elastic model. In: International scientific and expert symposium nonmetal inorganic materials, Zenica, Bosnia-Herzegovina, pp 249–257 (2000)
69. Martinović D, Horman I, Demirdžić I (2001) Numerical and experimental analysis of wood drying process. Wood Sci Technol 35:143–156
70. Martinović D (2002) A numerical method for analysis of thermo-deformational processes during the welding. PhD thesis, University of Sarajevo (in Bosnian)
71. Horman I, Martinović D, Hajdarević S (2008) Numerical analysis of a phenomena in the wood caused by heat. Moisture or External Load, vol 21. In: Proceedings of international scientific conference: challanges in forestry and wood technology in the University of Zagreb, Faculty of Forestry, Zageb, pp 31–34
72. Martinović D, Horman I, Hajdarević S (2008) Stress distribution in wooden corner joints. Strojarstvo 50:193–204
73. Horman I, Martinović D, Hajdarević S (2009) Finite volume method for analysis of stress and strain in wood. Drv Ind 60:27–32
74. Horman I, Hajdarević S, Martinović D, Vukas N (2010) Numerical analysis of stress and strain in a wooden chair. Drv Ind 61:151–158
75. Horman I, Martinović D, Bijelonja I, Hajdarević S (2012) Wood subjected to hydro-thermal and/or mechanical loads. In: Petrova R (ed) Finite volume method—powerful means of engineering design
76. Fu R (2018) Thermo-mechanical coupling for ablation. PhD thesis, University of Kentucky
77. Holzmann T, Ludwig A, Raninger P (2018) Yield strength prediction in 3D during local heat treatment of structural A356 alloy components in combination with thermal-stress analysis. In: Lambotte G, Lee J, Allanore A, Wagstaff S (eds) Materials processing fundamentals. The minerals, metals and materials series
78. Tang T, Hededal O, Cardiff P (2015) On finite volume method implementation of poro-elasto-plasticity soil model. Int J Numer Anal Methods Geomech 39:1410–1430. https://doi.org/10.1002/nag.2361
79. Bryant EC, Hwang J, Sharma MM (2015) Arbitrary fracture propagation in heterogeneous poroelastic formations using a finite volume-based cohesive zone model. In: SPE hydraulic fracturing technology conference, The Woodlands, Texas
80. Cardiff P, Manchanda R, Bryant EC, Lee D, Ivanković A, Sharma MM (2015) Simulation of fractures in OpenFOAM: from adhesive joints to hydraulic fractures. In: 10th OpenFOAM workshop, University of Michigan, Ann Arbor, MI, USA
81. Cardiff P, Manchanda R, Bryant EC, Ivanković A, Sharma MM (2015) Finite volume method for the simulation of hydraulic fractures. In: Joint symposium of Irish mechanics society and Irish society for scientific and engineering computation advances in mechanics. University College Dublin, Dublin, Ireland
82. Lee D, Cardiff P, Bryant EC, Manchanda R, Wang H, Sharma AMM (2015) New model for hydraulic fracture growth in unconsolidated sands with plasticity and leak-off. In: SPE annual technical conference and exhibition, pp 28–30
83. Elsafti H, Oumeraci H (2016) A numerical hydro-geotechnical model for marine gravity structures. Comput Geotech 79:105–129. https://doi.org/10.1016/j.compgeo.2016.05.025
84. Manchanda R, Bryant EC, Bhardwaj P, Cardiff P, Sharma MM (2017) Strategies for effective stimulation of multiple perforation clusters in horizontal wells. SPE, Preprint, pp 28–30. https://doi.org/10.2118/179126-PA
85. Asadollahi M (2017) Finite volume method for poroelasticity. Master's thesis, Delft University of Technology
86. Fainberg J, Leister HJ (1996) Finite volume multigrid solver for thermo-elastic stress analysis in anisotropic materials. Comput Methods Appl Mech Eng 137:167–174
87. Horman I (1999) Finite volume method for analysis of timber drying. PhD thesis, University of Sarajevo (in Bosnian)
88. Cardiff P, Karač A, Ivanković A (2014) A large strain finite volume method for orthotropic bodies with general material orientations. Comput Methods Appl Mech Eng 268:318–335. https://doi.org/10.1016/j.cma.2013.09.008
89. Golubović A, Demirdžić I, Muzaferija S (2017) Finite volume analysis of laminated composite plates. Int J Numer Methods Eng 109(11):1607–1620
90. Tuković Ž, Ivanković A, Karač A (2012) Finite-volume stress analysis in multi-material linear elastic body. Int J Numer Methods Eng 93:400–419
91. Carolan D, Tuković Ž, Murphy N, Ivanković A (2013) Arbitrary crack propagation in multi-phase materials using the finite volume method. Comput Mater Sci 69:153–159
92. Cardiff P (2012) Development of the finite volume method for hip joint stress analysis. PhD thesis, University College Dublin. https://www.researchgate.net/publication/262772501_Development_of_the_Finite_Volume_Method_for_Hip_Joint_Stress_Analysis
93. Greenshields CJ, Weller HG, Ivanković A (1999) The finite volume formulation for fluid–structure interaction. In: Vilsmeirer Haenel R, Benkhaldoun F (eds) Finite volumes for complex applications, II—problems and perspectives. Hermes Science, pp 467–474
94. Greenshields CJ, Weller HG, Ivanković A (1999) The finite volume method for coupled fluid flow and stress analysis. Comput Model Simul Eng 4:213–218
95. Bijelonja I, Demirdžić I, Muzaferija S (2005) A finite volume method for large strain analysis of incompressible hyperelastic materials. Int J Numer Methods Eng 64:1594–1609

96. Greenshields CJ, Weller HG (2005) A unified formulation for continuum mechanics applied to fluid–structure interaction in flexible tubes. Int J Numer Methods Eng 64:1575–1593
97. Bijelonja I, Demirdžić I, Muzaferija S (2006) A finite volume method for incompressible linear elasticity. Comput Methods Appl Mech Eng 195:6378–6390
98. Giannopapa CG, Papadakis G (2006) New formulations of the dynamic equations of elastic solids suitable for a unified methodology for fluid–structure interaction problems. Comput Methods Appl Mech Eng
99. Giannopapa CG, Papadakis G (2008) Linear stability analysis and application of a new solution method of the elastodynamic equations suitable for a unified fluid–structure-interaction approach. ASME J Pressure Vessels Technol 130:31303-1
100. Bijelonja I, Demirdžić I, Muzaferija S (2017) Mixed finite volume method for linear thermoelasticity at all Poisson's ratios. Numer Heat Transf Part A Appl 72:215–235
101. Jasak H, Weller HG (2000) Finite volume methodology for contact problems of linear elastic solids. In: Proceedings of 3rd Congress of Croatian Society of Mechanics. Dubrovnik, Croatia, pp 253–260
102. Cardiff P, Karač A, Flavin R, FitzPatrick D, Ivanković A (2011) Contact stress analysis in OpenFOAM—application to hip joint bones. In: OpenFOAM Workshop, Penn State University, Penn State, PA, USA
103. Cardiff P, Karač A, Ivanković A (2011) Development of a finite volume methodology for linear elastic contact problems. In: 21st international workshop on computational mechanics of materials, IWCMM, Limerick, Limerick, Ireland
104. Cardiff P, Karač A, Ivanković A (2012) Development of a finite volume contact solver based on the penalty method. Comput Mater Sci 64:283–284
105. Cardiff P, Karač A, FitzPatrick D, Flavin R, Ivanković A (2014) Development of a hip joint model for finite volume simulations. J Biomech Eng 136:1–8. https://doi.org/10.1115/1.4025776
106. Maneeratana K, Ivanković A (1999) Finite volume method for structural applications involving material and geometrical nonlinearities. In: European council of computational mechanics Technische Universität München, Proceedings of the European conference on computational mechanics (ECCM'99), pp 874–875
107. Maneeratana K, Ivanković A (1999) Finite volume method for geometrically non-linear stress analysis applications. In: Proceedings of the seventh annual conference of the association for computational mechanics in engineering (ACME'1999)
108. Maneeratana K, Ivanković A (1999) Finite volume method for large deformation with linear hypoelastic materials. In: Vilsmeier R, Benkhaldoun F (eds) second international symposium on finite volumes for complex applications (FVCA II) for complex applications II: problems and perspectives. Hermes Science Publication, University Duisburg, Germany, pp 459–466
109. Maneeratana K, Ivanković A (2000) Modelling of high strain rate behaviour of a series 7108 aluminium alloy. In: Proceedings of the 14th conference of the mechanical engineering network of Thailand, pp 227–233
110. Bašić H (2012) Application of the finite volume method to the analysis of plastic metal flow in extrusion technologies. PhD thesis, University of Sarajevo (in Bosnian)
111. Bijelonja I (2002) Finite volume method for incremental analysis of small and large thermo-elasto-plastic deformations. PhD thesis, University of Sarajevo (in Bosnian)
112. Tuković Ž, Jasak H (2007) Updated Lagrangian finite volume solver for large deformation dynamic response of elastic body. Trans FAMENA 31:55–70
113. Tuković Ž, Jasak H (2007) FVM for fluid–structure interaction with large structural displacements. In: 2nd OpenFOAM Workshop, Zagreb, Croatia
114. Cardiff P, Karač A, Tuković Ž, Ivanković A (2012) Development of a finite volume based structural solver for large rotation of non-orthogonal meshes. In: 7th OpenFOAM Workshop, Darmstadt, Germany
115. Cardiff P, Karač A, Tuković Ž, Ivanković A (2013) An open-source finite method for computational solid mechanics. In: Joint symposium of Irish mechanics society and Irish society for scientific and engineering computation. University College Dublin, Dublin, Ireland
116. Cardiff P, Tuković Ž, Karač A, Ivanković A (2014) Nonlinear solid mechanics in OpenFOAM. In: 9th OpenFOAM Workshop. University of Zagreb, Croatia
117. Liu Q, Ming P-J, Zhang W-P (2018) Research on the nonlinear finite volume numerical method for the large rotating of disk. J Harbin Eng Univ 39:1012–1018
118. Ivanković A, Demirdžić I, Williams JG, Leevers PS (1993) A new numerical method for analysing dynamic fracture problems. In: ESIS symposium on impact and dynamic fracture of polymers and composites, Potro Cervo, Sardinia, Italy
119. Ivanković A, Demirdžić I, Williams JG, Leevers PS (1994) Application of the finite volume method to the analysis of dynamic fracture problems. Int J Fract 66:357–371
120. Ivanković A, Muzaferija S, Demirdžić I (1997) Finite volume method and multigrid acceleration in modelling of rapid crack propagation in full-scale pipe test. Comput Mech 20:46–52
121. Ivanković A, Venizelos GP (1998) Rapid crack propagation in plastic pipe: predicting full-scale critical pressure from S4 test results. Eng Fract Mech 59:607–622
122. Ivanković A (1999) Finite volume modelling of dynamic fracture problems. Comput Model Simul Eng 4:227–235
123. Ivanković A, Hillmansen S (2001) Evoluton of dynamic fractures in PMMA. Plast Rubber Compos 30:88–93
124. Stylianou V, Ivanković A (2002) Finite volume analysis of dynamic fracture phenomena I: a node release methodology. Int J Fract 113:107–123
125. Stylianou V, Ivanković A (2002) Finite volume analysis of dynamic fracture phenomena II: a cohesive zone type methodology. Int J Fract 113:125–151
126. Ivanković A, Williams JG, Pandya KC (2004) Crack growth predictions in polyethylene using measured traction–separation curves. Eng Fract Mech, pp 657–668
127. Rager A, Williams JG, Ivanković A (2005) Numerical analysis of the three point bend impact test for polymers. Int J Fract 135(1–4):199–215
128. Murphy N, Ivanković A (2005) The prediction of dynamic fracture evolution in PMMA using a cohesive zone model. Eng Fract Mech 72:861–875
129. Murphy N, Ali M, Ivanković A (2006) Dynamic crack bifurcation in PMMA. Eng Fract Mech 73(16):2569–2587
130. Tropša V, Georgiou I, Ivanković A, Kinloch AJ, Williams JG (2006) OpenFOAM in non-linear stress analysis: modelling of adhesive joints. In: 1st OpenFOAM workshop, Zagreb, Croatia
131. Tuković Ž (2010) Arbitrary crack propagation model in OpenFOAM. Technical report, Faculty of Mechanical Engineering and Naval Architecture, University of Zagreb, in association with the School of Mechanical and Materials Engineering, University College Dublin
132. Karač A, Blackman BRK, Cooper V, Kinloch AJ, Rodriguez Sanchez S, Teo WS, Ivanković A (2011) Modelling the fracture behaviour of adhesively-bonded joints as a function of test rate. Eng Fract Mech 78:973–989
133. Ivanković A, Tropša V, Williams JG (1997) Finite volume modelling of residual stresses in cast plastic slabs. In: Fifth

international conference on residual stresses, Linkoping, Sweden, pp 392–399
134. Tropša V, Ivankovic A, Williams JG (2000) Predicting residual stresses due to solidification in cast plastic plates. Plast Rubber Compos 29(9):468–474. https://doi.org/10.1179/146580100101541319
135. Sato A, Ohnaka I, Iwane J (2006) Stress analysis by finite volume method for prediction of porosity and deformation defects of spheroidal graphite castings. J Jpn Found Eng Soc 78:231–237 (in Japanese)
136. Teskeredžić A, Demirdžić I, Muzaferija S (2015) Numerical method for calculation of complete casting process—part I: theory. Numer Heat Transf Part B Fundam An Int J Comput Methodol 68:295–316
137. Teskeredžić A, Demirdžić I, Muzaferija S (2015) Numerical method for calculation of complete casting process—part II: validation and application. Numer Heat Transf Part B Fundam An Int J Comput Methodol 68:317–335
138. Henry FS, Collins MW (1993) A novel predictive model with compliance for arterial flows. BED-vol 26, Advances in Bioengineering. ASME
139. Henry FS, Collins MW (1993) Prediction of transient wall movement of an incompressible elastic tube using finite volume procedure. In: Proceedings of BIOMED93, Bath, UK
140. Greenshields CJ, Vanizelos GP, Ivanković A (2000) A fluid-structure model for fast brittle fracture in plastic pipes. J Fluids Struct 14:221–234
141. Ivanković A, Karač A, Dendrinos E, Parker K (2001) Blood flow in deformable arteries: the finite volume method for fluid–structure interaction problem. In: Proceedings of the 9th ACME conference on computational mechanics in engineering, Birmingham, UK
142. Schäfer M, Teschauer I (2001) Numerical simulation of coupled fluid–solid problems. Comput Methods Appl Mech Eng 190:3645–3667
143. Schäfer M, Teschauer I, Kadinski L, Selder M (2002) A numerical approach for the solution of coupled fluid–solid and thermal stress problems in crystal growth processes. Comput Mater Sci 24:409–419
144. Ivanković A, Karač A, Dendrinos E, Parker K (2002) Towards early diagnosis of artherosclerosis: the finite volume method for fluid–structure interaction. Biorheology 39:401–407
145. Torlak M, Muzaferija S (2002) Finite volume approach to computation of elastic plates and their interaction with fluid flows. In: Finite volumes for complex applications III—problems and perspectives. Kogan Page Science
146. Torlak M, Muzaferija S, Perić M (2002) Application of a finite volume method to the computation of interaction between thin linearly elastic structures and incompressible fluid flows. In: VDI-Berichte 1862, VDI Tagung Fluid-Struktur-Wechselwirkung, Wiesloch
147. Kovačević A, Stošić N, Smith IK, Numerical A (2004) A numerical study of fluid–solid interaction in screw compressors. Int J Comput Appl Technol 21:148–158. https://doi.org/10.1504/IJCAT.2004.006651
148. Stošić N, Smith I, Kovačević A (2005) Screw compressors. Springer, Berlin
149. Shaw G, Stone T (2005) Finite volume methods for coupled stress/fluid flow in commercial reservoir simulations. In: SPE reservoir simulation symposium, Houston, Texas. SPE 93430
150. Torlak M (2006) A finite-volume method for coupled numerical analysis of incompressible fluid flow and linear deformation of elastic structures. PhD thesis, Technischen Universitaet Hamburg-Harburg
151. Kovačević A, Stošić N, Smith IK (2006) Numerical simulation of combined screw compressor–expander machines for use in high pressure refrigeration systems. Simul Model Pract Theory 14:1143–1154
152. Kovačević A, Stošić N, Mujić E, Smith IK (2007) CFD integrated design of screw compressors. J Eng Appl Comput Fluid Mech 1:96–108
153. Stošić N, Smith I, Kovačević A (2007) Screw compressors. three dimensional computational fluid dynamics and solid–fluid interaction. Springer, Berlin
154. Papadakis G (2008) A novel pressure–velocity formulation and solution method for fluid–structure interaction problems. J Comput Phys 227:3383–3404
155. Jasak H, Jemcov A, Tuković Ž (2007) OpenFOAM: A C++ library for complex physics simulations. In: International workshop on coupled methods in numerical dynamics, Dubrovnik, Croatia
156. Kanyanta V, Ivanković A, Karač A (2009) Validation of a fluid–structure interaction numerical model for predicting flow transients in arteries. J Biomech 42:1705–1712
157. Jagad P, Puranik BP, Date AW (2011) A finite volume procedure on unstructured meshes for fluid-structure interaction problems. World Acad Sci Eng Technol Int J Mech Aerosp Ind Mechatron Manuf Eng 5:1406–1412
158. Wiedemair W, Tuković Ž, Jasak H, Poulikakos D, Kurtcuoglu V (2012) On ultrasound-induced microbubble oscillation in acapillary blood vessel and its implications for the blood–brain barrier. Phys Med Biol 57:1019–1045
159. Habchi C, Russeil S, Bougeard D, Harion J-L, Lemenand T, Ghanem A, Della Valle D, Peerhossaini H (2013) Partitioned solver for strongly coupled fluid–structure interaction. Comput Fluids 71:306–319
160. Tuković Ž, Cardiff P, Ivanković A, Karač A (2014) OpenFOAM library for fluid–structure interaction. In: 9th OpenFOAM Workshop, Zagreb, Croatia, Zagreb, Croatia
161. Smith I, Stošić N, Kovačević A (2014) Power recovery from low grade heat sources by the use of screw expanders. Chandos Publishing
162. Šekutkovski B, Kostić I, Simonović A, Cardiff P, Jazarević V (2016) Three-dimensional fluid–structure interaction simulation with a hybrid RANS-LES turbulence model for applications in transonic flow domain. Aerosp Sci Technol 49:1–16
163. Jagad P (2016) A numerical procedure for elastic solids. GIT-J Eng Technol 9:113–124
164. Cardiff P, Karač A, De Jaeger P, Jasak H, Nagy J, Ivanković A, Tuković Ž (2017) Towards the development of an extendable solid mechanics and fluid–solid interactions toolbox for OpenFOAM. In: 12th OpenFOAM Workshop, vol 12, University of Exeter, UK
165. Jagad P, Puranik BP, Date AW (2017) A numerical analysis of fluid–structure interaction problem with a flow channel embedded in a structural material. Proc Indian Natl Sci Acad 83:655–667
166. Jagad P, Puranik BP, Date AW (2018) A finite volume procedure for fluid flow, heat transfer and solid-body stress analysis. Int J Comput Methods Eng Sci Mech. https://doi.org/10.1080/15502287.2018.1434839
167. Demirdžić I, Ivanković A (1997) Finite volume approach to modelling of plates. In: Proceedings of 2nd Congress of Croatian Society of mechanics, Brac, Croatia, pp 101–108
168. Fallah N (2004) A cell vertex and cell centred finite volume method for plate bending analysis. Comput Methods Appl Mech Eng 193:3457–3470
169. Fallah N (2006) A finite volume method for plate buckling analysis. In: Mota Soares CA et al. (eds) III European conference on computational mechanics, solids, structures and coupled problems in engineering, Lisbon, Portugal, pp 5–8

170. Fallah N, Hatami F (2006) A displacement formulation based on finite volume method for analysis of Timoshenko beam. In: Proceedings of the 7th international conference on civil engineering Tehran, Iran, pp 8–10
171. Fallah N (2006) On the use of shape functions in the cell centered finite volume formulation for plate bending analysis based on Mindlin–Reissner plate theory. Comput Struct 84:1664–1672
172. Fallah N, Hatami F (2006) Extension of the finite volume method for instability analysis of columns with shear effects. In: Proceedings of the eighth international conference on computational structures technology, Stirlingshire, Scotland. Civil-Comp Press. Paper 192
173. Hatami F, Fallah N, Pourzeynali S (2006) Application of the finite volume method for shell analysis: a membrane study. In: Topping BHV, Montero G, Montenegro R (eds) Proceedings of the eighth international conference on computational structures technology. Civil-Comp Press, Stirlingshire, UK. https://doi.org/10.4203/ccp.83.160
174. Isić S, Doleček V, Karabegović I (2007) A comparison between finite element and finite volume methods on the problem of stability of Timoshenko beam. In: The 12th international conference on problems of material engineering, Jasna, Slovakia
175. Isić S, Doleček V, Karabegović I (2007) Numerical and experimental analysis of postbuckling behaviour of prismatic beam under displacement dependent loading. In: Proceedings of the first Serbian congress on theoretical and applied mechanics, Kopaonik, Serbia
176. Isić S, Doleček V, Karabegović I (2007) A comparison of finite element and finite volume method on stability analysis of rectangular plate. In: Doleček Karabegović V, Jurković M (eds) I. 6th international scientific conference on production engineering, development and modernization of production, RIM Bihac, BiH
177. Isić S (2008) Numerical and experimental analysis of nonlinear stability phenomena in elastic systems. PhD thesis, University of Bihac, Bosnia and Herzegovina (in Bosnian)
178. Fallah N (2013) Finite volume method for determining the natural characteristics of structures. J Eng Sci Technol 8:93–106
179. Fallah N, Parayandeh-Shahrestany A (2014) A novel finite volume based formulation for the elasto-plastic analysis of plates. Thin-Walled Struct 77:153–164
180. Fallah N, Ebrahimnejad M (2014) Finite volume analysis of adaptive beams with piezoelectric sensors and actuators. Appl Math Model 38:727–737
181. Jing L-L, Ming P-J, Zhang W-P, Fu L-R, Cao Y-P (2016) Static and free vibration analysis of functionally graded beams by combination Timoshenko theory and finite volume method. Compos Struct 138:192–213
182. Fallah N, Ghanbari A (2017) A displacement finite volume formulation for the static and dynamic analysis of shear deformable circular curved beams. Sci Iran. https://doi.org/10.24200/sci.2017.4259
183. Fallah N, Parayandeh-Shahrestany A, Golkoubi H (2017) A finite volume formulation for the elasto-plastic analysis of rectangular Mindlin–Reissner plates, a non-layered approach. Civil Eng Infrastruct J 50:293–310
184. Mohebi B, Kaboudan AR, Yazdanpanah O (2017) Damage detection in beam-like structures using finite volume method. J Rehabil Civ Eng 5:77–92
185. Fallah N, Ghanbary A (2018) A displacement finite volume formulation for the static and dynamic analysis of shear deformable curved beams. Sci Iran 25(3):999–1014
186. Amraei A, Fallah N (2018) A cell-centered finite volume formulation for the calculation of stress intensity factors in Mindlin–Reissner cracked plates. Civ Eng J 3:1366–1385
187. Tuković Ž, De Jaeger P, Cardiff P, Ivanković A (2019) A finite volume solver for geometrically exact Simo–Reissner beams. In: ECCOMAS MSF Thematic conference. Sarajevo, Bosnia and Herzegovina
188. Das S, Mathur SR, Murthy JY (2011) An unstructured finite-volume method for structure–electrostatic interactions in MEMS. Numer Heat Transf Part B Fundam 60:425–451
189. Das S, Koslowski M, Mathur SR, Murthy JY, Finite volume method for simulation of creep in RF MEMS devices. In ASME, (2011) International mechanical engineering congress and exposition: nano and micro materials, devices and systems; microsystems integration, vol 11. Denver, Colorado, p 2011
190. Dioh NN, Ivanković A, Demirdžić I (1995) Dynamic thermo elastic plastic deformation of solids using finite volume technique. In: Oñate E, Owen DRJ (ed) Computational plasticity, fundamentals and applications. Pineridge Press, pp 1947–1957
191. Dioh NN, Ivanković A, Leevers PS, Williams JG (1995) Stress wave propagation effects in split Hopkinson pressure bar tests. In: Proceedings of The Royal Society; proceedings: mathematical and physical sciences, pp 187–204
192. Djapic Oosterkamp L, Ivankovic A, Venizelos G (2000) High strain rate properties of selected aluminium alloys. Mater Sci Eng A 278(1):225–235. https://doi.org/10.1016/S0921-5093(99)00570-5
193. Weller HG, Tabor G, Jasak H, Fureby C (1998) A tensorial approach to computational continuum mechanics using object orientated techniques. Comput Phys 12:620–631
194. Jasak H, Weller HG (2000) Application of the finite volume method and unstructured meshes to linear elasticity. Int J Numer Methods Eng 48:267–287
195. Suvanjumrat C, Chaichanasiri E (2011) Implementation and validation of finite volume C++ codes for plane stress analysis. In: CST02, The Second TSME, Krabi. International conference on mechanical engineering
196. Haider J, Lee CH, Gil AJ, Huerta A, Bonet J (2018) An upwind cell centred total Lagrangian finite volume algorithm for nearly incompressible explicit fast solid dynamic applications. Comput Methods Appl Mech Eng 340:684–727
197. Demirdžić I, Muzaferija S, Perić M (1997) Benchmark solutions of some structural analysis problems using finite-volume method and multigrid acceleration. Int J Numer Methods Eng 40:1893–1908
198. Cardiff P, Tuković Ž, Jasak H, Ivanković AA (2014) Block-coupled finite volume methodology for linear elasticity. In: 9th OpenFOAM Workshop, vol 9. University of Zagreb, Croatia
199. González I, Naseri A, Chiva J, Rigola J, Pérez-Segarra CD (2018) An enhanced finite volume based solver for thermoelastic materials in fluid–structure coupled problems. In: 6th European conference on computational mechanics (ECCM 6), 7th European conference on computational fluid dynamics (eCFD 7), Glasgow, UK, 15 June 2018
200. Fowler BL, Yee RK (2003) Application of finite volume method for solid mechanics. In: Proceedings of the ASME IMECE conference international mechanical engineering congress and RD&D Expo, pp 15–21, November 2003. IMECE2003-44297
201. Bijelonja I (2011) A numerical method for almost incompressible body problem. In: Katalinić (ed) Proceedings of the 22nd international DAAAM symposium, Vienna, Austria, pp 321–322
202. Oliveira PJ, Rente CJ (1999) Development and application of a finite volume method for static and transient stress analysis. In: Proceedings of NAFEMS world congress '99 on effective engineering analysis, pp 297–309
203. Demirdžić I (2016) A fourth-order finite volume method for structural analysis. Appl Math Model 40:3104–3114

204. Fallah N (2008) A method for calculation of face gradients in two-dimensional cell centred finite volume formulation for stress analysis in solid problems. Sci Iran 15:286–294
205. Nordbotten JM (2014) Cell-centered finite volume discretizations for deformable porous media. Int J Numer Methods Eng 100:399–418
206. Nordbotten JM (2015) Convergence of a cell-centered finite volume discretization for linear elasticity. SIAM J Numer Anal 53:2605–2625
207. Keilegavlen E, Nordbotten JM (2017) Finite volume methods for elasticity with weak symmetry. Int J Numer Methods Eng. https://doi.org/10.1002/nme.5538
208. Tuković Ž, Karač A, Cardiff P, Jasak H, Ivanković A (2018) OpenFOAM finite volume solver for fluid–solid interaction. Trans FAMENA 42(3):1–31. https://doi.org/10.21278/TOF.42301
209. Fallah N (2008) Finite volume based formulations for the analysis of Bernouli and Timoshenko beams. J Numer Simul Eng 1(3):259–268
210. Golubović A (2017) Finite volume analysis of laminated composite plates. PhD thesis, University of Sarajevo
211. Godunov SK (1959) A difference method for numerical calculation of discontinuous solutions of the equations of hydrodynamics. Mat Sborn 47:271–306
212. Godunov SK (1962) The problem of a generalized solution in the theory of quasi-linear equations and in gas dynamics. Russ Math Surv 17:145–156
213. Trangenstein JA, Pember RB (1992) Numerical algorithms for strong discontinuities in elastic–plastic solids. J Comput Phys 103(1):63–89
214. Trangenstein JA (1994) Second-order Godunov algorithm for two-dimensional solid mechanics. Comput Mech 13:343–359
215. Miller GH, Puckett EG (1996) A high-order Godunov method for multiple condensed phases. J Comput Phys 128:134–164
216. Tang H, Sotiropoulos F (1999) A second-order Godunov method for wave problems in coupled solid water gas systems. J Comput Phys 151:790–815
217. Berezovski A, Maugin GA (2001) Simulation of thermoelastic wave propagation by means of a composite wave-propagation algorithm. J Comput Phys 168:249–264
218. Howell BP, Ball GJ (2002) A free-Lagrange augmented Godunov method for the simulation of elastic–plastic solids. J Comput Phys 175:128–167
219. Berezovski A, Maugin GA (2003) Simulation of wave and front propagation in thermoelastic materials with phase transformation. Comput Mater Sci 28:478–485
220. Kluth G, Després B (2008) F. V. schemes for hyperelastic–plastic models in finite deformations. In: Reymard B, Hérard J-M (eds) Finite volumes for complex applications V-problems and perspectives. Wiley, London
221. Carré G, Del Pino S, Després B, Labourasse E (2009) A cell-centered Lagrangian hydrodynamics scheme on general unstructured meshes in arbitrary dimension. J Comput Phys 228:5160–5183
222. Maire P-H, Abgrall R, Breil J, Loubère R, Rebourcet B (2013) A nominally second-order cell-centered Lagrangian scheme for simulating elastic–plastic flows on two-dimensional unstructured grids. J Comput Phys 235:626–665
223. Sambasivan SK, Shashkov M-J, Burton DE (2013) A finite volume cell-centered lagrangian hydrodynamics approach for solids in general unstructured grids. Int J Numer Method Fluids 72:770–810
224. Sijoy CD, Chaturvedi S (2015) An Eulerian multi-material scheme for elastic–plastic impact and penetration problems involving large material deformations. Eur J Mech B/Fluids 53:85–100. https://doi.org/10.1016/j.euromechflu.2015.04.004
225. Després B, Labourasse E (2015) Angular momentum preserving cell-centered Lagrangian and Eulerian schemes on arbitrary grids. J Comput Phys 290:28–54. https://doi.org/10.1016/j.jcp.2015.02.032
226. Ndanou S, Favrie N, Gavrilyuk S (2015) Multi-solid and multi-fluid diffuse interface model: applications to dynamic fracture and fragmentation. J Comput Phys 295:523–555. https://doi.org/10.1016/j.jcp.2015.04.024
227. Cheng J-B, Toro EF, Jiang S, Yu M, Tang W (2015) A high-order cell-centered Lagrangian scheme for one-dimensional elastic–plastic problems. Comput Fluids 122:136–152. https://doi.org/10.1016/j.compfluid.2015.08.029
228. Loubere R, Maire P-H, Rebourcet B (2016) Staggered and colocated finite volume schemes for Lagrangian hydrodynamics. In: Abgrall R, Shu C-W (eds) Handbook of numerical methods for hyperbolic problems, vol 17, pp 319 – 352. https://doi.org/10.1016/bs.hna.2016.07.003
229. Boscheri W, Dumbser M, Loubére R (2016) Cell centered direct arbitrary-Lagrangian–Eulerian ADER-WENO finite volume schemes for nonlinear hyperelasticity. Comput Fluids 134–135:111–129. https://doi.org/10.1016/j.compfluid.2016.05.004
230. Vilar F, Shu C-W, Maire P-H (2016) Positivity-preserving cell-centered Lagrangian schemes for multi-material compressible flows: from first-order to high-orders. Part I: the one-dimensional case. J Comput Phys 312:385–415. https://doi.org/10.1016/j.jcp.2016.02.027
231. Georges G, Breil J, Maire P-H (2017) A 3D finite volume scheme for solving the updated Lagrangian form of hyperelasticity. Int J Numer Methods Fluids 84(1):41–54. https://doi.org/10.1002/fld.4336
232. Heuzé T (2017) Lax–Wendroff and TVD finite volume methods for unidimensional thermomechanical numerical simulations of impacts on elastic-plastic solids. J Comput Phys 346:369–388. https://doi.org/10.1016/j.jcp.2017.06.027
233. Cheng J-B, Jia Y, Jiang S, Toro EF, Ming Yu (2017) A second-order cell-centered Lagrangian method for two-dimensional elastic–plastic flows. Commun Comput Phys 22(5):1224–1257. https://doi.org/10.4208/cicp.OA-2016-0173
234. Cheng J-B, Huang W, Jiang S, Tian B (2017) A third-order moving mesh cell-centered scheme for one-dimensional elastic–plastic flows. J Comput Phys 349:137–153. https://doi.org/10.1016/j.jcp.2017.08.018
235. Fridrich D, Liska R, Wendroff B (2017) Cell-centered Lagrangian Lax–Wendroff HLL hybrid method for elasto-plastic flows. Comput Fluids 157:164–174. https://doi.org/10.1016/j.compfluid.2017.08.030
236. Heuzé T (2018) Simulation of impacts on elastic–viscoplastic solids with the flux-difference splitting finite volume method applied to non-uniform quadrilateral meshes. Adv Model Simul Eng Sci 5(1):9, 2018 https://doi.org/10.1186/s40323-018-0101-z
237. Aguirre M, Gil AJ, Bonet J, Lee CH (2015) An upwind vertex centred finite volume solver for Lagrangian solid dynamics. J Comput Phys 300:387–422
238. Selim MM, Koomullil RP, Mcdaniel DR (2016) Linear elasticity finite volume based structural dynamics solver. In: AIAA modeling and simulation technologies conference, Washington, DC, USA. https://doi.org/10.2514/6.2016-4418
239. Selim MM, Koomullil R, McDaniel DR (2017) Finite volume based fluid–structure interaction solver. In: 58th AIAA/ASCE/AHS/ASC structures, structural dynamics, and materials conference, Grapevine, TX
240. Baliga BR, Patankar SV (1980) A new finite-element formulation for convection–diffusion problems. Numer Heat Trans Part B Fundam 3(4):393–409. https://doi.org/10.1080/01495728008961767

241. Taylor GA, Bailey C, Cross M (2003) A vertex-based finite volume method applied to non-linear material problems in computational solid mechanics. Int J Numer Methods Eng 56:507–529
242. Wheel MA (1996) A geometrically versatile finite volume formulation for plane elastostatic stress analysis. J Strain Anal Eng Des 31:111–116
243. Wheel MA (1996) A finite-volume approach to the stress analysis of pressurised axisymmetric structures. Int J Press Vessels Pip 68:311–317
244. Wheel MA (1998) Applying the finite volume approach to structural analysis. In: O'Donoghue PE, Atluri SN (ed) Modelling and simulation in engineering, pp 229–234
245. Wheel MA (1999) A mixed finite volume formulation for determining the small strain deformation of incompressible materials. Int J Numer Methods Eng 44:1843–1861
246. Costa VAF, Sousa ACM (2000) A control volume-based fem for the solution of the three-dimensional, elastic stress–strain equations. In: WSEAS Proceedings 2nd World MCME (Mathematics and Computers in Mechanical Engineering, MCME 2000), Vouliagmeni, Greece
247. Fallah N (2005) Using shape function in cell centred finite volume formulation for two dimensional stress analysis. Lecture series on computer and computational sciences (ICCMSE 2005), vol 4. Brill Academic Publishers, The Netherlands
248. Xia GH, Zhao Y, Yeo JH, Lv X (2007) A 3D implicit unstructured-grid finite volume method for structural dynamics. Comput Mech 40:299–312
249. Tsui Y-Y, Huang Y-C, Huang C-L, Lin S-W (2013) A finite-volume-based approach for dynamic fluid–structure interaction. Numer Heat Transf Part B Fundam 64(4):326–349. https://doi.org/10.1080/10407790.2013.806691
250. Wu Y, Xie X, Chen L (2013) Hybrid stress finite volume method for linear elasticity problems. Int J Numer Anal Model 10:634–656
251. Taylor GA, Bailey C, Cross M (1995) Solution of the elastic/visco-plastic constitutive equations: a finite volume approach. Appl Math Model 19:746–760
252. Ferguson WJ (1998) The control volume finite element numerical solution technique applied to creep in softwoods. Int J Solids Struct 35:1325–1338
253. Hambleton JP, Sloan SW, Pyatigorets AV, Voller VR (2011) Lower bound limit analysis using the control volume finite element method. In: 13th international conference of the IACMAG, Melbourne, Australia, pp 88–93
254. Fallah N, Bailey C, Cross M (1999) Finite volume method for stress analysis. In: Proceedings ASME The 7th annual conference of the association for computational mechanics in engineering, vol 99, Durham, UK, pp 135–138
255. Fallah N, Bailey C, Cross M, Taylor GA (2000) Comparison of finite element and finite volume methods application in geometrically nonlinear stress analysis. Appl Math Model 24:439–455
256. Fallah N, Bailey C, Cross M (2000) CFD approach for solid mechanics analysis. In: European congress on computational methods in applied sciences and engineering, ECCOMAS 2000, Barcelona, Spain, 11–14 September 2000
257. Fallah N (2000) Computational stress analysis using finite volume methods. PhD thesis, University of Greenwich
258. Slone AK, Fallah N, Bailey C, Cross M (2002) A finite volume approach to geometrically nonlinear stress analysis. In: Third international symposium on finite volumes for complex applications—problems and perspectives, pp 663–670
259. Teran J, Blemker S, Hing VNT, Fedkiw R (2003) Finite volume methods for the simulation of skeletal muscle. In: Eurographics/SIGGRAPH symposium on computer animation
260. Limache AC, Idelsohn SR (2007) On the development of finite volume methods for computational solid mechanics. Mec Comput 26:827–843
261. Wheel MA (1997) A finite volume method for analyzing the bending deformation of thick and thin plates. Comput Methods Appl Mech Eng 147:199–208
262. Beveridge AJ, Wheel M (2009) A control volume based formulation of the discrete Kirchoff triangular thin plate bending element. In: The 17th UK national conference on computational mechanics in engineering, Nottingham, UK, pp 287–290
263. Taylor GA (1996) A vertex based discretisation scheme applied to material non-linearity within a multi-physics framework. PhD thesis, University of Greenwich
264. Bailey C, Chow P, Cross M, Fryer Y, Pericleous K (1996) Multiphysics modelling of metals casting process. Proc R Soc Lond Math Phys Eng Sci, pp 459–486
265. Bailey C, Taylor GA, Bounds SM, Moran G, Cross M (1997) PHYSICA: a multiphysics computational framework and its application to casting. Miner Metal Process Power Gener, pp 419–425
266. Bailey C, Bounds S, Cross M, Moran G, Pericleous K, Taylor GA (1999) Multiphysics modeling and its application to the casting process. Comput Model Simul Eng 4:206–212
267. Bailey C, Taylor GA, Cross M, Chow P (1999) Discretisation procedures for for multi-physics phenomena. J Comput Appl Math 103:3–17
268. Oldroyd AB, Wheel MA, Scanlon TJ (1999) An integrated volume based approach for analysing flow induced vibrations. In: Proceedings European conference on computational mechanics (ECCM), Munich, Germany, September 1999
269. Wheel MA, Oldroyd A, Scanlon TJ, Wenke P (1999) Integrating finite volume based structural analysis procedures with CFD software to analyse fluid–structure interaction. In: Proceedings of 2nd international confernce on finite volumes for complex applications, Duisburg, Germany
270. Slone AK (2000) A finite volume unstructured mesh approach to dynamic fluid–structure interactions between fluids and linear elastic solids. PhD thesis, University of Greenwich
271. Slone AK, Pericleous K, Bailey C, Cross M (2001) Details of an integrated approach to three- dimensional dynamic fluid–structure interaction. Fluid–structure interaction. WIT Press, London, pp 57–66
272. Slone AK, Pericleous K, Bailey C, Cross M (2002) Dynamic fluid–structure interaction using finite volume unstructured mesh procedures. Comput Struct 80:371–390
273. Slone AK, Bailey C, Cross M (2003) Dynamic solid mechanics using finite volume methods. Appl Math Model 27:69–87
274. Slone AK, Pericleous K, Bailey C, Cross M, Bennett C (2004) A finite volume unstructured mesh approach to dynamic fluid–structure interaction: an assessment of the challenge of predicting the onset of flutter. Appl Math Model 28:211–239
275. Slone AK, Croft TN, Williams AJ, Cross M (2007) An alternative mixed Eulerian–Lagrangian approach to high speed collision between solid structures on parallel clusters. Adv Eng Softw 38(4): 244–255. https://doi.org/10.1016/j.advengsoft.2006.09.015
276. Cross M, Croft TN, Slone AK, Williams AJ, Christakis N, Patel MK, Bailey C, Pericleous K (2007) Computational modelling of multi-physics and multi-scale processes in parallel. Int J Comput Methods Eng Sci Mech 8(2):63–74. https://doi.org/10.1080/15502280601149510
277. Lv X, Zhao Y, Huang XY, Xia GH, Su XH (2007) A matrix-free implicit unstructured multigrid finite volume method for simulating structural dynamics and fluid–structure interaction. J Comput Phys 225:120–144

278. Croft TN, Williams AJ, Slone AK, Cross M (2008) A two-dimensional prototype multi-physics model of the right ventricle of the heart. Int J Numer Methods Fluids 57(5):583–600. https://doi.org/10.1002/fld.1764
279. Xia GH, Lin Cl (2008) An unstructured finite volume approach for structural dynamics in response to fluid motions. Comput Struct 86:684–701
280. Hejranfar K, Azampour MH (2016) Simulation of 2D fluid–structure interaction in inviscid compressible flows using a cell-vertex central difference finite volume method. J Fluids Struct 67:190–218
281. Taylor GA (1995) Material non-linearity within a finite volume framework for the simulation of a metal casting process. Comput Plast Fundam Appl II:1459–1470
282. Taylor GA, Bailey C, Cross M (1998) A three dimensional finite volume approach to the thermomechanical modelling of the shape casting of metals. In: Proceedings of 8th international conference on modelling of casting, welding and advanced solidification processes
283. Cross M (1996) Computational issues in the modelling of materials-based manufacturing processes. J Comput Aided Mater Des 3:100–116
284. Bounds S, Moran G, Pericleous K, Cross M, Croft TN (2000) A computational model for defect prediction in shape castings based on the interaction of free surface flow, heat transfer, and solidification phenomena. Metall Mater Trans B 31:515–527
285. Williams AJ, Croft TN, Cross M. (2001) Computational modelling of metals extrusion and forging processes. In: Cross M, Ewans JW, Bailey C (eds) Computational modelling of materials, minerals and metals processing, TMS, pp 481–490 (2001)
286. Williams AJ, Croft TN, Cross M (2002) Computational modelling of metal extrusion and forging processes. J Mater Process Technol 125:573–582. https://doi.org/10.1016/S0924-0136(02)00401-6
287. Williams AJ, Slone AK, Croft TN, Cross M (2010) A mixed Eulerian–Lagrangian method for modelling metal extrusion processes. Comput Methods Appl Mech Eng 199:2123–2134
288. Taylor GA, Hughes M, Pericleous K (2000) The application of three dimensional finite volume methods to the modelling of welding phenomena. In: Sahm PR, Hansen PN, Conley JG (eds) Welding and advanced solidification processes IX, modeling of casting
289. Taylor GA, Hughes M, Strusevich N, Pericleous K (2002) Finite volume methods applied to the computational modelling of welding phenomena. Appl Math Model 26:309–320
290. Taylor GA, Breiguine V, Bailey C, Cross M (2000) An augmented Lagrangian contact algorithm employing a vertex-based finite volume method. In: ACME, 2000. http://www.brunel.ac.uk/ eesrgat/research/ps_pubs
291. Gong J-F, Xuan L-K, Ming P-J, Zhang W-P (2013) Thermoelastic analysis of functionally graded solids using a staggered finite volume method. Compos Struct 104:134–143
292. Gong J-F, Ming P-J, Xuan L-K, Zhang W-P (2014) Thermoelastic analysis of three-dimensional functionally graded rotating disks based on finite volume method. J Mech Eng Sci. https://doi.org/10.1177/0954406213489933
293. Perré P, Passard J (1995) A control-volume procedure compared with the finite-element method for calculating stress and strain during wood drying. Drying Technol 13:635–660
294. Salinas C, Chávez C, Gatica Y, Ananias R (2011) Two-dimensional wood drying stress simulation using control control-volume mixed finite element methods (CVFEM). Ingenere Investig 31:171–183
295. Wheel MA (2008) A control volume-based finite element method for plane micropolar elasticity. Int J Numer Methods Eng 75:992–1006
296. Beveridge AJ, Wheel M, Nash D (2013) A higher order control volume based finite element method to predict the deformation of heterogeneous materials. Comput Struct 129:56–62
297. Zhu M, Ming P-J, Xuan L, Zhang W-P (2012) An unstructured finite volume time domain method for structural dynamics. Appl Math Model 36:183–192
298. Xuan L, Ming P-J, Gong J, Zheng D, Zhang W-P (2014) A finite volume time domain method for in-plane vibration on mixed grids. J Vib Acoust. https://doi.org/10.1177/1687814017690068
299. Xuan L, Ming P-J, Zhang W-P, Jin G, Gong J (2014) Time domain finite volume method for the transient response and natural characteristics of structural–acoustic coupling in an enclosed cavity. Shengxue Xuebao/Acta Acoust 39:215–225
300. Wenke P, Wheel MA (2003) A finite volume method for solid mechanics incorporating rotational degrees of freedom. Comput Struct 81:321–329
301. Pan W, Wheel M, Qin Y (2010) Six-node triangle finite volume method for solids with a rotational degree of freedom for incompressible material. Comput Struct 88:1506–1511
302. Pan W, Wheel M (2011) A finite-volume method for solids with a rotational degrees of freedom based on the 6-node triangle. Int J Numer Methods Biomed Eng 27:1411–1426
303. McManus K, Cross M, Walshaw C, Johnson S, Leggett P, Scalable A (2000) Strategy for the parallelization of multiphysics unstructured mesh-iterative codes on distributed-memory systems. Int J High Perform Comput Appl 14:137–174
304. McManus K, Cross M, Walshaw C, Croft TN, Williams AJ (2002) Parallel performance in multi-physics simulation. In: ICCS '02 Proceedings of the international conference on computational science—part II. Springer, London, pp 806–815
305. Maitre JF, Rezgui A, Souhail H, Zine AM (2002) High order finite volume schemes: application to non-linear elasticity problems. In: Finite volumes for complex applications, III (Porquerolles), Hermes Science Publishers, Paris, pp 391–398
306. Souhail H (2004) Schéma volumes finis: estimation d'erreur a posteriori hiérarchique par éléments finis mixtes. Résolution de problémes d'élasticité non-linéaire. PhD thesis, Ecole Centrale de Lyon
307. Zhang J, Liu T (1999) P-SV wave propagation in heterogeneous media: grid method. Geophys J Int 136:431–438
308. Zhang J, Liu T (2002) Elastic wave modelling in 3-D heterogeneous media: 3-D grid method. Geophys J Int 150:780–799
309. Zhang J (2004) Wave propagation across fluid–solid interfaces: a grid method approach. Geophys J Int 159:240–252
310. Liu T, Liu K, Zhang J (2004) Unstructured grid method for stress wave propagation in elastic media. Comput Methods Appl Mech Eng 193:2427–2452
311. Liu T, Liu K, Zhang J (2005) Triangular grid method for stress-wave propagation in 2-D orthotropic materials. Arch Appl Mech 74:477–488
312. Gao H, Zhang J (2006) Parallel 3-D simulation of seismic wave propagation in heterogeneous anisotropic media: a grid method approach. Geophys J Int 165:875–888
313. Dormy E, Tarantola A (1995) Numerical simulation of elastic wave propagation using a finite volume method. J Geophys Res 100:2123–2133. https://doi.org/10.1029/94JB02648
314. Harlow FH, Welch JE (1965) Numerical calculation of the time-dependent viscous incompressible flow of fluid with free surface. Phys Fluids 8:2182
315. Spalding DB (1993) Simulation of fluid flow, heat transfer and solid deformation simultaneously. In: NAFEMS Conference No 4, Brighton, UK
316. Spalding DB (1997) Simultaneous fluid-flow, heat-transfer and solid-stress computation in a single computer code. In: Keynote lecture 4th international colloquium on process simulation. Helsinki University of Technology, Espoo, Finland

317. Spalding DB (1998) Fluid–structure interaction in the presence of heat transfer and chemical reaction. In: ASME/JSME point pressure vessels and piping conference, San Diego, CA, USA
318. Spalding DB (1998) Fluid–structure interaction in the presence of heat transfer and chemical reaction. In: Kudriavtsev V, Cheng W (eds) Computational technologies for fluid/thermal/structural/chemical systems with industrial applications
319. Spalding DB (2002) Simultaneous prediction of solid stress, heat transfer and fluid flow by a single algorithm. In: ASME pressure vessels and piping conference, Vancouver, British Columbia, Canada
320. Spalding DB (2006) Extending the boundaries of heat transfer. In: The 13th international heat transfer conference, Sydney, Australia
321. Spalding DB (2008) Enlarging the frontiers of computational fluid dynamics. In: International symposium heat and mass transfer and hydrodynamics in swirling flow, Moscow, Russia
322. Patanker SV, Spalding DB (1972) A calculation procedure for heat, mass, and momentum transfer in three-dimensional parabolic flows. Int J Heat Mass Transf 15:1787
323. Patankar SV (1980) Numerical hear transfer and fluid flow. Hemisphere Publishing Corporation, McGraw-Hill Book Company, Washington
324. Hattel JH, Hansen P, Hansen LF (1993) Analysis of thermally induced stresses in die casting using a novel control volume technique. In: Piwonka T (ed) Modelling of casting and welding and advanced solidification processes advanced solidification processes minerals advanced solidification processes minerals metals and materials society. TMS
325. Hattel JH, Hansen PN, Andersen S (1993) Modeling of thermal induced stresses in high pressure die casting dies. In: NADCA 19th international die casting congress, NADC, Transactions, Rosemant, IL, USA
326. Hattel JH (1993) Stress calculations using a control volume based finite difference method. Revnedannelse og Brudmekanik, DMS Vintermderbog
327. Hattel JH (1993) Control volume based finite difference method—numerical modeling of thermal and mechanical conditions in casting and heat treatment processes. PhD thesis, Institute of Manufacturing Engineering, Technical University of Denmark
328. Hattel JH, Hansen PN (1994) 1-D analytical model for the thermally induced stresses in the mold surface during die casting. Appl Math Model 18:550–559
329. Hattel JH, Hansen PN (1995) A control volume-based finite difference method for solving the equilibrium equations in terms of displacements. Appl Math Model 19:210–243
330. Hattel JH (1997) Numerical modelling of stresses and deformations in casting processes. In: Proceedings of CASTING international ADI and simulation conference. Helsinki University of Technology, Helsinki
331. Pryds N, Hattel JH (1997) Numerical modelling of rapid solidification. Model Simul Mater Sci Eng 5(5):451–472
332. Hattel JH, Thorborg J, Andersen S (1998) Stress/strain modelling of casting processes in the framework of the control-volume method. In: Modeling of casting and advanced solidification processes VIII, Warrendale, USA: TMS, The Minerals, Metals and Materials Society, pp 763–770
333. Hattel JH, Pryds N (2001) Modelling rapid solidification with the control volume method. In: Dinesen AR, Eldrup M, Juul Jensen D, Linderoth S, Pedersen TB, Pryds NH, Schrder Pedersen A, Wert JA (eds) Proceedings of science of metastable and nanocrystalline alloys—structure, properties and modelling, Roskilde, Ris National Laboratory, pp 241–247
334. Thorborg J (2001) Nonlinear constitutive modelling in thermomechanical processes with the control volume method. PhD thesis, Department of Manufacturing Engineering, Technical University of Denmark
335. Hattel JH, Thorborg J (2003) A numerical model for predicting the thermomechanical conditions during hydration of early-age concrete. Appl Math Model 27:1–26
336. Thorborg J, Hattel JH (2003) Thermo-elasto-plasticity in solidification processes using the control volume method on staggered grid. In: Stefanescu et al (ed) Modelling of casting, welding and advanced solidification processes. Warrendale: TMS—The Minerals, Metals and Materials Society
337. Wang L, Melnik R (2007) Finite volume analysis of nonlinear thermo-mechanical dynamics of shape memory alloys. Heat Mass Transf 43:535
338. Rajagopal KR, Srinivasa AR, Ponnalagu A (2014) Thermo-inelastic response of polymeric solids. Technical report, Final Report, Texas Engineering Experiment Station, Harvey Mitchell Parkway South, Suite 300, College Station, TX
339. Aboudi J, Pindera M-J, Arnold SM (1999) Higher-order theory for functionally graded materials. Compos B Eng 30:777–832
340. Aboudi J (2001) Micromechanical analysis of fully coupled electro–magneto–thermo–elastic multiphase composites. Smart Mater Struct 10:867–877
341. Aboudi J, Pindera M-J, Arnold SM (2001) Linear thermoelastic higher-order theory for periodic multiphase materials. ASME J Appl Mech 68:697–707
342. Haj-Ali R, Aboudi J (2009) Nonlinear micromechanical formulation of the high fidelity generalized method of cells. Int J Solids Struct 46:2577–2592
343. Haj-Ali R, Aboudi J (2012) Discussion paper: has renaming the high fidelity generalized method of cells been justified? Int J Solids Struct 49:2051–2058
344. Bansal Y, Pindera M-J (2005) A second look at the higher-order theory for periodic multiphase materials. ASME J Appl Mech 72:177–195
345. Bansal Y, Pindera M-J (2006) Finite-volume direct averaging micromechanics of heterogeneous materials with elastic–plastic phases. Int J Plast 22:775–825
346. Aboudi J (1982) A continuum theory for fiber-reinforced elastic–viscoplastic composites. Int J Eng Sci 20:605–621
347. Aboudi J (1991) Mechanics of composite materials: a unified micromechanical approach. Elsevier, Amsterdam
348. Paley M, Aboudi J (1992) Micromechanical analysis of composites by the generalized cells model. Mech Mater 14:127–139
349. Cavalcante MAA, Pindera M-J (2016) Generalized FVDAM theory for elastic–plastic periodic materials. Int J Plast 77:90–117
350. Aboudi J (2004) The generalized method of cells and high-fidelity generalized method of cells micromechanical models: a review. Mech Adv Mater Struct 11:329–366
351. Pindera M-J, Khatam H, Drago AS, Bansal Y (2009) Micromechanics of spatially uniform heterogeneous media: a critical review and emerging approaches. Compos B Eng 40:349–378
352. Charalambakis N, Murat F (2006) Homogenization of stratified thermoviscoplastic materials. Q Appl Math 64(2):359–99
353. Aboudi J, Arnold SM, Bednarcyk BA (2007) Micromechanical analyses of smart composite materials. Nova Science Publishers, New York
354. Aboudi J (2008) Finite strain micromechanical modeling of multiphase composites. Int J Multiscale Comput Eng 6:411–434
355. Atluri SN, Shen S (2002) The meshless local Petrov–Galerkin (MLPG) method: a simple & less-costly alternative to the finite element and boundary element methods. Comput Model Eng Sci 3:11–51
356. Atluri SN, Zhu T (1998) A new meshless local Petrov–Galerkin (MLPG) approach in computational mechanics. Comput Mech 22:117–127. https://doi.org/10.1007/s004660050346

357. Ching H-K, Batra RC (2001) Determination of crack tip fields in linear elastostatics by the meshless local Petrov–Galerkin (MLPG) Method. Comput Model Eng Sci 2:273–289
358. Warlock A, Ching H-K, Kapila AK, Batra RC (2002) Plane strain deformations of an elastic material compressed in a rough rectangular cavity. Int J Eng Sci 40:991–1010
359. Qian L, Batra R, Chen L (2003) Elastostatic deformations of a thick plate by using a higher-order shear and normal deformable plate theory and two meshless local Petrov–Galerkin (MLPG) methods. Comput Model Eng Sci 4(1):161–76
360. Raju I, Phillips D (2003) Further developments in the MLPG method for beam problems. Comput Model Eng Sci 4(1):141–60
361. Atluri SN, Han Z, Rajendran A (2004) A new implementation of the meshless finite volume method, through the MLPG "mixed" approach. Comput Model Eng Sci 6(6):491–514
362. Han Z, Atluri SN (2004) Meshless local Petrov–Galerkin (MLPG) approaches for solving 3D problems in elasto-statics. Comput Model Eng Sci 6:169–88
363. Batra RC, Porfiri M, Spinello D (2004) Treatment of material discontinuity in two meshless local Petrov–Galerkin (MLPG) formulations of axisymmetric transient heat conduction. Int J Numer Methods Eng 61:2461–2479
364. Han Z, Rajendran A, Atluri SN (2005) Meshless local Petrov–Galerkin (MLPG) approaches for solving nonlinear problems with large deformations and rotations. Comput Model Eng Sci 10(1):1
365. Sladek J, Sladek V, Solek P, Saez A (2008) Dynamic 3D axisymmetric problems in continuously non-homogeneous piezoelectric solids. Int J Solids Struct 45(16):4523–4542. https://doi.org/10.1016/j.ijsolstr.2008.03.027
366. Moosavi MR, Khelil A (2008) Accuracy and computational efficiency of the finite volume method combined with the meshless local Petrov-Galerkin in comparison with the finite element method in elasto-static problem. ICCES 5:211–38
367. Moosavi MR, Khelil A (2009) Finite volume meshless local Petrov–Galerkin method in elastodynamic problems. Eng Anal Bound Elem 33:1016–1021
368. Moosavi MR, Delfanian F, Khelil A (2011) Orthogonal meshless finite volume method in elasticity. Thin-Walled Struct 49:708–712
369. Moosavi MR, Delfanian F, Khelil A (2011) The orthogonal meshless finite volume method for solving Euler–Bernoulli beam and thin plate problems. Thin-Walled Struct 49:923–932
370. Hosseini SM, Sladek J, Sladek V (2011) Meshless local Petrov–Galerkin method for coupled thermoelasticity analysis of a functionally graded thick hollow cylinder. Eng Anal Bound Elem 35(6):827–835. https://doi.org/10.1016/j.enganabound.2011.02.001
371. Soares D, Sladek V, Sladek J (2012) Modified meshless local Petrov–Galerkin formulations for elastodynamics. Int J Numer Methods Eng 90(12):1508–1828. https://doi.org/10.1002/nme.3373
372. Moosavi MR, Delfanian F, Khelil A (2012) Orthogonal meshless finite volume method applied to crack problems. Thin-Walled Struct 52:61–65
373. Moosavi M, Delfanian F, Khelil A (2012) Orthogonal meshless finite volume method in shell analysis. Finite Elem Anal Des 62:1–7
374. Moosavi MR (2013) Orthogonal meshless finite volume method applied to elastodynamic crack problems. Int J Fract 179:1–7. https://doi.org/10.1007/s10704-012-9752-9
375. Ebrahimnejad M, Fallah N, Khoei AR (2015) Adaptive refinement in the meshless finite volume method for elasticity problems. Comput Math Appl 69:1420–1443
376. Ebrahimnejad M, Fallah N, Khoei AR (2017) Three types of meshless finite volume method for the analysis of two-dimensional elasticity problems. Comput Appl Math 36(2):971–990
377. Fallah N (2018) Mesh-free and mesh based finite volume methods for solid mechanics analysis. In: 41st solid mechanics conference (SOLMECH 2018), Warsaw, Poland
378. Davoudi-Kia A, Fallah N (2017) Comparison of enriched meshless finite-volume and element-free Galerkin methods for the analysis of heterogeneous media. Eng Comput. https://doi.org/10.1007/s00366-017-0573-3
379. Davoudi-Kia A, Fallah N (2018) An enriched meshless finite volume method for the modeling of material discontinuity problems in 2D elasticity. Latin Am J Solids Struct 15(2):209–219. https://doi.org/10.1590/1679-78254121
380. Fallah N, Nikraftar N (2018) Meshless finite volume method for the analysis of fracture problems in orthotropic media. Eng Fract Mech. https://doi.org/10.1016/j.engfracmech.2018.09.029
381. Bašić H, Demirdžić I, Muzaferija S (2001) Analysis of plastic flow of metals during extrusion processes using finite volume method. In: Proceedings of 3rd international conference on industrial tools, Slovenia, pp 22–26
382. Bašić H (2008) Friction models comparison in finite volume method simulation of bulk metal forming technologies. J Technol Plast 33:113–122
383. Bašić H (2009) The constitutive models in numerical simulation of steady-state metal forming processes. J Technol Plast 34:27–36
384. Chen ZZ, Lou ZL, Ruan XY (2007) Finite volume simulation and mould optimization of aluminum profile extrusion. J Mater Process Technol 190(1–3):382–386. https://doi.org/10.1016/j.jmatprotec.2007.01.032
385. Jafari MR, Zebarjad SM, Kolahan F (2007) Simulation of thixoformability of A356 aluminum alloy using finite volume method. Mater Sci Eng A 454:558–563. https://doi.org/10.1016/j.msea.2006.11.124
386. Lou S, Zhao G, Wang R, Wu X (2008) Modeling of aluminum alloy profile extrusion process using finite volume method. J Mater Process Technol 206:481–490
387. Al-Athel KS, Gadala MS (2011) Eulerian volume of solid (VOS) approach in solid mechanics and metal forming. Comput Methods Appl Mech Eng 200:2145–2159
388. Wang R, Li HZ (2011) Modeling of aluminum extrusion process using non-orthogonal block structured grids based FVM. Adv Mater Res 189:1749–1752
389. Wang R (2012) Body fitted grids based FVM simulation of aluminum extrusion process. Adv Mater Res 418:2102–2105
390. Bressan JD, Martins MM, Button ST (2013) Aluminium extrusion analysis by the finite volume method. In: Nate O, Owen DRJ, Peric D, Suárez B (eds) XII international conference on computational plasticity. Fundamentals and applications COMPLAS XII
391. Zhang C, Chen H, Zhao G, Zhang L, Lou S (2016) Optimization of porthole extrusion dies with the developed algorithm based on finite volume method. Int J Adv Manuf Technol 85:1–13
392. de Brauer A, Iollo A, Milcent T (2016) A Cartesian scheme for compressible multimaterial models in 3D. J Comput Phys 313:121–143. https://doi.org/10.1016/j.jcp.2016.02.032
393. de Brauer A, Iollo A, Milcent T (2017) A Cartesian scheme for compressible multimaterial hyperelastic models with plasticity. Commun Comput Phys 22(5):1362–1384. https://doi.org/10.4208/cicp.OA-2017-0018
394. Teng JG, Chen SF, Hu JL (1999) A finite volume method for deformation analysis of woven fabrics. Int J Numer Methods Eng 46:2061–2098

395. Chen SF, Hu JL, Teng JG (2001) A finite-volume method for contact drape simulation of woven fabrics and garments. Finite Elem Anal Des 37:513–531
396. Martin B, Pascal F (2011) Discrete duality finite volume method applied to linear elasticity. Finite Vol Complex Appl VI Prob Perspect 4:663–671
397. Martin B (2012) Elaboration de solveurs volumes finis 2D/3D pour résoudre le problème de l'elasticité linéaire. PhD thesis, Ecole normale supérieure de Cachan - ENS Cachan, Francais
398. Di Pietro DA, Eymard R, Lemaire S, Masson R (2011) Hybrid finite volume discretization of linear elasticity models on general meshes. In: Fürst J, Halama J, Herbin R, Hubert F (eds) Finite Volumes for Complex Applications: VI Problems & Perspectives, volume 4 of Springer proceedings in mathematics. Springer, Berlin, pp 331–339
399. Wilkins ML (1963) Calculation of elastic–plastic flow, T3 - UCRL; 7322. Technical report, Lawrence Radiation Laboratory, Lawrence Livermore Laboratory, University of California, Berkeley. https://catalog.hathitrust.org/Record/007293160
400. Wilkins ML (1964) Calculations of elastic–plastic flow. In: Adler B, Fernback S, Rotenberg M (eds) Methods of computational physics, vol 3. Lawrence Radiation Laboratory, Livermore
401. Wilkins ML (1999) Computer simulation of dynamic phenomena. Springer, Berlin
402. Bessonov NM, Golovashchenko SF, Volpert VA (2009) Numerical modelling of contact elastic-plastic flows. Math Model Nat Phenomena 4(1):44–87
403. Rhie CM, Chow WL (1983) Numerical study of the turbulent flow past an airfoil with trailing edge separation. AIAA J 21:1525–1532. https://doi.org/10.2514/3.8284
404. Jameson A, Schmidt W, Turkel E (1981) Numerical solution of the Euler equations by finite volume methods using Runge–Kutta time-stepping schemes. In: AIAA 5th computational fluid dynamics conference, vol 81, p 1259
405. Jacobs DAH (1980) Preconditioned conjugate gradient methods for solving systems of algebraic equations. Technical report, Central Electricity Research Laboratories Report (RD/L/N193/80)
406. Hassan OII (2019) A vertex centred finite volume algorithm for fast solid dynamics: total and updated Lagrangian descriptions. PhD thesis, University of Swansea
407. Belytschko T, Liu WK, Moran B, Elkhodary KI (2014) Nonlinear finite elements for continua and structures, 2nd edn. Wiley, Chichester
408. Bathe KJ (1996) Finite element procedures. Prentice Hall, New Jersey
409. Schäfer M (2006) Computational engineering—introduction to numerical methods. Springer, Berlin
410. Zienkiewicz OC, Taylor RL (2000) The finite element method, solid mechanics, vol 2, 5th edn. Butterworth Heinemann, Oxford
411. Laursen TA (2002) Computational contact and impact mechanics. Springer, Berlin
412. Dassault Systémes Simulia Corp. Abaqus 6.14 (2018) http://www.simulia.com/products/abaqus_fea.html
413. Oñate E, Cervera M (1993) Derivation of thin plate bending elements with one degree of freedom per node. Eng Comput 10:543–561
414. Oñate E (1998) Elementos finitos y volumenes finitos puntos de encuentro y posibilidad de nuevas aplicaciones. Technical report, CIMNE, Barcelona
415. Oñate E, Zarate F (2000) Rotation-free triangular plate and shell elements. Int J Numer Methods Eng 47:557–603
416. Zienkiewicz OC (1995) Origins, milestones and directions of the finite element method: a personal view. Arch Comput Methods Eng State Art Rev 2(1):1–48
417. Lahrmann A (1992) An element formulation for the classical finite difference and finite volume method applied to arbitrarily shaped domains. Int J Numer Methods Eng 35:893–913
418. Harrild DM, Henriquez CS (1997) A finite volume model of cardiac propagation. Ann Biomed Eng 25:315–334
419. Fang Q, Tsuchiya T, Yamamoto T (2002) Finite difference, finite element and finite volume methods applied to two-point boundary value problems. J Comput Appl Math 139:9–19
420. Yamamoto T, Fang Q, Tsuchiya T (2002) Finite element and finite volume methods applied to two-point boundary value problems. J Comput Appl Math 139:9–19
421. Jacquemet V, Henriquez CS (2005) Finite volume stiffness matrix for solving anisotropic cardiac propagation in 2-D and 3-D unstructured meshes. IEEE Trans Biomed Eng 52:1490–1492
422. Jacquemet V (2005) Link between the FEM and FVM formulations of anisotropic cardiac propagation in unstructured meshes. Technical report, ITS Technical Report, TR-ITS 021:2005
423. Filippini G, Maliska CR, Vaz M Jr (2014) A physical perspective of the element-based finite volume method and FEM-Galerkin methods within the framework of the space of finite elements. Int J Numer Methods Eng 98:24–43
424. Demirdžić I (2020) Finite volumes vs finite elements. There is a choice. Coupled Syst Mech 9(1):5–28. https://doi.org/10.12989/csm.2020.9.1.005
425. Hassan OI, Ghavamian A, Lee CH, Gil AJ, Bonet J, Auricchio F (2019) An upwind vertex centred finite volume algorithm for nearly and truly incompressible explicit fast solid dynamic applications: total and updated lagrangian formulations. J Comput Phys 3:100025. https://doi.org/10.1016/j.jcpx.2019.100025
426. Smith IM, Griffiths DV, Margetts L (2013) Programming the finite element method, 5th edn. Wiley, London
427. Reed WH, Hill TR (1973) Triangular mesh methods for the neutron transport equation. Technical report, Los Alamos Scientific Lab., New Mexico (USA). Technical Report 836, LA-UR-73-479; CONF-730414-2
428. Cockburn B (2003) Discontinuous Galerkin methods. Technical report, School of Mathematics, Univeristy of Minnesota
429. Cockburn B, Gopalakrishnan J, Lazarov R (2009) Unified hybridization of discontinuous Galerkin, mixed, and continuous Galerkin methods for second order elliptic problems. SIAM J Numer Anal 47:1319–1365. https://doi.org/10.1137/070706616
430. Fu G, Cockburn B, Stolarski H (2015) Analysis of an HDG method for linear elasticity. Int J Numer Methods Eng 102(3–4):551–575. https://doi.org/10.1002/nme.4781
431. Qiu W, Shen J, Shi K (2018) An hdg method for linear elasticity with strong symmetric stresses. Math Comput 87:69–93. https://doi.org/10.1090/mcom/3249
432. Sevilla R, Giacomini M, Karkoulias A, Huerta A (2018) A superconvergent hybridisable discontinuous Galerkin method for linear elasticity. Int J Numer Methods Eng 116:91–116. https://doi.org/10.1002/nme.5916
433. Hesthaven JS, Warburton T (2007) Nodal discontinuous Galerkin methods: algorithms, analysis, and applications (texts in applied mathematics). Springer, New York
434. Slone AK, Pericleous K, Bailey C, Cross M (1997) Dynamic fluid–structure interactions using finite volume unstructured mesh procedures. In: International forum on aero-elasticity and structural dynamics, pp 417–424
435. Demirdžić I (1998) Finite volume approach to multi-physics problems. In: Alturi SN, O'Donoghue PE (eds) Modelling and simulation based engineering. Tech Science Press, Palmdale, pp 1757–1762
436. Schäfer M, Meynen S, Sieber R, Teschauer I (2000) Multigrid methods for coupled fluid–solid problems. In: European congress on computational methods in applied sciences and engineering, ECCOMAS 2000, Barcelona, Spain

437. Slone AK, Cross M, Pericleous K, Bailey C (2000) A finite volume approach to dynamic fluid–structure interaction. In: 8th annual conference of the association for computational mechanics in engineering (ACME 2000). Greenwich University, London, UK, pp 218–221
438. Slone AK, Pericleous K, Bailey C, Cross M (2000) Dynamic fluid–structure interactions using finite volume unstructured mesh procedures. In: 8th symposium on multidisciplinary analysis and optimization, multidisciplinary analysis optimization conferences. American Institute of Aeronautics and Astronautics. https://doi.org/10.2514/6.2000-4788
439. Slone AK, Pericleous K, Bailey C, Cross M (2001) Dynamic fluid–structure interactions using finite volume unstructured mesh procedures. In: ECCOMAS computational fluid dynamics conference
440. Slone AK, Cross M, Pericleous K, Bailey C, Cross M (2001) Using finite volume unstructured mesh approach to dynamic fluid–structure interaction: an assessment of the challenge of flutter analysis. In: Wall WA, Bletzinger KU, Schweizerhof K (eds) Trends in computational structural mechanics. CIMNE: International Centre for Numerical Methods in Engineering, 2001, pp 741–750
441. Džaferović E (2002) Interaction of viscoplastic fluid and viscoelastic solid—numerical modelling. PhD thesis, University of Sarajevo (in Bosnian)
442. Karač A, Ivanković A (2002) Drop impact of fluid-filled plastic containers: finite volume method for coupled fluid-structure-fracture problems. In: Mang HA, Rammerstorfer FG, Eberhardsteiner J (eds) WCCM V. Fifth world congress on computational mechanics, Vienna, Austria
443. Slone AK, Croft TCN, Williams AJ, Cross M (2002) A two fluid approach to high impact interaction amongst solid structures. In: Mang HA, Rammerstorfer FG, Eberhardsteiner J (eds) Fifth world congress on computational mechanics Proceedings. Vienna University of Technology, Vienna, Austria
444. Slone AK, Grossman D, Williams AJ, Pericleous K, Bailey C, Cross M (2002) A time and space accurate numerical approach to closely coupled fluid–structure interaction problems. In: 11th international colloquium on numerical analysis and computer science with applications, Plovdiv, Bulgaria
445. Karač A, Ivanković A (2003) Fully predictive model of the drop impact and fracture of fluid-filled plastic containers. In: Proceedings of 11th ACME conference on computational mechanics in engineering, Glasgow. University of Strathclyde Publishing, pp 113–116
446. Karač A, Ivanković A (2003) Modelling the drop impact behaviour of fluid-filled polyethylene containers. In: Blackman BRK, Pavan A, Williams JG (eds) Fracture of polymers. ESIS publication 32. Composites and adhesives, pp 253–264
447. Karač A (2003) Drop impact of fluid-filled polyethylene containers. PhD thesis, Imperial College London
448. Cross M, Slone AK, Croft TN, Williams AJ (2004) Computational modelling of thermal fluid–structure interaction processes. In: Topping BHV (ed) Progress in engineering computational technology, pp 111–126. Saxe-Coberg Publications
449. Karač A, Ivanković A (2004) Modelling drop impact and fracture of fluid-filled plastic containers. In: Proceedings of The 15th European conference on fracture—advanced fracture mechanics for life and safety assessments, Stockholm, Sweden
450. Giannopapa CG (2004) Fluid–structure interaction in flexible vessels. PhD thesis, University of London
451. Giannopapa CG, Papadakis G (2004) A new formulation for solids suitable for a unified solution method for fluid–structure interaction problems. In: ASME PVP, San Diego, CA, vol 491-1, pp 111–117
452. Slone AK, Cross M (2006) A comparison of finite element and finite volume methods for computational structural mechanics and their application in multi-physics problems. In: 5th international conference on engineering computational technology. Civil-Comp Press
453. Slone AK, Croft TN, Williams AJ, Cross M (2006) A mixed Eulerian–Lagrangian approach to high speed collision between solid structures on parallel clusters. In: 5th international conference on engineering computational technology. Civil-Comp Press
454. Cross M, Croft TN, McBride D, Slone AK, Williams AJ (2006) Using mixed discretisation schemes in multi-physics simulation. In: Innovation in engineering computational technology, pp 309–324
455. Papadakis G, Giannopapa CG (2006) Towards a unified solution method for fluid–structure interaction problems: progress and challenges. In: Proceedings of PVP 2006-ICPVT11 10th international symposium on emerging technology in fluids, Vancouver, Canada
456. Giannopapa CG, Papadakis G (2007) Indicative results and progress on the development of the unified single solution method for fluid–structure interaction problems (CASA-report, No. 0711). Technical report, Technische Universiteit Eindhoven, Eindhoven
457. Karač A, Ivanković A (2009) Investigating the behaviour of fluid-filled polyethylene containers under base drop impact: a combined experimental/numerical approach. Int J Impact Eng 36:621–631
458. Safari A, Ivanković A, Tuković Ž, Casey E, Walter M (2009) A fluid–structure interaction study of biofilm detachment. In: 1st international conference on mathematical and computational biomedical engineering—CMBE2009, June 29–July 1, Swansea, UK
459. Slone AK, Williams AJ, Croft TN, Cross M (2009) Dynamic fluid–structure interaction in parallel: a challenge for scalability. In: Topping BHV, Ivanyi P (eds) Parallel, distributed and grid computing for engineering. Saxe-Coburg Publications, pp 329–350
460. Das S, Mathur SR, Murthy JY (2010) An unstructured finite-volume method for structure–electrostatic interactions in MEMS. In Proceedings of IMECE2010. ASME International mechanical engineering congress and exposition, Vancouver, Canada, p 2010
461. Kelly A, O'Rourke M-J (2010) Two system, single analysis, fluid–structure interaction modelling of the abdominal aortic aneurysms. Proc Inst Mech Eng Part H J Eng Med 224(H8):955–970
462. Kelly A, O'Rourke M-J (2012) Fluid, solid and fluid–structure interaction simulations on patient-based abdominal aortic aneurysm models. Proc Inst Mech Eng Part H J Eng Med 226(4):288–304
463. Das S (2013) Fluid–structure interactions in microstructures. PhD thesis, University of Texas at Austin
464. de Oliveira IL, Gasche JL, Militzer J, Baccin CE (2017) Using FOAM-extend to assess the influence of fluid–solid interaction on the flow in intracranial Aneurismus. In: COBEM-2017-0851, 24th ABCM international congress of mechanical engineering, Curitiba, PR, Brazil
465. de Oliveira IL (2017) Using FOAM-extend to assess the influence of fluid–structure interaction on the rupture of intracranial aneurysms. PhD thesis, Sao Paulo State University, Júlio De Mesquita Filho
466. Cardiff P, Karač A, De Jaeger P, Jasak H, Nagy J, Ivanković A, Tuković Ž (2018) Towards the development of an extendable solid mechanics and fluid–solid interactions toolbox for

OpenFOAM. preprint. arXiv:1808.10736 [math.NA], available at https://arxiv.org/abs/1808.10736
467. Tuković Ž, Bukač M, Cardiff P, Jasak H, Ivanković A (2018) Added mass partitioned fluid–structure interaction solver based on a robin boundary condition for pressure. In: OpenFOAM selected papers of the 11th workshop. Springer, Berlin, pp 1–23
468. Leevers PS, Venizelos G, Ivanković A (1993) Rapid crack propagation along pressurized pipe: small-scale testing and numerical modelling. Constr Build Mater 7:179–184
469. Demirdžić I, Ivanković A, MacGillivray HJ, Maneeratana K (1996) Numerical modelling of high-rate tensile tests using finite volume formulation. In: Proceedings of IUTAM symposium on innovative computational methods for fracture and damage, Dublin, Ireland
470. Murphy N, Ivanković A (1999) Dynamic fracture simulation of brittle material characterised by microcrack-dominated failure mechanisms. In: Proceedings of 7th ACME conference computation mechanics in engineering, pp 99–102, Durham, UK
471. Stylianou V (1999) Finite volume modelling of rapid crack propagation (RCP) in brittle polymers. PhD thesis, Imperial College, London
472. Pandya KC, Ivanković A, Williams JG (2000) Cohesive zone modelling of crack growth in polymers—part 2—numerical simulation of crack growth. Plast Rubber Compos 29:447–452
473. Pandya KC, Ivanković A, Williams JG (2000) Predicting crack growth in tough polyethylene from measured cohesive zone traction-separation curves. In: Proceedings of 11th international confernce on deformation, yield and fracture of polymers
474. Pandya KC, Ivanković A, Williams JG (2000) Predictive fracture modelling in tough polyethylenes using experimentally measured cohesive zone traction curves. In: Proceedings of 13th European conference on fracture—ECF13, San Sebastian, Spain
475. Ivanković A, Jasak H, Karač A, Tropša V, Leevers P (2002) Fully predictive model of RCP in plastic pipes. In: Proceedings of 14th European conference on fracture, Kracow, Poland
476. Ivanković A, Jasak H, Karač A, Tropša V (2002) Prediction of dynamic fracture in pressurised plastic pipes. Annu Conf Assoc Comput Mech Eng 10:173–176
477. Ivanković A, Murphy N, Hillmansen S (2004) Evolution of dynamic fractures in PMMA: experimental and numerical investigations. In: Aliabadi MH, Ivanković A (eds) Advances in fracture mechanics, vol 9. WIT Press/Computational Mechanics Publications, Southampton
478. Murphy N (2007) Dynamic fracture of PMMA: a combined experimental and numerical investigation. PhD thesis, University College Dublin
479. McAuliffe D, Karač A, Murphy N, Ivanković A (2011) Transferability of adhesive fracture toughness measurements between peel and TDCB test methods for a nano-toughened epoxy. Adhesion Society. http://hdl.handle.net/10197/4765
480. McAuliffe D, Karač A, Murphy N, Ivanković A (2012) Determination of the cohesive strength and toughening mechanisms of a nano-modified adhesive under a triaxial stress. Adhesion Society
481. McAuliffe D (2012) Fracture toughness characterisation of a nano-modified structural adhesives. PhD thesis, University College Dublin
482. Cooper V, Ivankovic A, Karač A, McAuliffe D, Murphy N (2012) Effects of bond gap thickness on the fracture of nano-toughened epoxy adhesive joints. Polymer 53(24):5540–5553. https://doi.org/10.1016/j.polymer.2012.09.049
483. Georgiou I, Ivanković A, Kinloch AJ, Tropša V (2003) Rate dependent fracture behaviour of adhesively bonded joints. In: Pavan A, Blackman BRK, Williams JG (eds) Fracture of polymers, composites and adhesives II, volume 32 of European Structural Integrity Society, pp 317 – 328. Elsevier, Amsterdam
484. Georgiou I, Hadavinia H, Ivanković A, Kinloch AJ, Tropša V, Williams JG (2003) Cohesive zone models and the plastically-deforming peel test. J Adhes 79:239–265
485. Cooper V, Ivanković A, Karač A (2008) A mode I fracture behaviour analysis of adhesively bonded joints. In: European conference on fracture, volume 17, Brno, Czech Republic
486. Cooper VJ (2010) The fracture behaviour of nano-toughened structural epoxy adhesives. PhD thesis, University College Dublin
487. Tabaković A, Karač A, Ivanković A, Gibney A, McNally C, Gilchrist MD (2010) Modelling the quasi-static behaviour of bituminous material using a cohesive zone model. Eng Fract Mech 77:2403–2418
488. Carolan D (2011) Mechanical and fracture properties of PCBN as a function of rate and temperature. PhD thesis, University College Dublin
489. Petrović M (2011) The behaviour of polycrystalline diamonds as a function of rate and temperature. PhD thesis, University College Dublin
490. Carolan D, Ivanković A, Murphy N (2012) Numerical investigation into dynamic fracture of pcbn. Key Eng Mater 488:553–556
491. Carolan D, Ivanković A, Murphy N (2013) A combined experimental-numerical investigation of fracture of polycrystalline cubic boron nitride. Eng Fract Mech 99:101–117
492. Alveen P, McNamara D, Carolan D, Murphy N, Ivanković A (2014) Analysis of two-phase ceramic composites using micromechanical models. Comput Mater Sci 92:318–324
493. McNamara D, Alveen P, Carolan D, Murphy N, Ivanković A (2014) Micromechanical study of strength and toughness of advanced ceramics. Proc Mater Sci 3:1810–1815
494. Alveen P (2015) An experimental-numerical investigation into the properties of polycrystalline cubic boron nitride towards materials optimisation. PhD thesis, University College Dublin
495. Manchanda R (2015) A general poro-elastic model for pad-scale fracturing of horizontal wells. A general poro-elastic model for pad-scale fracturing of horizontal wells. PhD thesis, University of Texas at Austin
496. McNamara D, Alveen P, Carolan D, Murphy N, Ivanković A (2015) Numerical analysis of the strength of polycrystalline diamond as a function of microstructure. Int J Refract Metal Hard Mater 52:195–202
497. McNamara D (2015) The mechanical and fracture properties of polycrystalline diamond as a function of microstructure. PhD thesis, University College Dublin
498. Lee D (2017) A model for hydraulic fracturing and proppant placement in unconsolidated sands. PhD thesis, University of Texas at Austin
499. Yi S (2018) Development of computationally efficient 2D and pseudo-3D multi-fracture models with applications to fracturing and refracturing. PhD thesis, University of Texas at Austin
500. Sabbagh-Yazdi SR, Farhoud A, Gharebaghi SA (2018) Simulation of 2D linear crack growth under constant load using GFVM and two-point displacement extrapolation method. Appl Math Model. https://doi.org/10.1016/j.apm.2018.05.022
501. Pindera M-J (1991) Local/global stiffness matrix formulation for composite materials and structures. Compos Eng 1(2):69–83
502. Aboudi J, Pindera M-J, Arnold SM (1994) Elastic response of metal matrix composites with tailored microstructures to thermal gradients. Int J Solids Struct 31:1393–1428
503. Aboudi J (2002) Micromechanical analysis of the fully coupled finite thermoelastic response of rubberlike matrix composites. Int J Solids Struct 39:2587–2612
504. Aboudi J, Pindera M-J, Arnold SM (2002) High-fidelity generalized method of cells for inelastic periodic multiphase materials. Technical report, NASA TM-2002-211469

505. Zhong Y, Pindera M-J, Arnold S (2002) Efficient reformulation of HOTFGM: heat conduction with variable thermal conductivity. NASA CR 2002-211910
506. Aboudi J, Pindera M-J, Arnold SM (2003) Higher-order theory for periodic multiphase materials with inelastic phases. Int J Plast 19:805–847
507. Bansal Y, Pindera M-J (2003) Efficient reformulation of the thermo-elastic higher-order theory for FGMs. J Therm Stresses 26(11–12):1055–1092
508. Arnold SM, Bednarcyk B, Aboudi J (2004) Comparison of the computational efficiency of the original versus reformulated high-fidelity generalized method of cells. Technical report, NASA/TM-2004-213438
509. Bansal Y, Pindera M-J (2004) Testing the predictive capability of the high-fidelity generalized method of cells using an efficient reformulation. Technical report, NASA/CR-2004-213043
510. Bednarcyk BA, Arnold SM, Aboudi J, Pindera M-J (2004) Local field effects in titanium matrix composites subject to fiber-matrix debonding. Int J Plast 20:1707–1737
511. Pindera M-J, Bansal Y, Zhong Y (2004) Finite-Volume Direct Averaging Theory for Functionally Graded Materials (FVDAT-FGM). Technical report, NASA Disclosure of Invention and New Technology Form 1679
512. Zhong Y, Bansal Y, Pindera M-J (2004) Efficient reformulation of the thermal higher-order theory for FGM's with variable thermal conductivity. Int J Comput Eng Sci 5(4):795–831
513. Aboudi J (2005) Micromechanically established constitutive equations for multiphase materials with viscoelastic–viscoplastic phases. Mech Time-Depend Mater 9:121–145
514. Aboudi J, Gilat R (2005) Micromechanical analysis of lattice blocks. Int J Solids Struct 42:4372–4392
515. Cavalcante MAA (2006) Modelling of the transient thermo-mechanical behavior of composite material structures by the finite-volume theory. Master's thesis, Federal University of Alagoas, Maceio, Alagoas, Brazil
516. Pindera M-J, Bansal Y (2006) Finite volume direct averaging micromechanics of heterogeneous materials with elastic–plastic phases. Int J Plast 22:775–825
517. Bruck HA, Gilat R, Aboudi J, Gershon AL (2007) A new approach for optimizing the mechanical behavior of porous microstructures for porous materials by design. Modell Simul Mater Sci Eng 15:653–674
518. Cavalcante MAA, Marques SPC, Pindera M-J (2007) Parametric formulation of the finite-volume theory for functionally graded materials—part I: analysis. ASME J Appl Mech 74:935–945
519. Cavalcante MAA, Marques SPC, Pindera M-J (2007) Parametric formulation of the finite-volume theory for functionally graded materials—part II: numerical results. ASME J Appl Mech 74:946–957
520. Drago AS, Pindera M-J (2007) Micro-macromechanical analysis of heterogeneous materials: macroscopically homogeneous vs periodic microstructures. Compos Sci Technol 67(6):1243–63
521. Gattu M (2007) Parametric finite volume theory for periodic heterogeneous materials. Master's thesis, University of Virginia, Charlottesville, VA, USA
522. Pindera M-J, Bansal Y (2007) On the micromechanics-based simulation of metal–matrix composite response. J Eng Mater Technol 129(3):468–82
523. Ryvkin M, Aboudi J (2007) The effect of fiber loss in periodic composites. Int J Solids Struct 44:3497–3513
524. Bednarcyk BA, Aboudi J, Arnold SM, Sullivan RM (2008) Analysis of space shuttle external tank spray-on foam insulation with internal pore pressure. J Eng Mater Technol 130:041005–0410016
525. Cavalcante MAA, Marques SPC, Pindera M-J (2008) Computational aspects of the parametric finite-volume theory for functionally graded materials. Comput Mater Sci 44:422–438
526. Gattu M, Khatam H, Drago AS, Pindera M-J (2008) Parametric finite-volume micromechanics of uniaxial, continuously-reinforced periodic materials with elastic phases. J Eng Mater Technol 130:31015–31030
527. Paulino GH, Pindera M-J, Dodds RH, Rochinha FE, Dave EV, Chen L (2008) Multiscale and functionally graded materials. In: AIP conference proceedings, vol 973. Melville, New York
528. Cavalcante MAA, Marques SPC, Pindera M-J (2009) Transient thermo-mechanical analysis of a layered cylinder by the parametric finite-volume theory. J Therm Stresses 32:112–134
529. Gao X, Song Y, Sun Z (2009) Quadrilateral subcell based finite volume micromechanics theory for multiscale analysis of elastic periodic materials. ASME J Appl Mech 76:011013–1
530. Khatam H, Pindera M-J (2009) Parametric finite-volume micromechanics of periodic materials with elastoplastic phases. Int J Plast 25:1386–1411
531. Khatam H, Pindera M-J (2009) Thermo-elastic moduli of lamellar composites with wavy architectures. Compos B Eng 40(1):50–64
532. Khatam H, Chen L, Pindera M-J (2009) Elastic and plastic response of perforated plates with different porosity architectures. Trans ASME J Eng Mater Technol 131(3):031014–031015
533. Aboudi J, Freed Y (2010) Shape memory alloys: manufacture properties and applications. Micromechanical modeling of shape memory alloy composites. Nova Science Publishers, New York
534. Bednarcyk BA, Aboudi J, Arnold SM, Sullivan RM (2010) Micromechanics modeling of composites subjected to multiaxial progressive damage in the constituents. AIAA J 48:1367–1378
535. Haj-Ali R, Aboudi J (2010) Formulation of the high-fidelity generalized method of cells with arbitrary cell geometry for refined micromechanics and damage in composites. Int J Solids Struct 47:3447–3461
536. Khatam H, Pindera M-J (2010) Plasticity-triggered architectural effects in periodic multilayers with wavy microstructures. Int J Plast 26(2):273–287
537. Aboudi J (2011) The effect of anisotropic damage evolution on the behavior of ductile and brittle matrix composites. Int J Solids Struct 48:2102–2119
538. Cavalcante MAA, Marques SPC, Pindera M-J (2011) Transient finite-volume analysis of a graded cylindrical shell under thermal shock loading. Mech Adv Mater Struct 18:53–67
539. Cavalcante MAA, Khatam H, Pindera M-J (2011) Homogenization of elastic–plastic periodic materials by FVDAM and FEM approaches—an assessment. Compos B Eng 42:1713–1730
540. Chareonsuk J, Vessakosol P (2011) Numerical solution for functionally graded solids under thermal and mechanical loads using a high-order control volume finite element method. Appl Therm Eng 31:213–27
541. Khatam H, Pindera M-J (2011) Plastic deformation modes in perforated sheets and their relation to yield and limit surfaces. Int J Plast 27(10):1537–59
542. Carolan D, Tuković Ž, McNamara D, Alveen P, Murphy N, Ivanković A (2012) Effect of microstructure on the fracture toughness of polycrystalline cubic boron nitride. In: 7th OpenFOAM workshop, Darmstadt, Germany
543. Cavalcante MAA, Pindera M-J (2012) Generalized finite-volume theory for elastic stress analysis in solid mechanics—Part I: framework. ASME J Appl Mech 79:051006
544. Cavalcante MAA, Pindera M-J (2012) Generalized finite-volume theory for elastic stress analysis in solid mechanics—part II: results. ASME J Appl Mech 79:051007

545. Cavalcante MAA (2012) Generalized finite-volume micromechanics theory for heterogeneous materials. PhD thesis, University of Virginia
546. Khatam H, Pindera M-J (2012) Microstructural scale effects in the nonlinear elastic response of bio-inspired wavy multilayers undergoing finite deformation. Compos B Eng 43(3):869–84
547. Cavalcante MAA, Pindera M-J (2013) Generalized FVDAM, theory for periodic materials with elastic- plastic phases. In: CILAMCE, (2013) Proceedings of the XXXIV Iberian Latin-American Congress on Computational Methods in Engineering. ABMEC, Pirenpólis, GO, Brazil
548. Cavalcante MAA, Pindera M-J (2014) Generalized FVDAM theory for periodic materials undergoing finite deformations—part I: framework. ASME J Appl Mech 81(2):021005–021010
549. Cavalcante MAA, Pindera M-J (2014) Generalized FVDAM theory for periodic materials undergoing finite deformations—part II: numerical results. ASME J Appl Mech 81(2):021006–021012
550. Cardiff P, Leonard M, Murphy N, Ivanković A (2014) Fracture toughness optimization of nano-toughened structural adhesives: a representative volume element approach. In: Proceedings of the 37th annual meeting of the Adhesion Society, San Diego, CA, USA
551. Leonard M (2014) Micro-mechanical modelling of toughening mechanisms in nano-toughened structural adhesives. PhD thesis, University College, Dublin
552. Tu W, Pindera M-J (2014) Cohesive zone-based damage evolution in periodic materials via finite volume homogenization. ASME J Appl Mech 81(10):1–12
553. Carolan D, Ivankovic A, Chong HM, Kinloch AJ, Taylor AC (2015) Co-continuous polymer systems: a numerical investigation. Comput Mater Sci 98:24–33
554. Tu W (2016) CZM-based finite-volume homogenization and optimization of periodic composites. PhD thesis, University of Virginia
555. Chen Q, Wang G, Chen X, Geng J (2017) Finite-volume homogenization of elastic/viscoelastic periodic materials. Compos Struct 182:457–470
556. Chen Q, Wang G, Pindera M-J (2018) Finite-volume homogenization and localization of nanoporous materials with cylindrical voids. Part 1: theory and validation. Eur J Mech A Solids. https://doi.org/10.1016/j.euromechsol.2018.02.004
557. Chen Q, Tu W, Liu R, Chen X (2018) Parametric multiphysics finite-volume theory for periodic composites with thermo-electro-elastic phases. J Intell Mater Syst Struct 29:530–552
558. Ye J, Hong Y, Cai H, Wang Y, Zhai Z, Shi B (2018) A new three-dimensional parametric FVDAM for investigating the effective elastic moduli of particle-reinforced composites with interphase. Mech Adv Mater Struct. https://doi.org/10.1080/15376494.2018.1452321
559. Bijelonja I, Muzaferija S, Demirdžić I (2000) Some computational aspects of finite volume analysis of solid body deformation. In: Proceedings of 3rd congress of Croatian Society of Mechanics, Dubrovnik, Croatia, pp 261–267
560. Cross M, Walshaw C, Williams AJ, Slone AK, Croft TN, McManus K (2003) Parallel processing for nonlinear problems. In: Oñate E, Owen DRJ (eds) VII international conference on computational plasticity, CIMNE, Barcelona, Spain
561. Demirdžić I, Džaferović E, Ivanković A (2003) Predicting residual stresses due to solidification in cast plastic plates. In: 4th international congress of Croatian Society of Mechanics
562. Williams AJ, Slone AK, Croft TN, Cross M (2003) A mixed Eulerian–Lagrangian approach for metal forming. In: 6th ESAFORM conference on Metal Forming, Salerno, Italy
563. Kalkan H (2011) A combined experimental-numerical investigation on aluminium extrusion. Master's thesis, Atilim University, Ankara, Turkey
564. Mohan J, Karač A, Murphy N, Ivanković A (2011) An experimental and numerical investigation of the mixed-mode fracture toughness and lap shear strength of aerospace grade composite joints. Key Eng Mater 488:549–552
565. Cardiff P, De Jaeger P, Tuković Ž, Ivanković A (2014) A finite approach to simulation of wire rolling. In: Joint symposium of Irish Mechanics Society and Irish Society for Scientific and Engineering Computation, Galway
566. Cardiff P, Tuković Ž, Ivankovic A, De Jaeger P (2018) Development of an arbitrary Lagrangian–Eulerian finite volume method for metal forming simulation in OpenFOAM. In: The 13th OpenFOAM workshop (OFW13), Shanghai, China, June 24–29
567. Clancy M, Cardiff P, De Jaeger P, Ivankovic A (2018) Implementation of advanced plasticity models in OpenFOAM. In: The 13th OpenFOAM Workshop (OFW13), Shanghai, China, June 24–29
568. Grossman D, Bailey C, Pericleous K, Slone AK (2002) Computational modelling of blood flow and artery wall interaction. In: 9th workshop on the finite element methods in biomedical engineering biomechanics and related fields, University of Ulm, Germany
569. Anthony CM (2003) Finite volume modelling of the human leg. Master's thesis, Imperial College London
570. Alakija O, Ivanković A, Karač A (2005) Finite volume solution to high rate wave propagation through a lung alveoli stack. In: IUTAM symposium on impact biomechanics: from fundamental insights to applications, pp 281–288
571. Quinn NM, Ivanković A, Karač A (2007) An experimental and numerical investigation into the deformation profiles of mock arteries. In: ASME Summer Bioengineering Conference
572. Quinn NM, Ivanković A, Karač A (2007) A combined experimental and numerical investigation into early atherosclerosis. In: The fifteenth UK conference of the association of computational mechanics in engineering, Glasgow, UK, 2–3 April, 2007. Civil-Comp Press. https://doi.org/10.4203/ccp.85.11
573. Safari A, Ivanković A, Tuković Ž (2008) Numerical modelling of viscoelastic response of bacterial biofilm to mechanical stress. In: Bioengineering in Ireland conference, Radisson Hotel, Sligo, January, pp 25–26
574. Kanyanta V, Ivanković A, Karač A (2009) Accurate prediction of blood flow transients: a fluid–structure interaction approach in hemodynamic wall shear stress. In: Nithiarasu P (ed) 1st international conference on mathematical and computational biomedical engineering—CMBE2009, Swansea, UK
575. Kanyanta V (2009) Towards early diagnosis of atherosclerosis: wall shear prediction. PhD thesis, University College Dublin, Ireland
576. Kelly S (2009) Thrombus growth and its influence on the stress distribution in patient-based abdominal aortic aneurysm models. PhD thesis, University College Dublin
577. Cardiff P, Karač A, Flavin R, FitzPatrick D, Ivanković A (2010) The development of a numerical model of the hip joint for complex soft tissue reconstructions around the hip joint. In: 13th annual Sir Bernard Crossland symposium, University College Dublin, Dublin, Ireland
578. Cardiff P, Karač A, Flavin R, FitzPatrick D, Ivanković A (2011) The development of a numerical model of the hip joint. In $17^{th}$ Bioengineering In Ireland, Galway, Ireland
579. Cardiff P, Karač A, Flavin R, FitzPatrick D, Ivanković A (2011) Numerical analysis of the hip joint bones in contact. In: ACME-UK Heriott-Watt University, Edinburgh, Scotland
580. Quinn N (2011) Towards early diagnosis of atherosclerosis: combined experimental and numerical investigation into the deformation of mock arterial models. PhD thesis, University College Dublin
581. Cardiff P, Karač A, Flavin R, FitzPatrick D, Ivanković A (2012) Modelling the muscles for hip joint stress analysis using a finite

volume methodology. In: 18th Bioengineering In Ireland, Belfast, Northern Ireland
582. Cardiff P, Karač A, FitzPatrick D, Flavin R, Ivanković A (2014) Development of mapped stress-field boundary conditions based on a Hill-type muscle model. Int J Numer Methods Biomed Eng. https://doi.org/10.1002/cnm
583. Khalili Parsa H (2014) Compression tests on fluid-filled gelatine microcapsules: a combined experimental/numerical study. PhD thesis, University College Dublin
584. Safari A (2015) A combined experimental and numerical study of biofilm detachment. PhD thesis, University College Dublin
585. Fitzgerald K, Cardiff P, Flavin R, Ivankovic A (2016) Calculation of hip joint contact pressures using a high resolution finite volume model with CT-based properties. In: Bioengineering in Ireland
586. Fitzgerald K, Cardiff P, Flavin R, Ivankovic A (2017) Towards in silico analysis of total hip arthroplasty mechanics. In: XXVI Congress of the International Society of Biomechanics, Brisbane, Australia
587. Muralidharan L, Cardiff P, Flavin R, Ivankovic A (2017) A numerical model for the calculation of ankle joint stresses. In: XXVI Congress of the International Society of Biomechanics, Brisbane, Australia
588. Kovačević A, Stošić N, Smith IK (2002) Solid–fluid interaction in screw compressors. In: XVI International Compressor Engineering Conference at Purdue
589. Kovačević A, Stošić N, Smith IK (2002) Three-dimensional modelling of solid–fluid interaction as a design tool in screw compressors. In: International design conference—DESIGN 2002, Dubrovnik, Croatia
590. Kovačević A, Stošić N, Smith IK (2002) The influence of rotor deflection upon the screw compressor process. In: Schraubencompressor tagung (Screw compressor meeting), Dortmund, Germany
591. Kovačević A, Stošić N, Smith IK (2002) Numerical simulation of fluid flow and solid structure in screw compressors. In: Proceedings of 2002 ASME Congress, New Orleans, USA, 2002. Symposium on the analysis and applications of heat pump and refrigeration systems
592. Kovačević A, Stošić N, Smith IK (2003) Fluid–solid interaction for extension of range in screw machine application. In: Advances of CFD in fluid machinery design, ImechE Seminar, London, UK
593. Kovačević A, Stošić N, Smith IK, Mujić E (2004) Fluid–solid interaction in the design of multifunctional screw machines. In: 8th international design conference—design 2004, vol 2. Dubrovnik, Croatia, pp 1289–1295
594. Kovačević A, Mujić E, Stošić N, Smith IK (2011) Extending the role of computational fluid dynamics in screw machines. J Process Mech Eng Part E Proc Inst Mech Eng, pp 83–97
595. I. Bijelonja (2011) A finite volume method for a geomechanics problem. In: Proceedings of the 22nd international DAAAM symposium, pp 323–324
596. Demirdžić I, Muzaferija S, Perić M (1977) Advances in computation of heat transfer, fluid flow, and solid body deformation using finite volume approaches. In: Sparrow EM, Minkowycz WJ (ed) Advances in numerical heat transfer. Taylor and Francis, pp 59–96
597. Bijelonja I (2005) Finite volume method analysis of large strain elasto-plastic deformation. In: The 16th DAAAM International Symposium, Opatia, Croatia
598. Sabbagh-Yazdi SR, Alkhamis MT, Mastorakis NE, Esmaili M (2008) Finite volume analysis of two-dimensional strain in a thick pipe with internal fluid pressure. Int J Math Models Methods Appl Sci 2:162–167
599. Sabbagh-Yazdi SR, Mastorakis NE, Esmaili M (2008) Explicit 2D matrix free Galerkin finite volume solution of plane strain structural problems on triangular meshes. Int J Math Comput Simul 2:1–8
600. Alkhamis MT, Sabbagh-Yazdi SR, Esmaeili M, Wegian FM (2008) Utilizing NASIR Galerkin finite volume analyzer for 2D plane strain problems under static and vibrating concentrated loads. Jordan J Civ Eng 2:335–343
601. Sabbagh-Yazdi SR, Alimohammadi S, Mastorakis NE (2009) Comparison of finite element and finite volume solvers results for plane-stress displacements in plate with oval hole. In: Proceedings of the 4th IASME/WSEAS international conference on continuum mechanics CM'09, pp 168–173
602. Sabbagh-Yazdi SR, Amiri-Saadatabadi T (2011) Sequential computations of two-dimensional temperature profiles and thermal stresses on an unstructured triangular mesh by GFVM method. Int J Civ Eng 9:171–182
603. Sabbagh-Yazdi SR, Esmaili M, Alkhamis MT (2011) Symmetric conditions for strain analysis in a long thick cylinder under internal pressure using NASIR unstructured GFVM solver. Jordan J Civ Eng 5:258–267
604. Sabbagh-Yazdi SR, Ali-Mohammadi S (2011) Performance evaluation of iterative GFVM on coarse unstructured triangular meshes and comparison with matrix manipulation based solution methods. Sci Iran 18:131–138
605. Sabbagh-Yazdi SR, AliMohammadi S, Pipelzadeh MK (2012) Unstructured finite volume method for matrix-free explicit solution of stress–strain fields in two-dimensional problems with curved boundaries in equilibrium condition. Appl Math Model 36:2224–2236
606. Sabbagh-Yazdi SR, Bayatlou M (2012) Equilibrium condition nonlinear modeling of a cracked concrete beam using a 2D Galerkin finite volume solver. Comput Methods Civ Eng 3:63–76
607. Bailey C, Chow P, Cross M, Pericleous K, Taylor GA, Croft TN, Wheeler D, Lu H (1999) Finite volume methods for multiphysics problems. In: Haenel D, Vilsmeirer R, Benkhaldoun F (eds) Finite volumes for complex applications, II—problems and perspectives, Duisburg, Germany
608. Hitchings D, Davies GAO, Kamoulakos A (1987) Linear static benchmarks. International Association for the Engineering Analysis Community and National Agency for Finite Element Methods and Standards (NAFEMS), Glasgow, UK
609. Voller VR (2009) Basic control volume finite element methods for fluids and solids. World Scientific, Singapore